"알고 있는 것을 알고 있는 것(known knowns)이 있고, 알고 있지만 모른다는 사실을 알고 있는 것(known unknowns)이 있다. 그러나 우리가 모른다는 사실조차 모르는 것, 즉 unknown unknowns도 존재한다." - 도널드 럼스펠트 (2002)

"There are known knowns; there are things we know we know. We also know there are known unknowns; that is to say, we know there are some things we do not know. But there are also unknown unknowns—the ones we don't know we don't know."

- Donald Rumsfeld (2002)

Scaling

Seung-Woo Son
Hanyang University ERICA

KPS Statistical Physics Division

통계물리 분과 구성

- 위원장: 김철민 교수 (UNIST)
- 간사: 이상훈 교수 (경상국립대학교)

https://sites.google.com/site/statphysmeeting

Winter School

KIAS-APCTP Winter School on Statistical Physics

- 22nd KIAS-APCTP Winter School on Statistical Physics 2025 (Homepage, lecture note)
- 21st KIAS-APCTP Winter School on Statistical Physics 2024 (Homepage, lecture note)
- 20th KIAS-APCTP Winter School on Statistical Physics 2023 (Homepage, lecture video)
- 19th KIAS-APCTP Winter School on Statistical Physics 2022 (Homepage, lecture video)
- 18th KIAS-APCTP Winter School on Statistical Physics 2021 (Homepage, poster)
- 17th KIAS-APCTP Winter School on Statistical Physics 2020 (Homepage, poster)
- 16th KIAS-APCTP Winter School on Statistical Physics 2019 (**Homepage**)
- 15th KIAS-APCTP Winter School on Statistical Physics 2018 (**Homepage**, **poster**)
- 14th KIAS-APCTP Winter School on Statistical Physics 2017 (**Homepage**, **poster**)
- 13rd KIAS-APCTP Winter School on Statistical Physics 2016 (**Homepage**, **poster**)
- 12nd KIAS-APCTP Winter School on Statistical Physics 2015 (**Homepage**, **poster**)
- 11st KIAS-APCTP Winter School on Statistical Physics 2014 (**Homepage**, **poster**)
- 10th KIAS-APCTP Winter School on Statistical Physics 2013 (**Homepage**, **poster**)
- 9th KIAS-APCTP Winter School on Statistical Physics 2012 (**poster**)

The 16th KIAS-APCTP Winter School on Statistical Physics

January 14 (Mon), 2019 ~ January 18 (Fri), 2019

■ Main Page

Venue | Period

The Ocean Resort, Yeosu, Korea | January 14-18, 2019

Overview

Statistical mechanics provides a powerful tool for understanding macroscopic systems on the basis of microscopic laws governing the dynamics of their constituents. Its ever-increasing use is not limited to physical sciences but extends to as diverse subjects as biological and social sciences. This annual event is intended to provide graduate students and early-career scientists in statistical physics and related disciplines with the conceptual framework and analytical tools for advanced studies in statistical physics and interdisciplinary research.

Topics

Thematic focus of the 19th School is the Phase Transitions and Critical Phenomena. 15 hours of lectures by three invited lecturers will be devoted to learn the fundamental concepts and the practical tools on the subject. The attending students will undertake a hands-on group project on the subjects, in order to make the School more engaging. Three lecture series (5 hours each) will be given under the tentative topics:

- Fundamentals of Phase Transitions and Critical Phenomena (HP)
- Renormalization Group 101 (JDN)
- Numerical Methods to Study Critical Phenomena (DHK)

제19차 KIAS-APCTP 통계물리 겨울학교

by STATPHYS

Playlist · 12 videos · 984 views

제19차 KIAS-APCTP 통계물리 겨울학교

Play all

1 

제19차 통계물리 겨울학교 - 박형규 교수님 1교시 (HP1)

STATPHYS • 180 views • 3 years ago

2 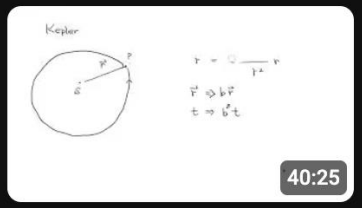

제19차 통계물리 겨울학교 - 노재동 교수님 1교시 (JDN1)

STATPHYS • 150 views • 3 years ago

3 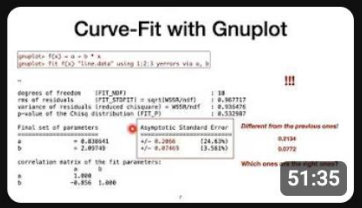

제19차 통계물리 겨울학교 - 김동희 교수님 1교시 (DHK1)

STATPHYS • 125 views • 3 years ago

4 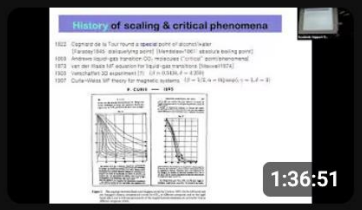

제19차 통계물리 겨울학교 - 박형규 교수님 2교시 (HP2)

STATPHYS • 68 views • 3 years ago

5 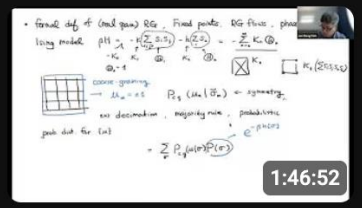

제19차 통계물리 겨울학교 - 노재동 교수님 2교시 (JDN2)

STATPHYS • 87 views • 3 years ago

6 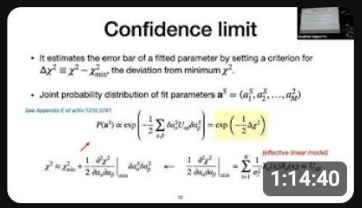

제19차 통계물리 겨울학교 - 김동희 교수님 2교시 (DHK2)

STATPHYS • 72 views • 3 years ago

- EQ spatial patterns

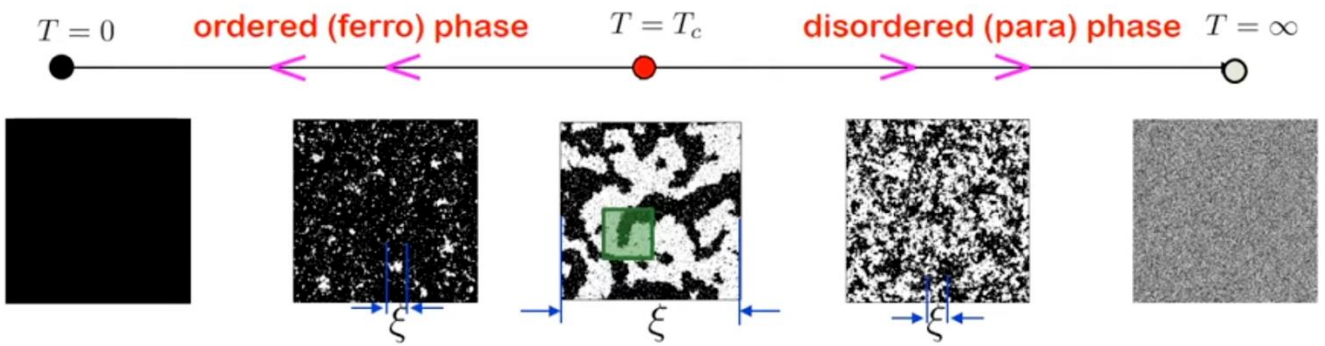

* Key question: What is "phase" ?

- How to classify seeming different patterns into a few groups (phases)?

Zoom out (coarsening) for scale transformation (RGT) ⇒ approaching a fixed point

- Stable f.p. represents phase & unstable f.p. represents critical point (fractal).
- Characteristics of f.p. patterns?? ⇒ fractal dimensions

* How to determine fractal dimensions? [a set of fractal dimensions]

$$A(\ell) = \sum_{w(\ell)} \mathcal{O}_A \quad (\mathcal{O}_A\text{: local observable like } S_i,\ S_iS_j,\ \ldots;\ w(\ell)\text{: window of linear size } \ell)$$

$$\sim \ell^{d_A} \text{ for large } \ell \quad (d_A\text{: fractal dimension of object 'A'})$$

- Critical patterns are (nontrivial) fractals. $P(s_A) \sim s^{-d_A}$ [no typical scale] [self-similar]

* Is it useful to know fractal dimensions?

- Critical exponents are simply related to fractal dimensions.

Scailing **scal·ing**

- 발음 미국·영국 [skéiliŋ]
- 명사 [물리] 스케일링, 비례 축소; [컴퓨터] 크기 조정; [치과] 치석 제거

- 물리학용어집 - 눈금 바꿈

  scaling behavior 눈금 바꿈 행동, scaling ansatz 눈금 바꿈 가설, scaling theory 눈금 바꿈 이론, scaling law 눈금 바꿈 법칙

KPS 한국물리학회 The Korean Physical Society

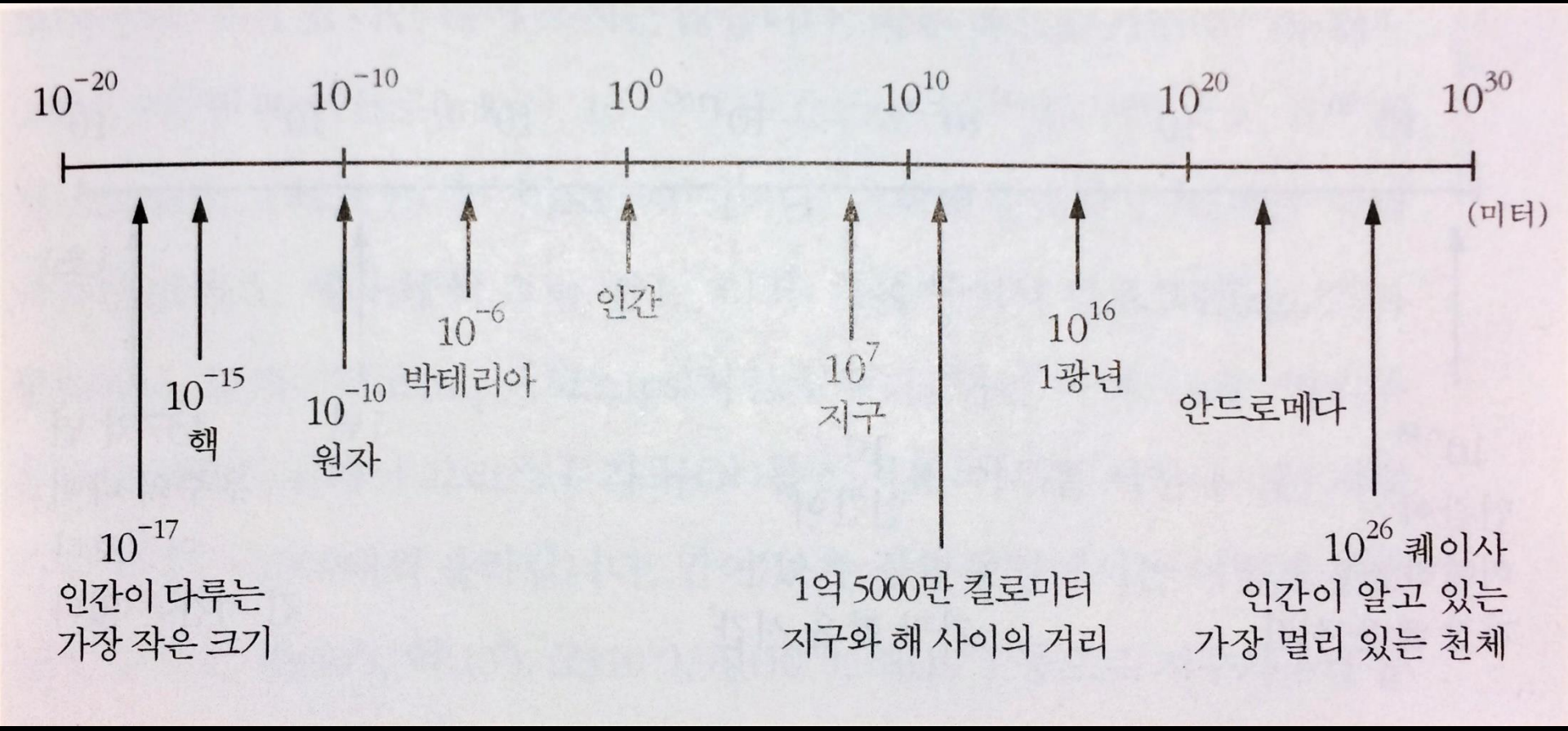

Image from <최무영 교수의 물리학 강의>

그림 8

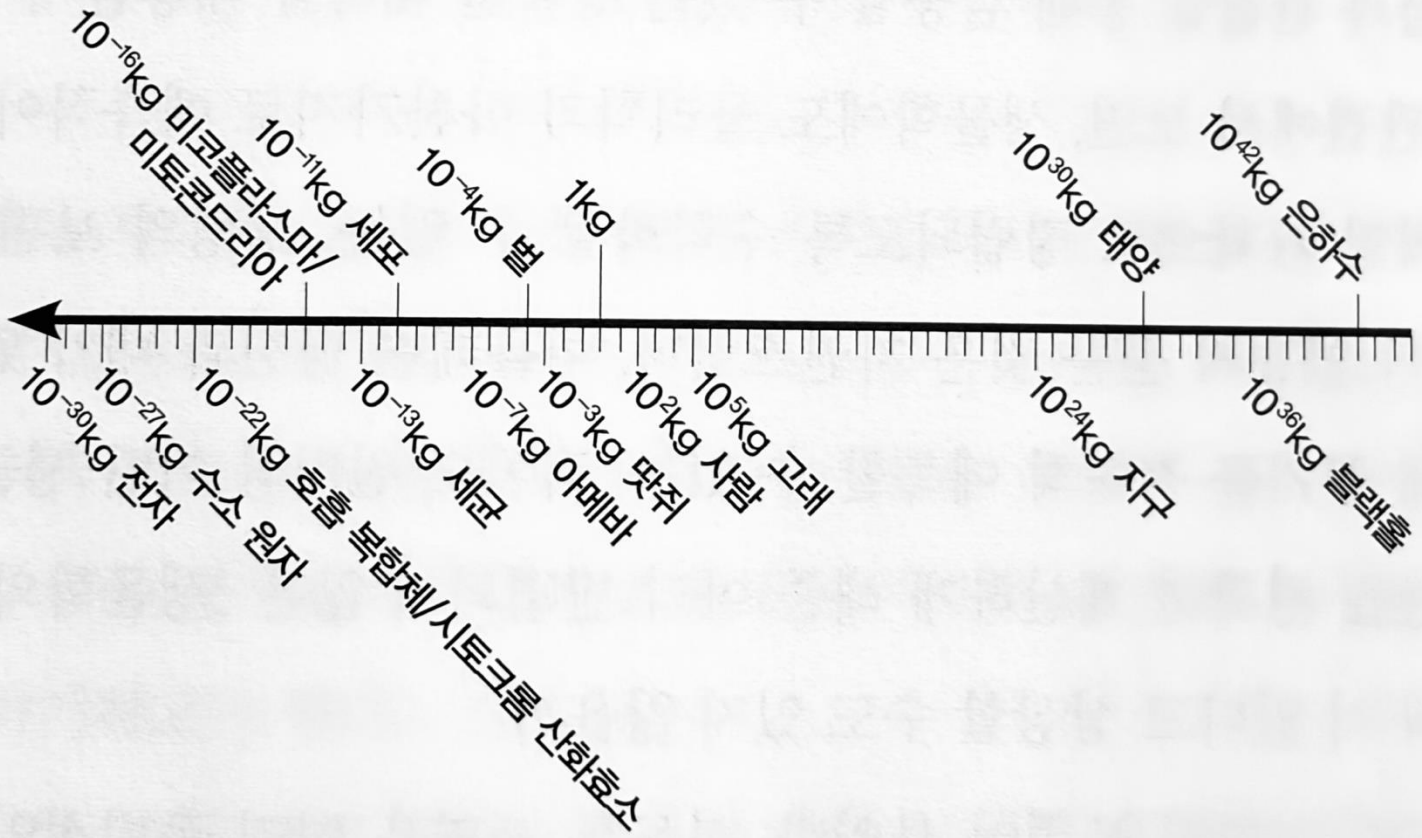

복잡한 분자와 미생물에서 고래와 세쿼이아에 이르는 생명의 놀라운 규모를 은하 및 소립자 규모와 관련지어 보았다.

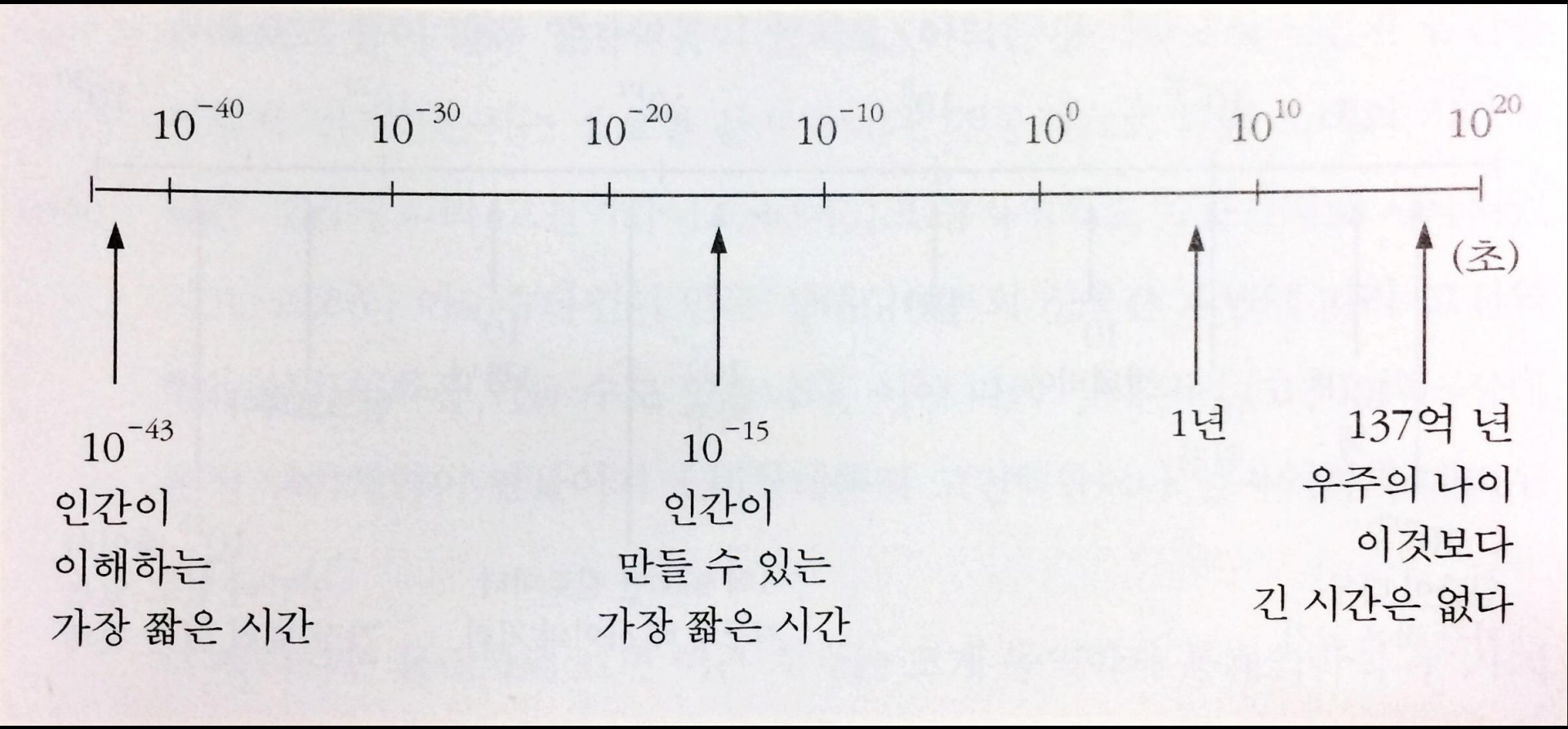

Image from <최무영 교수의 물리학 강의>

Video from Cosmic Eye

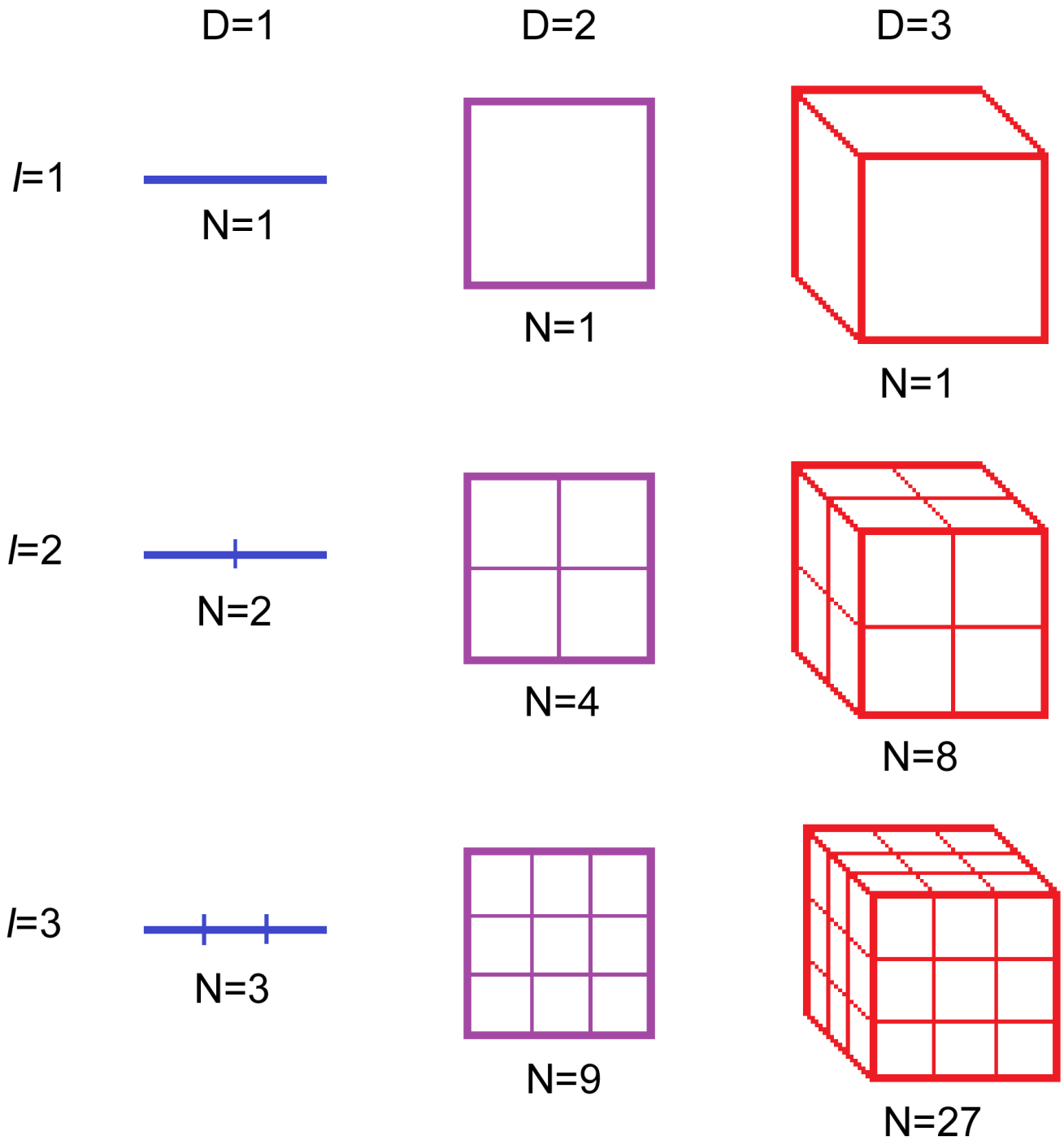
D=1
D=2
D=3
l=1
N=1
N=1
N=1
l=2
N=2
N=4
N=8
l=3
N=3
N=9
N=27

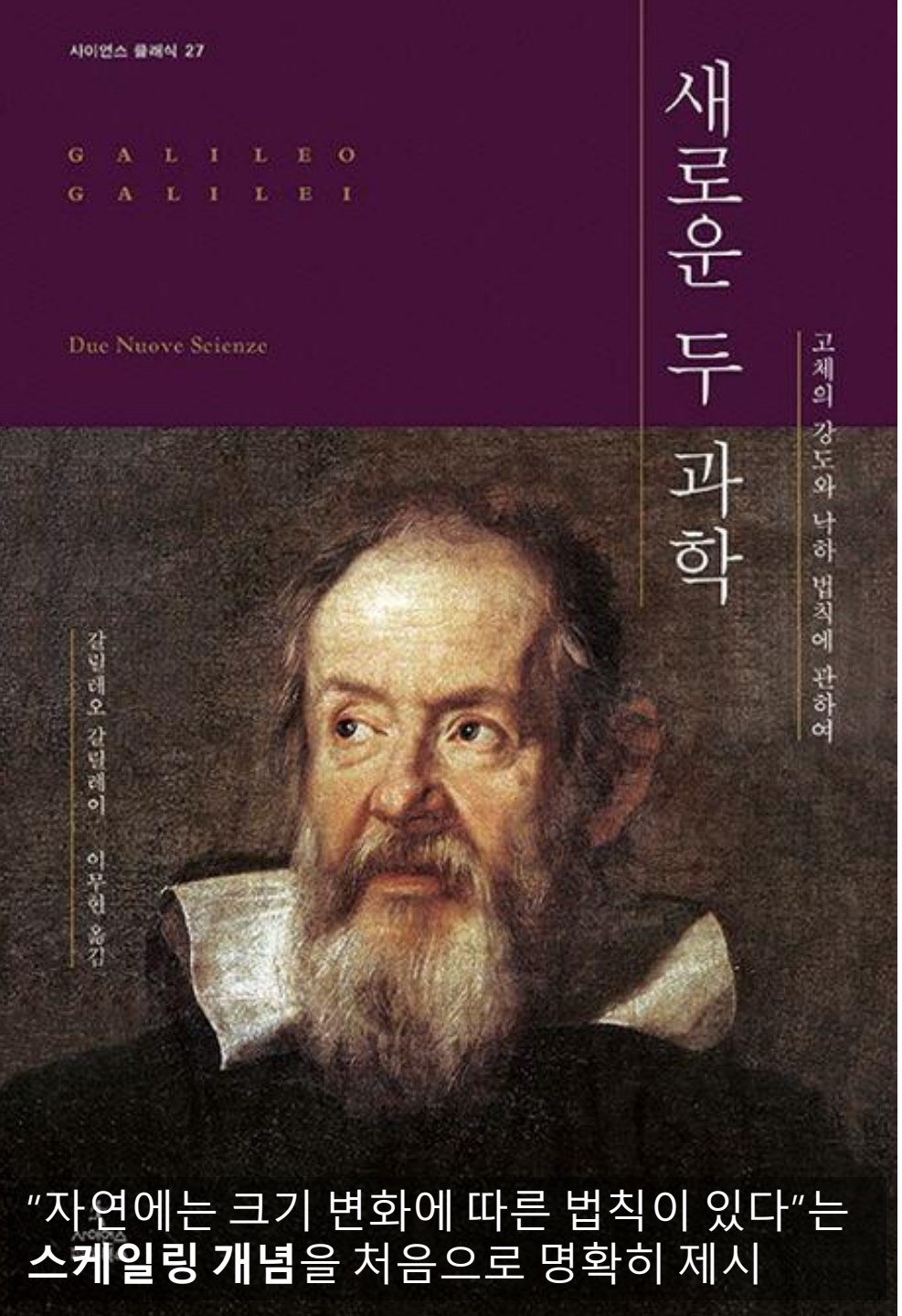

"자연에는 크기 변화에 따른 법칙이 있다"는 **스케일링 개념**을 처음으로 명확히 제시

<새로운 두 과학에 대한 논의와 수학적 논증> (1638)

둘째날, 밧줄과 들보의 강도에 대한 논의 중 살비아티의 말...

"이미 밝혀진 것들로부터, 기술에서든 자연에서든 구조물의 크기를 방대하게 늘린다는 것이 불가능함을 쉽게 알 수 있습니다. 즉 노, 활대, 들보, 쇠못 등 모든 부위가 하나로 결합되는 방식으로 엄청난 크기의 배, 궁전, 사원을 짓기란 불가능합니다. 게다가 나뭇가지들이 자신의 무게로 부러질 테니 자연도 아주 거대한 크기의 나무를 만들지 못합니다. 또 사람이나 말 같은 동물들이 엄청나게 커진다면, 형태를 유지하고 정상적인 기능을 수행할 수 있도록 뼈대 구조를 구축하기가 불가능할 겁니다. ... 키가 터무니없이 커지면, 그 자신의 무게로 무너지고 짓눌릴테니까요."


Entertainment
WEEKLY
JULY 2015
WWW.FB.COM/ANTMAN
EXCLUSIVE
MARVEL

square–cube law
(or **cube–square law**)

It was first described in 1638 by Galileo Galilei in his *Two New Sciences* as the "...ratio of two volumes is greater than the ratio of their surfaces".

Adolphe Quetelet

Lambert Adolphe Jacques Quetelet (22 February 1796 – 17 February 1874)[1] was a Belgian-French astronomer, mathematician, statistician, and sociologist

He also founded the science of anthropometry and developed the body mass index (BMI) scale, originally called the Quetelet Index.

$$\mathrm{BMI} = \frac{\mathrm{mass_{kg}}}{\mathrm{height_m}^2} = \frac{\mathrm{mass_{lb}}}{\mathrm{height_{in}}^2} \times 703$$

Corpulence Index (**CI**) or **Ponderal Index** (**PI**)

$$\mathrm{CI} = \frac{\mathrm{mass}}{\mathrm{height}^3}$$

SCIENTIFIC REPORTS

OPEN

Human bipedalism and body-mass index

Su Do Yi[1], Jae Dong Noh[2,3], Petter Minnhagen[4], Mi-Young Song[5], Tae-Soo Chon[6,7] & Beom Jun Kim[8]

Received: 15 April 2016
Accepted: 9 May 2017
Published online: 16 June 2017

Body-mass index, abbreviated as BMI and given by M/H^2 with the mass M and the height H, has been widely used as a useful proxy to measure a general health status of a human individual. We generalise BMI in the form of M/H^p and pursue to answer the question of the value of p for populations of animal species including human. We compare values of p for several different datasets for human populations with the ones obtained for other animal populations of fish, whales, and land mammals. All animal populations but humans analyzed in our work are shown to have $p \approx 3$ unanimously. In contrast, human populations are different: As young infants grow to become toddlers and keep growing, the sudden change of p is observed at about one year after birth. Infants younger than one year old exhibit significantly larger value of p than two, while children between one and five years old show $p \approx 2$, sharply different from other animal species. The observation implies the importance of the upright posture of human individuals. We also propose a simple mechanical model for a human body and suggest that standing and walking upright should put a clear division between bipedal human ($p \approx 2$) and other animals ($p \approx 3$).

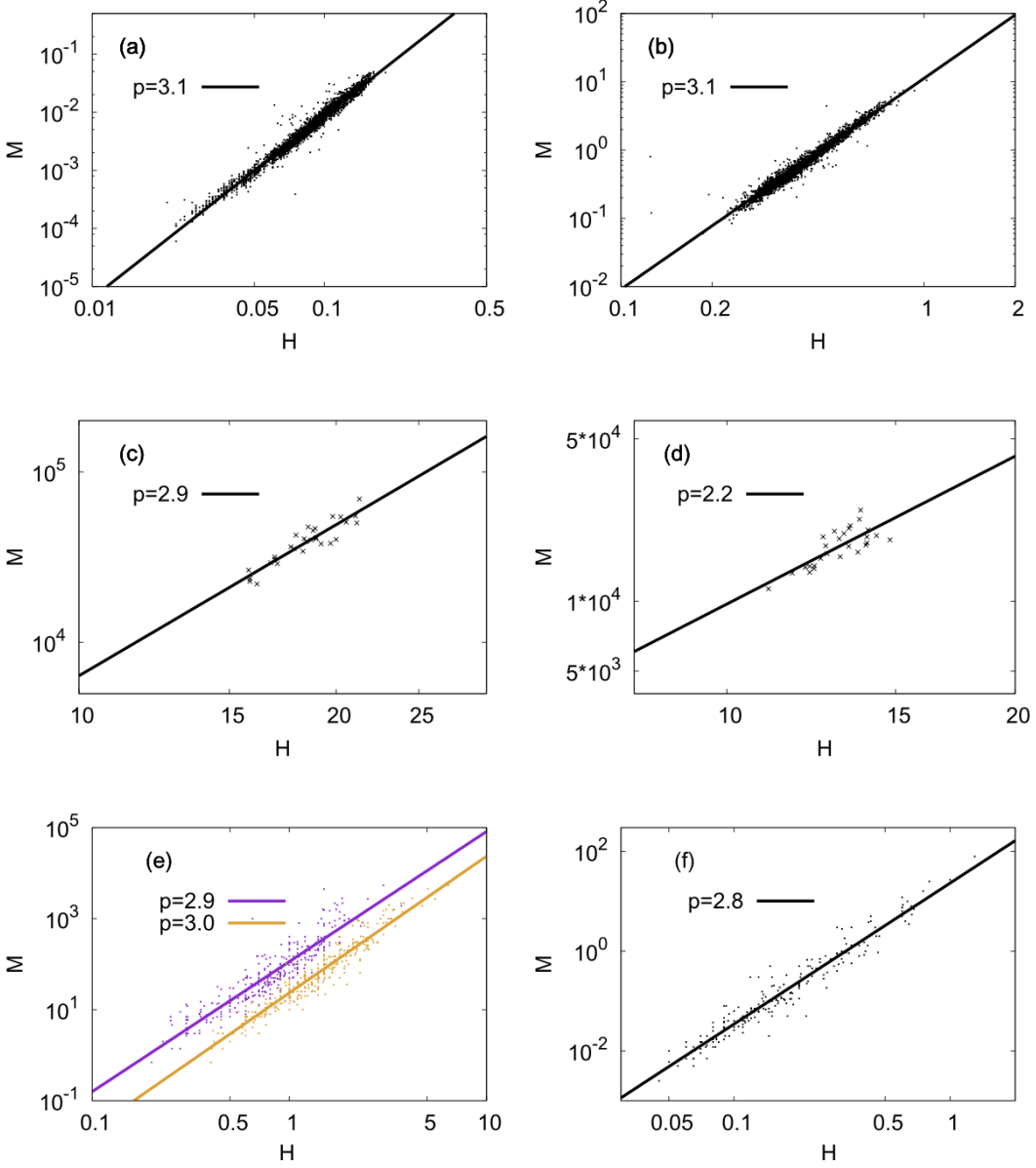

Figure 1. The mass M versus the linear body size H of animals: (**a**) Pale chub (*Zacco platypus*) ($N=3\,163$) and (**b**) Korean chub (*Zacco koreanus*) ($N=997$) are for fishes, (**c**) Fin ($N=29$) and (**d**) Sei ($N=27$) are for whales, and (**e**) and (**f**) are for land mammals, respectively. The data file used for (**e**) contains all 325 lines of the mass, the body length, and the shoulder height information of many different species of land mammals, while the file used for (**f**) contains 205 lines of the mass and the body length of species in order Rodentia. In (**e**) two different ways to measure the linear size, the shoulder height (upper points) and the body length (lower points) are displayed. In all datasets in (**a**)–(**f**), we observe that the Benn index $p \approx 3$, with (**d**) an exception, probably due to insufficient data size for Sei whales.

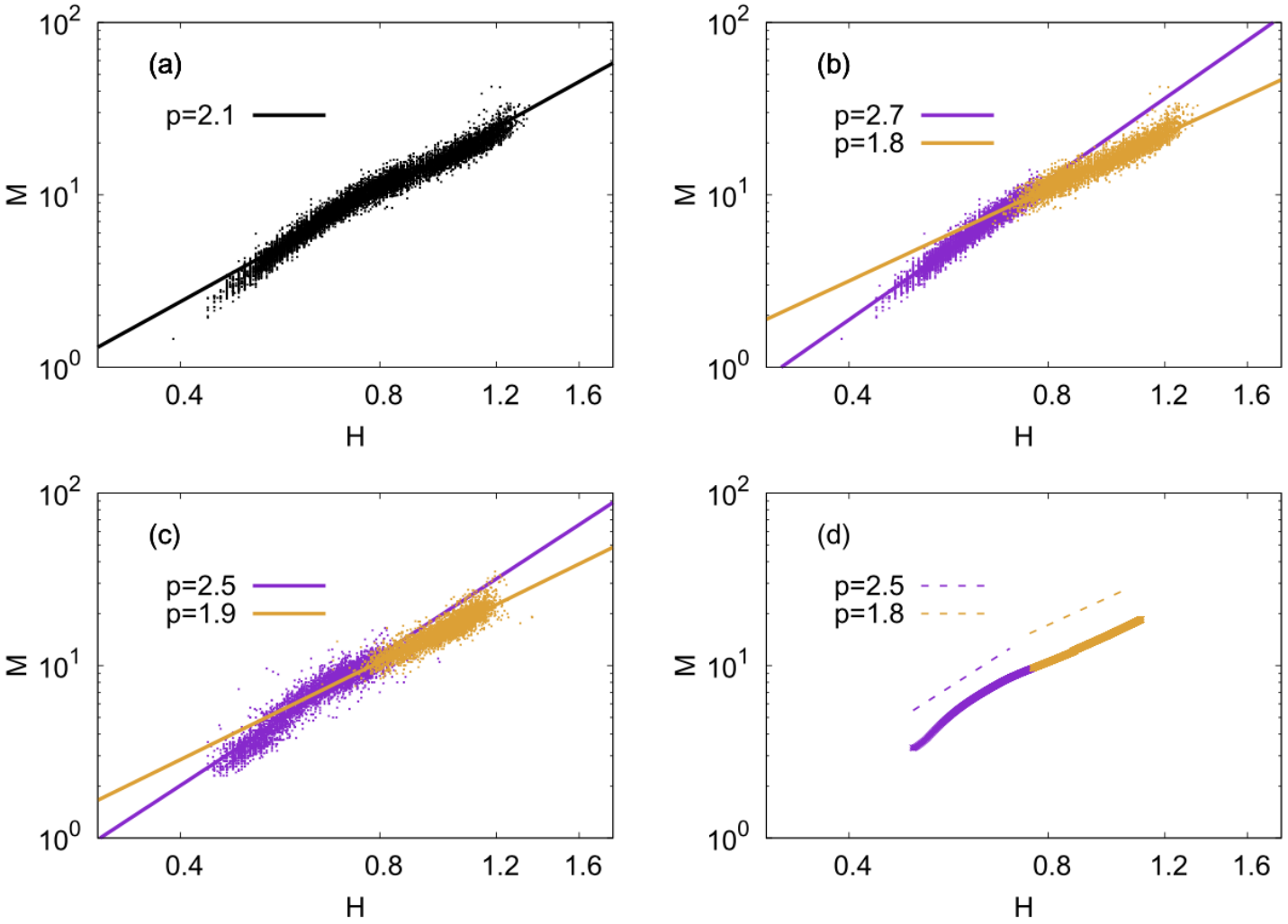

Figure 2. The mass M and the height H for humans: (**a**) and (**b**) for the data from Sweden, (**c**) from Korea, and (**d**) from WHO (see text for details of the used datasets). The linear regression for the entire data in (**a**) for Swedish children gives the Benn index $p = 2.1$. In (**b**), we divide all Swedish data into two groups depending on whether the child is younger or older than one year after birth. The left part of the data for children younger than one year old has $p \approx 2.8$ while children older than one year (the right part of the data) has $p \approx 1.8$. (**c**) Data for Korean children drawn in the same way as for (**b**), giving us $p \approx 2.5$ and $p \approx 1.9$ depending on the age group (younger and older than one year, respectively). (**d**) WHO data displayed in the same way. Again, we see the change of p value at around one year after birth. Although all data points in each dataset are used to perform the linear regressions in (**a**)–(**c**), we use only 10000 randomly chosen points in each scatter plot for (**a**)–(**c**), only for convenience of visibility.

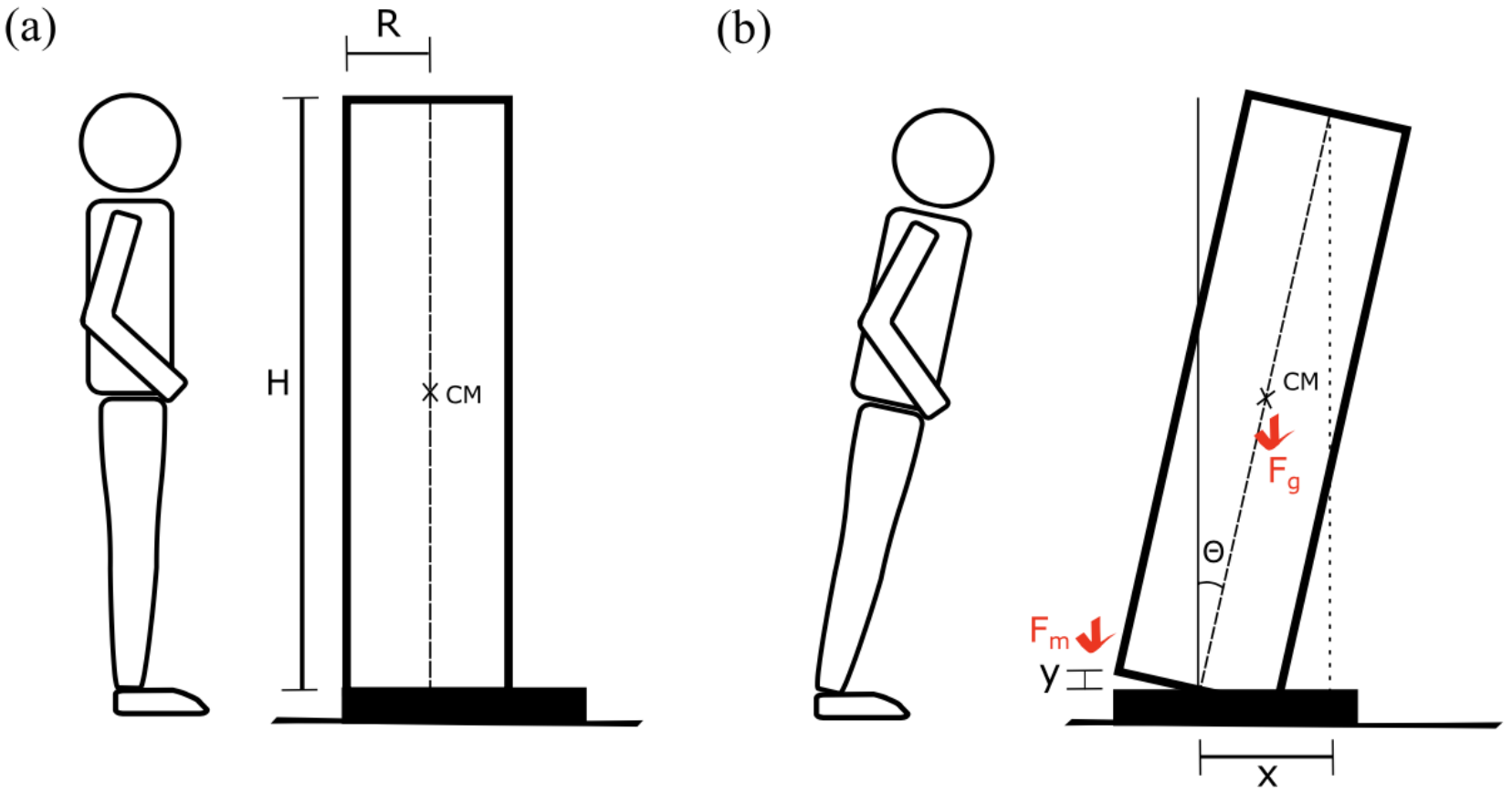

Figure 3. (**a**) We assume that the human body is a uniform cylinder with the radius R and the height H. It is supported on a rigid substrate (a representation of human feet). Suppose that the human body cylinder is tilted forward as shown in (**b**) by a small angle θ. To achieve the stability of the tilted posture, two competitive torques, one from the skeletal muscle force F_m and the other from the gravitational force F_g, must be balanced. The gravitational torque is written as $T_g = F_g(x/2)$ with $x/2$ being the shift of the horizontal position of the center of mass (CM). We assume that F_m depends on the extension y of muscles as shown in (**b**). For the tilting angle θ, we get $x = H \sin\theta$ and $y = R \sin\theta = xR/H$.

The total weight of the body is written as $F_g = \pi\rho R^2 H g$ with the mass density ρ and the gravitational acceleration g. As seen in Fig. 3(b), suppose that the body cylinder of a human is tilted forward in such a way that the top of the body is now shifted horizontally by the distance x. The gravitational torque, with the contact point of the body axis and the ground [see Fig. 3(b)] taken as the origin, reads

$$T_g = F_g \frac{x}{2}, \tag{1}$$

since the center of mass (CM) is horizontally shifted by the distance $x/2$. Upon tilting, the body cylinder is lifted from the substrate, which results in the extension y of the muscle as displayed in Fig. 3(b). The force F_m caused by the extension of the muscle then applies the torque

$$T_m = F_m c R \tag{2}$$

with c being a constant of $O(1)$. Skeletal muscles are collections of long muscle fibers, which are composed of repeating sections of the so-called sarcomeres. We expect that the total number of muscle fibers is proportional to R^2 and that the number of repeating building blocks (sarcomeres) along the muscle fiber must be proportional to H[17]. Accordingly, we believe that the muscle force F_m which can be provided by the human body cylinder can roughly be written as

$$F_m = R^2 H f(y), \tag{3}$$

where $f(y)$ is independent of body size but depends only on the extension y of the muscle. We note that in the study of jump heights of various animal species[18] the available energy produced by a body has been argued to be proportional to the body mass, i.e., R^2H, as in Eq. (3). The stability requirement for the tilted posture is given by the torque balance condition $T_g = T_m$, which yields $(\pi/2)\rho R^2 H g x = c R^3 H f(y)$, and we obtain $x \sim R f(y)$. We then use a general form $f(y) \sim y^b$ with an unspecified parameter b, and get $x \sim R y^b$. The final step is to use $x = H \sin\theta$ and $y = R \sin\theta = Rx/H$ as shown in Fig. 3, which gives us $x \sim R(Rx/H)^b$. In order to make this equation self-consistent, we now find $b = 1$, and we finally get

$$H \sim R^2, \tag{4}$$

yielding the Benn index $p = 2$ from $M \sim R^2 H \sim H^2$ for upright human body. Although our model results in $p = 2$ in accord with observations, we still believe that the model demands improvement to be more realistic. For example, the upper body length may scale differently than the total height H, which could be related with different values of p for different human population groups.

DIAGNOSIS: ANTHROPOMETRIC COMPONENT

Anthropometric Screening & Classification

Measure BMI
Clinically examine and confirm excess adiposity

+

Measure Waist Circumference
for BMI <35.0 kg/m^2, and
Calculate Waist-to-Height Ratio
for classifying abdominal obesity and cardiometabolic risk

Class	WHO BMI Classification
Overweight[a]	25.0 – 29.9 kg/m^2
Class I Obesity*	30.0 – 34.9 kg/m^2
Class II Obesity	≥35.0 – 39.9 kg/m^2
Class III Obesity	≥40.0 kg/m^2

[a] In the Asia-Pacific region, the BMI threshold for obesity is generally considered to be ≥25 kg/m^2 and for overweight 23 kg/m^2 to 24.9 kg/m^2. See text for additional information.

+

Assess Body Composition
Using, for example, bioelectrical impedance analysis or DXA if clinically needed and available

International Diabetes Federation Waist Circumference Criteria for Cardiometabolic Risk[b]			National Institute for Health and Care Excellence, and World Health Organization
Region/Ethnic Background[c]	Sex	Waist Circumference[d]	Waist-to-Height Ratio
Europe, Sub-Saharan Africa, and Middle East	Male	≥94 cm	≥0.5
	Female	≥80 cm	≥0.5
United States & Canada	Male	≥102 cm	≥0.5
	Female	≥88 cm	≥0.5
Asia, South & Central America	Male	≥90 cm	≥0.5
	Female	≥80 cm	≥0.5

[b] Darbandi M et al. Discriminatory Capacity of Anthropometric Indices for Cardiovascular Disease in Adults: A Systematic Review and Meta-Analysis. Prev Chronic Dis. 2020 Oct 22;17:E131.

[c] See text for additional information.

[d] Increasing waist circumference correlates with increased severity of obesity.

Obesity: identification, assessment and management. NICE Guideline, No. 189.

London: National Institute for Health and Care Excellence (NICE); 2023 Jul 26. Recommendations 1.2.11 and 1.2.12

Abbreviations: **BMI**, body mass index; **DXA**, dual-energy X-ray absorptiometry; **WHO**, World Health Organization

Algorithm Figure 3 - Diagnosis: Anthropometric Component

Endocrine Practice
Volume 31, Issue 11, November 2025, Pages 1351-1394

Adolphe Quetelet

Lambert Adolphe Jacques Quetelet (22 February 1796 – 17 February 1874)[1] was a Belgian-French astronomer, mathematician, statistician, and sociologist

He also founded the science of anthropometry and developed the body mass index (BMI) scale, originally called the Quetelet Index.

$$\mathrm{BMI} = \frac{\mathrm{mass_{kg}}}{\mathrm{height_m}^2} = \frac{\mathrm{mass_{lb}}}{\mathrm{height_{in}}^2} \times 703$$

Corpulence Index (**CI**) or **Ponderal Index** (**PI**)

$$\mathrm{CI} = \frac{\mathrm{mass}}{\mathrm{height}^3}$$

PHYSIOLOGICAL REVIEWS

VOL. 27 OCTOBER, 1947 No. 4

BODY SIZE AND METABOLIC RATE

MAX KLEIBER

Division of Animal Husbandry, College of Agriculture, University of California, Davis

CORRELATION BETWEEN BODY SIZE AND METABOLIC RATE. Günther (1944) introduces a recent review on body weight and metabolic rate with a motto which starts as follows:

"It is believed that far greater progress will be made by discarding all thoughts of a uniformity in heat loss and emphasizing the non-uniformity in heat production. . . ."

The sentence is a citation from Benedict's book, *Vital Energetics* (1938, p. 194).

It is rather difficult to understand how forgetting all thoughts of uniformity and emphasizing non-uniformity can stimulate a comparison of metabolic rates of large and small animals. Any comparison presupposes a common basis, and if I were convinced of the "futility of attempts to discover a unifying principle in metabolism" (Benedict, l.c., p. 178) I should not attempt to write a review on the relation of body size and metabolic rate.

The reader can be expected to spend time on this review only when he can be convinced that body size and metabolic rate are actually related. That these two variables are related is in fact common knowledge.

Does a horse produce more heat per day than a rat or do some rats produce

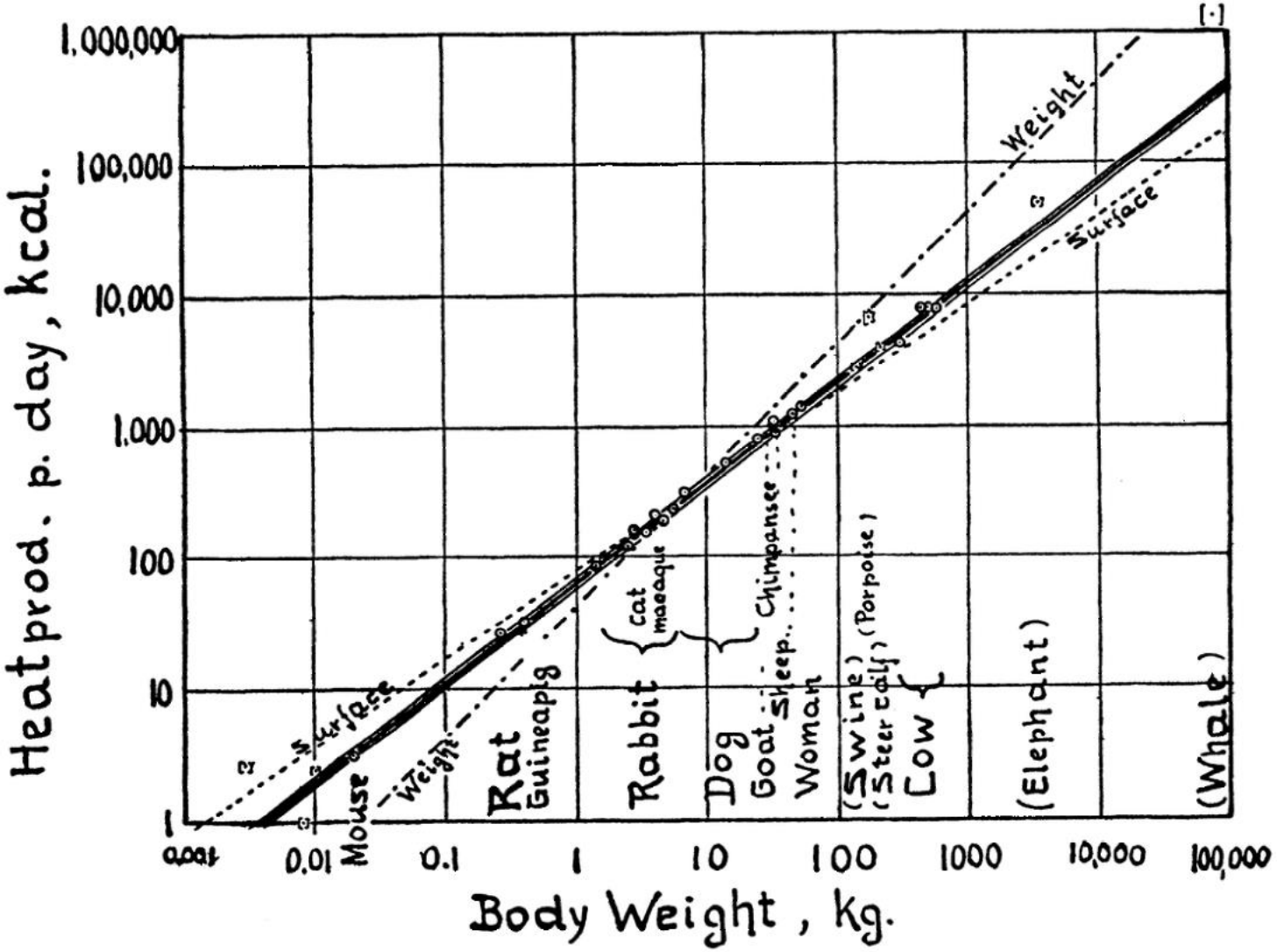

Fig. 1. Log. metabol. rate/log body weight

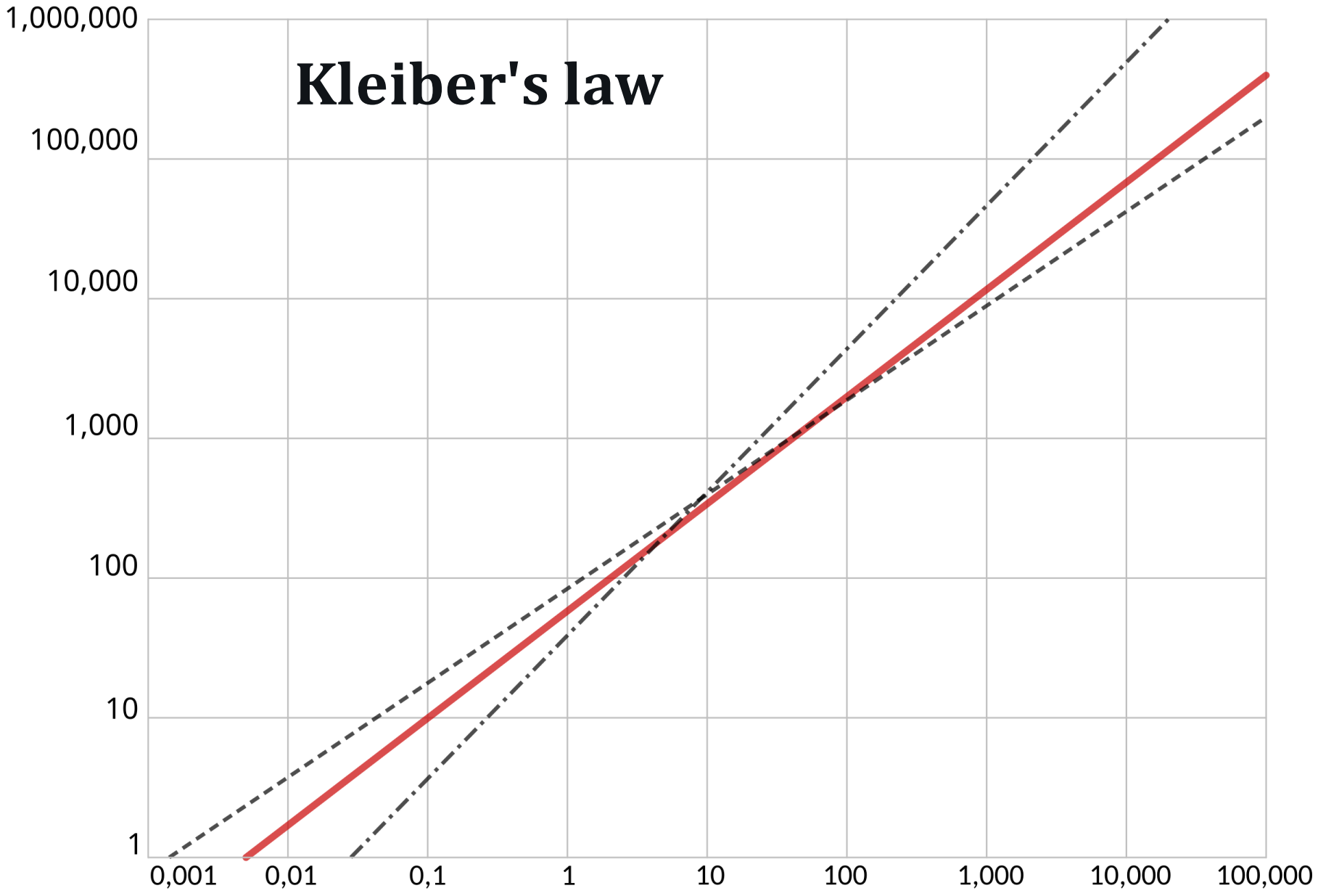
Kleiber's law
1,000,000
100,000
10,000
1,000
100
10
1
0,001
0,01
0,1
1
10
100
1,000
10,000
100,000

유사성 차원 (similarity dimension)

$$d = \frac{\ln m}{\ln r}$$

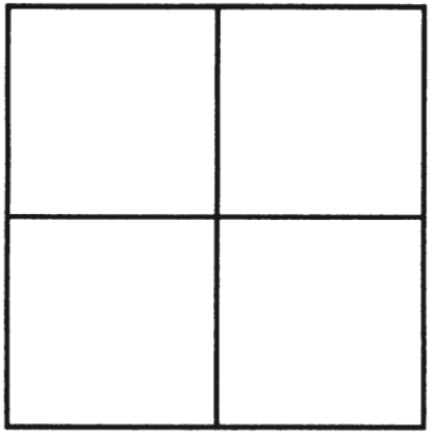

$m = 4$

$r = 2$

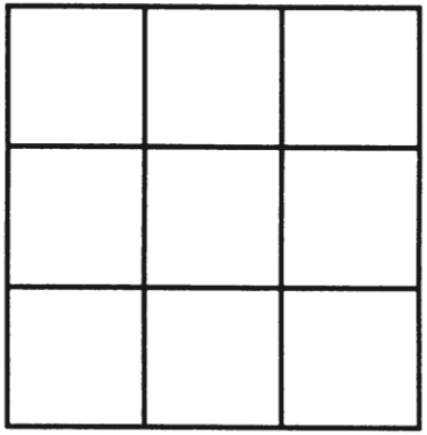

$m = 9$

$r = 3$

$m =$ number of copies
$r =$ scale factor

자기 유사 프랙탈의 차원

'차원'이란 무엇인가?
선과 부드러운 곡선 1차원,
표면은 2차원, 입체들은 3차원

차원은 집합의 모든 점을 설명하는 데 필요한 최소 좌표 수

코흐 곡선 K
- 1차원?
- 호의 길이가 무한!

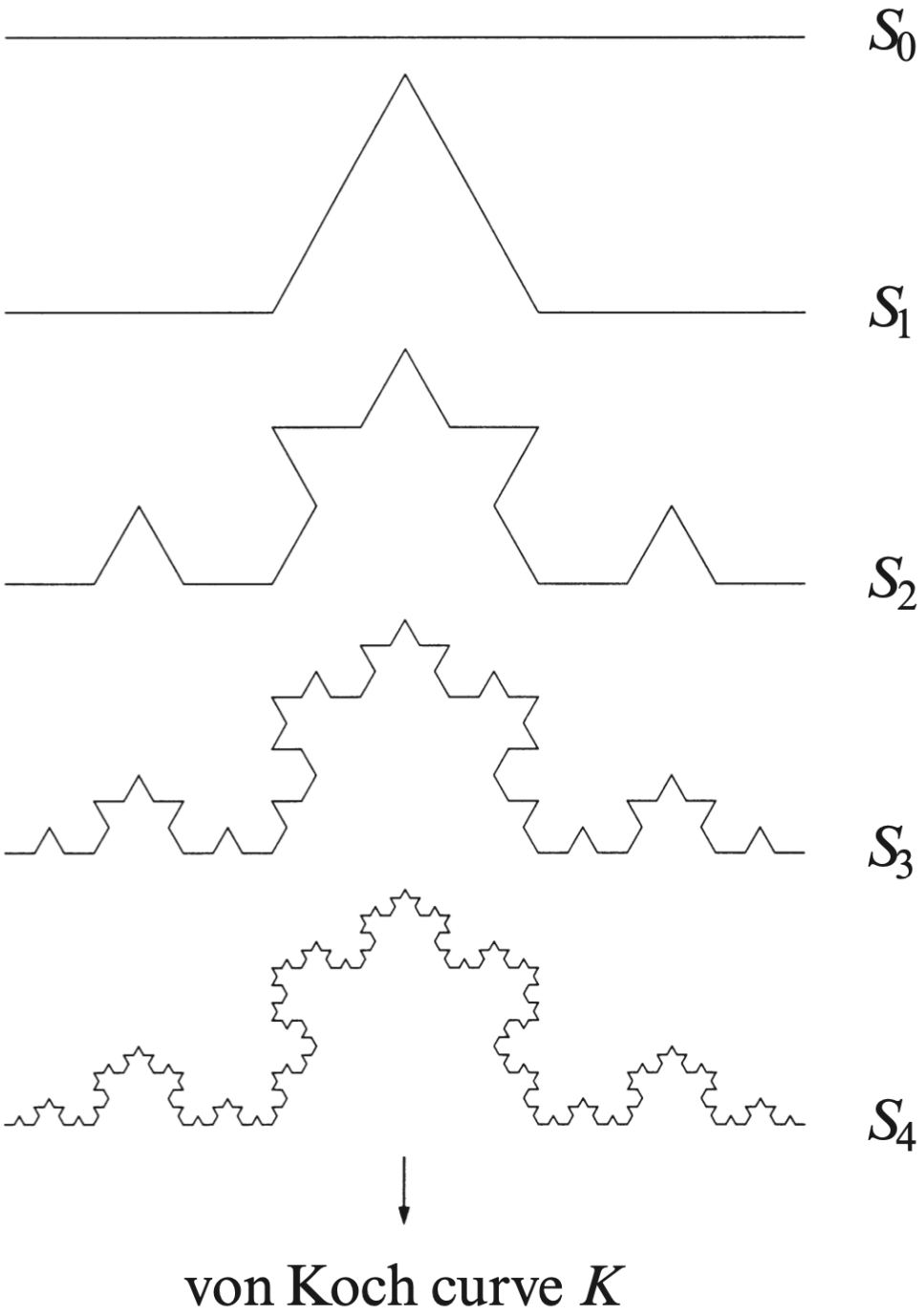

칸토어 집합의 유사성 차원 $d = \frac{\ln 2}{\ln 3} \approx 0.63$

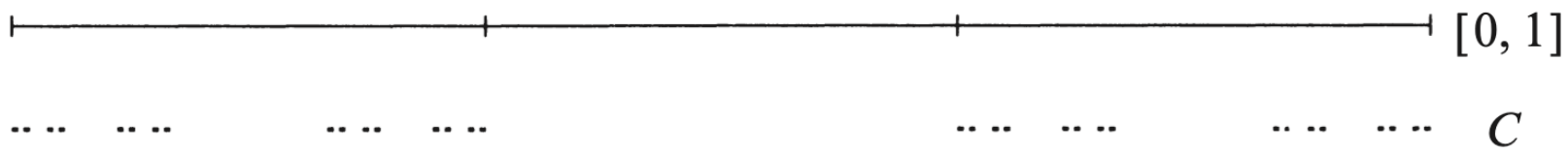

The left half of the Cantor set
is the original Cantor set,
scaled down by a factor of 3

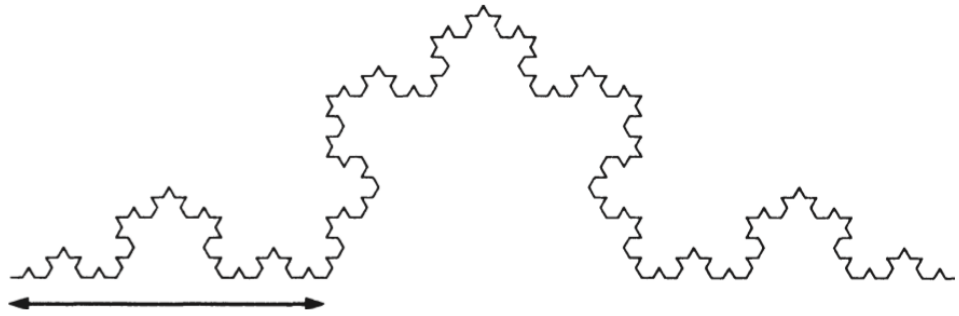

코흐 곡선의 유사성 차원

$$d = \frac{\ln 4}{\ln 3} \approx 1.26$$

칸토어 집합 (Cantor Set)

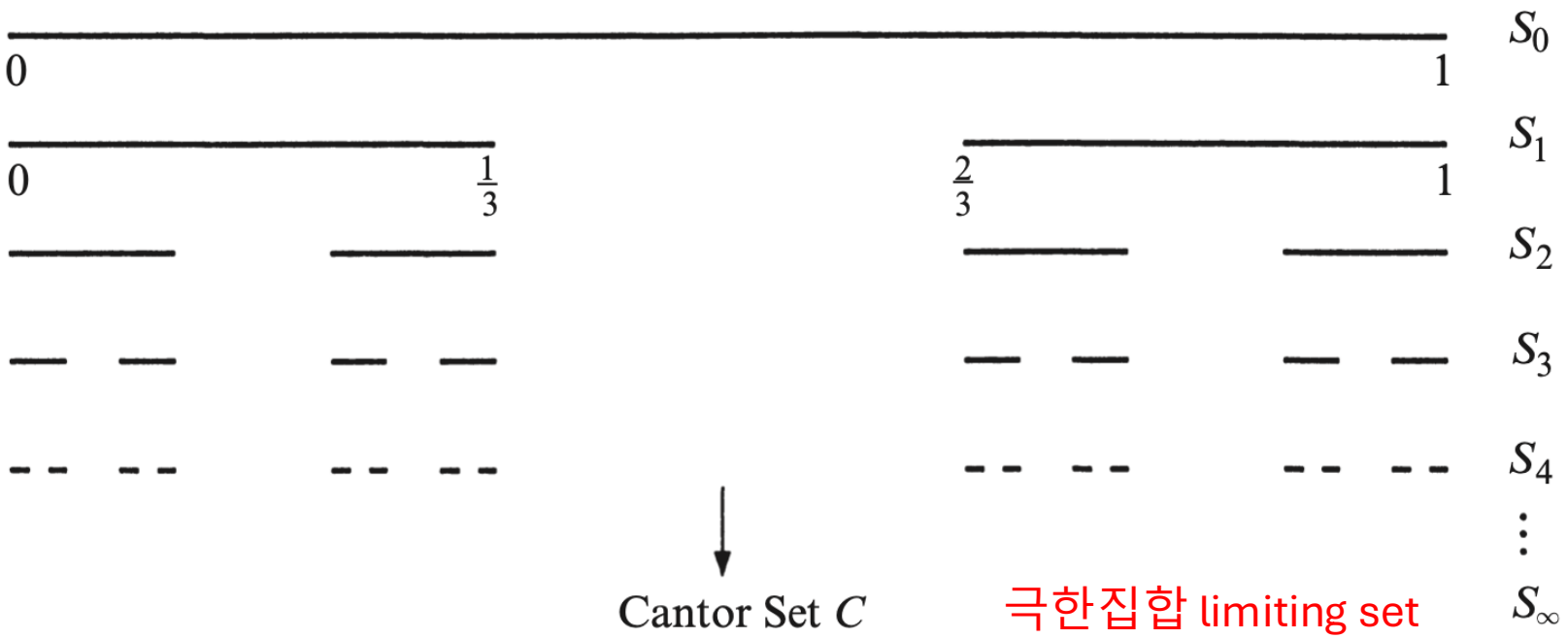

* 칸토어 집합은 프랙탈!

1. 임의의 작은 스케일 구조를 갖는다.
2. 자기 유사성이 있다.
3. 정수 차원이 아니다. 0.63 차원!

- 측정값 (measure) 0을 갖는다.
- 셀 수 없이 많은 점으로 구성된다.

박스 차원 (box dimension)

용량 차원 (capacity dimension)

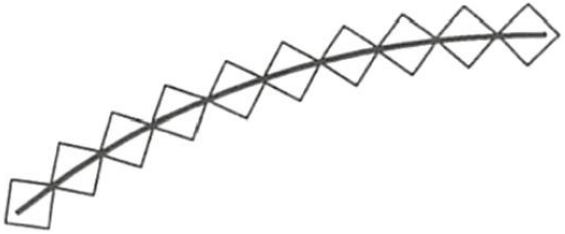

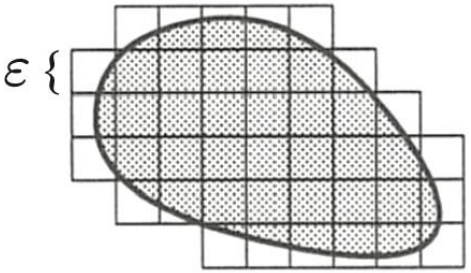

power law $N(\varepsilon) \propto 1/\varepsilon^d$

$$N(\varepsilon) \propto \frac{L}{\varepsilon}$$

$$N(\varepsilon) \propto \frac{A}{\varepsilon^2}$$

$$d = \lim_{\varepsilon \to 0} \frac{\ln N(\varepsilon)}{\ln(1/\varepsilon)}$$

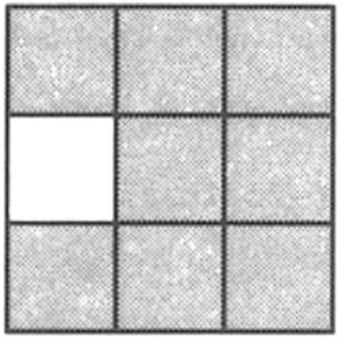

S_1

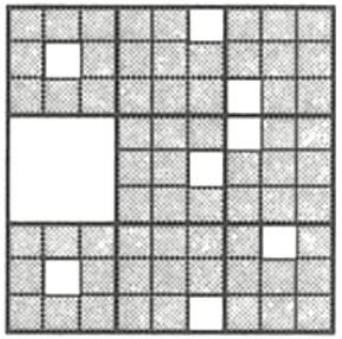

S_2

$$d = \frac{\ln 8}{\ln 3}$$

점별 상관관계 차원

점별 차원 (pointwise dimension)

$$N_{\mathbf{x}}(\varepsilon) \propto \varepsilon^{d}$$

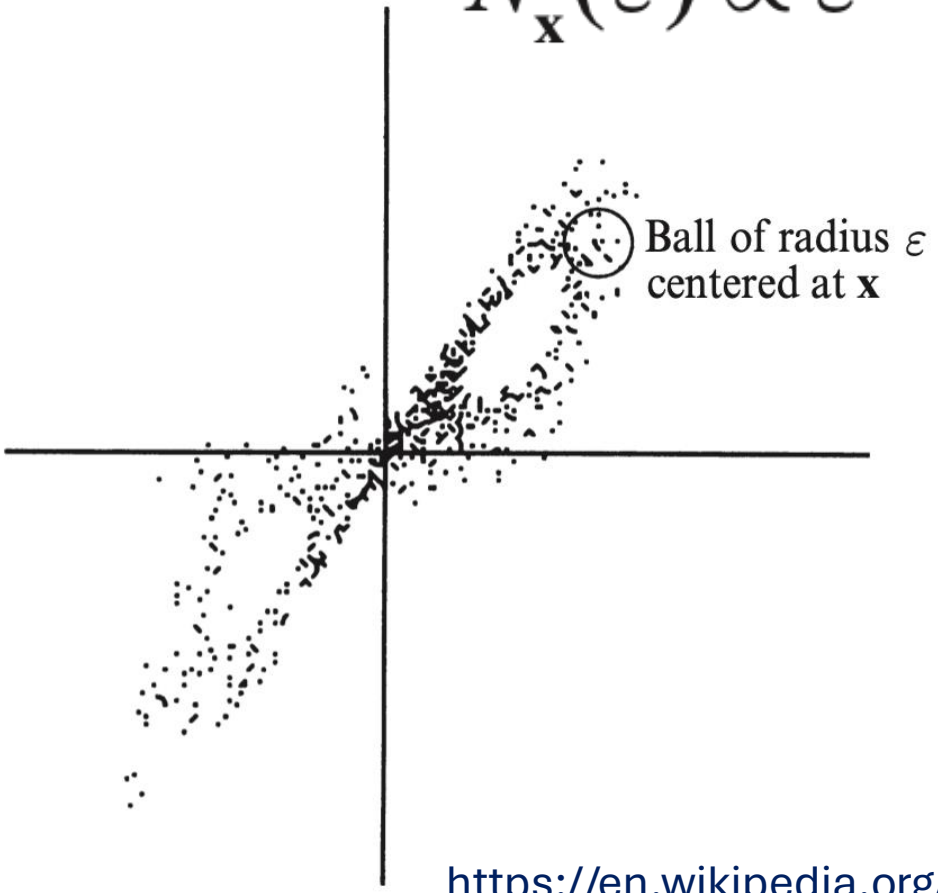

상관관계 차원 (correlation dimension)

$$C(\varepsilon) \propto \varepsilon^{d}$$

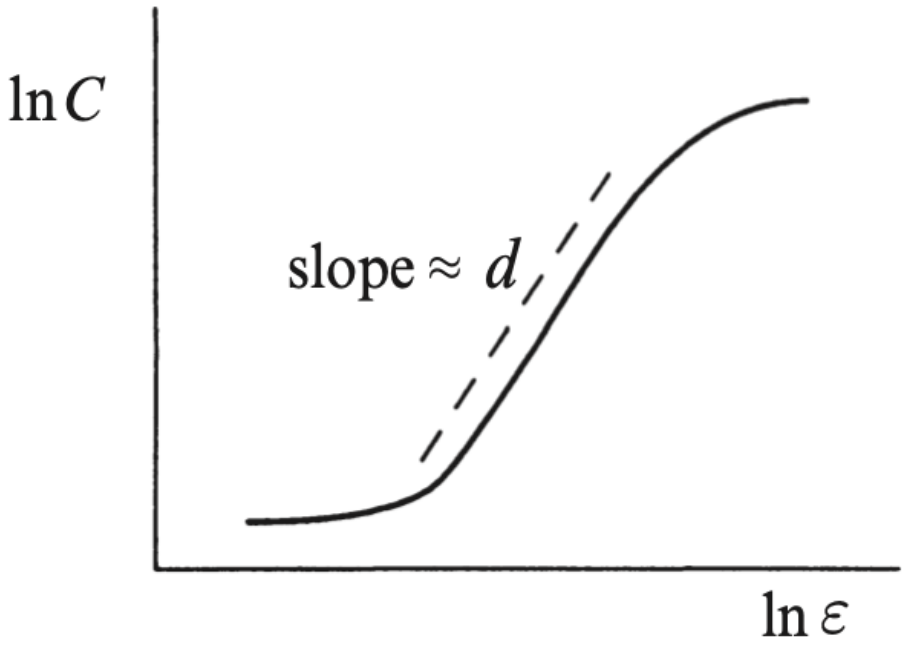

https://en.wikipedia.org/wiki/Correlation_dimension

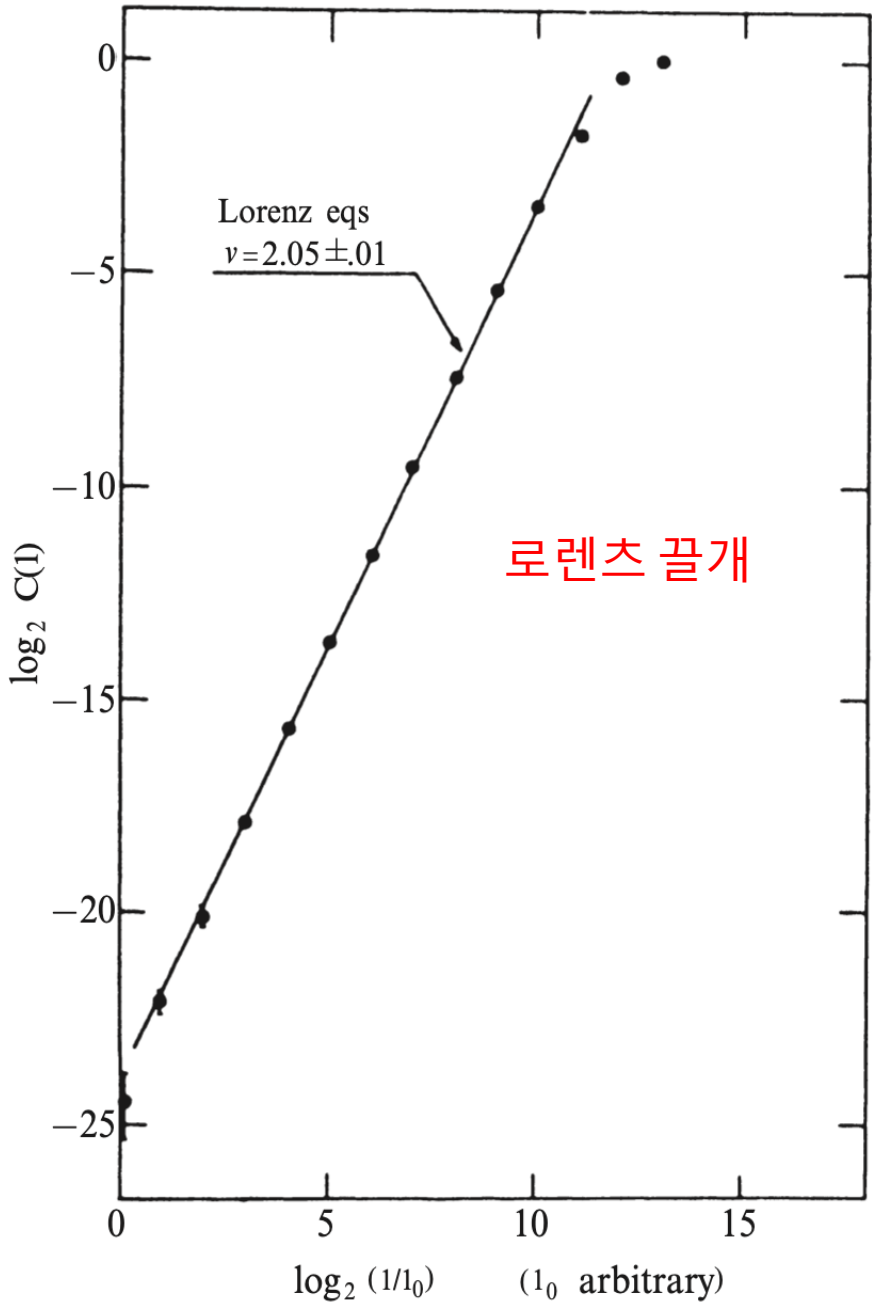

Figure 11.5.3 Grassberger and Procaccia (1983), p.196

Lewis Fry Richardson

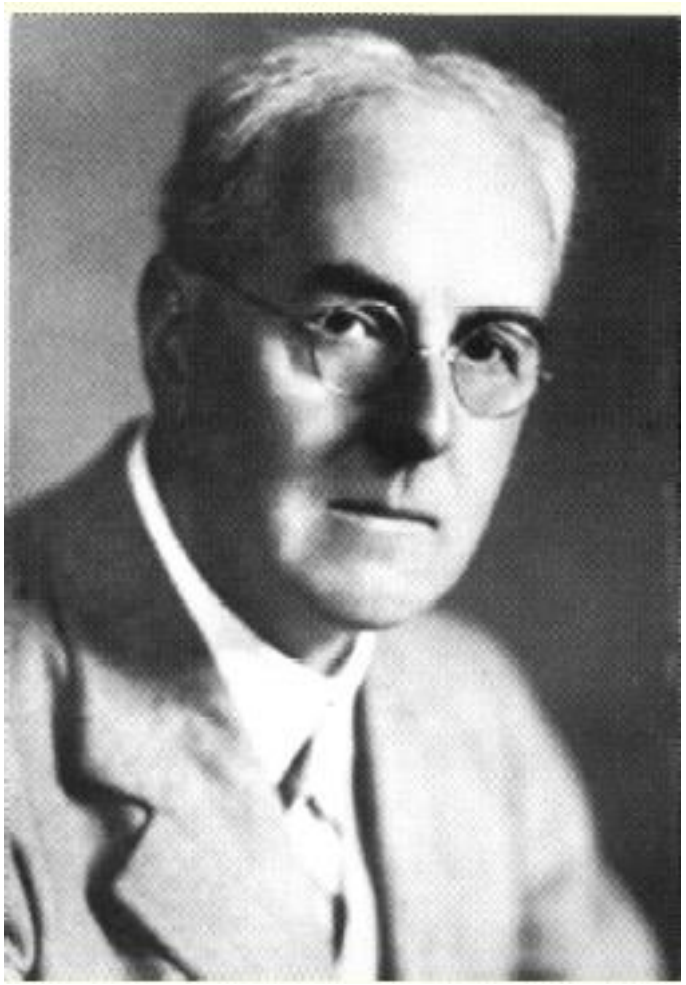

(1961) "The Problem of Contiguity: An Appendix to Statistics of Deadly Quarrels" is a significant 1961 article by Lewis Fry Richardson, published in the *General Systems Yearbook*

스페인과 포르투갈 사이의 접한 국경의 길이?
987 km? 1,214 km?

네덜란드와 벨기에 국경의 길이는?
380 km? 449 km?

Coastline paradox 해안선 역설

How Long Is the Coast of Britain?

Benoit Mandelbrot (1967)

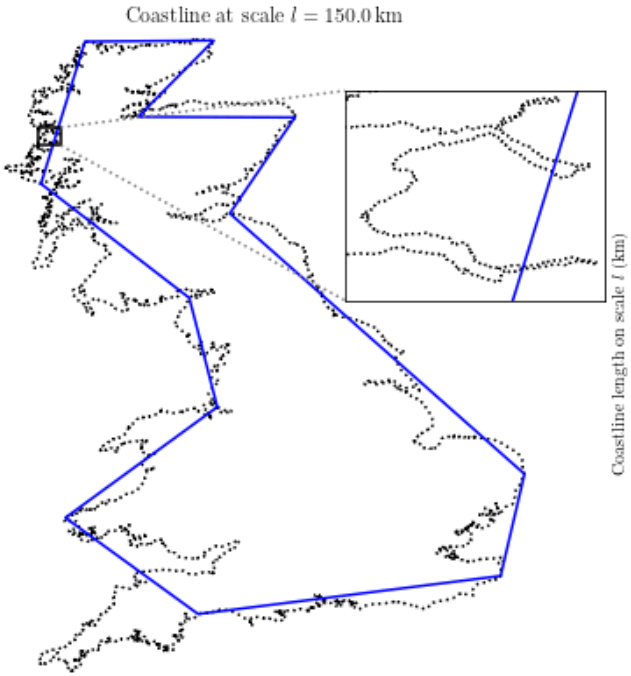

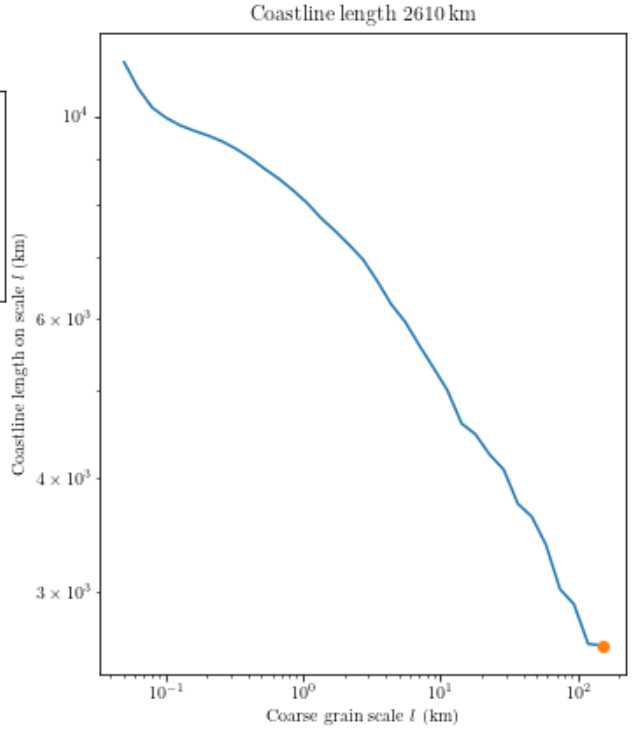

The smaller the ruler, the longer the resulting coastline. It might be supposed that these values would converge to a number representing the coastline's true length, but Richardson demonstrated that this is not so: the measured length of coastlines, and other natural features, increases without limit as the unit of measurement is made smaller.[17] This is known as the *Richardson effect*.[18]

Benoit Mandelbrot (1967)

Science
Volume 156,
Issue 3775
May 1967

How Long Is the Coast of Britain?

Statistical Self-Similarity and Fractional Dimension

Abstract. *Geographical curves are so involved in their detail that their lengths are often infinite or, rather, undefinable. However, many are statistically "self-similar," meaning that each portion can be considered a reduced-scale image of the whole. In that case, the degree of complication can be described by a quantity* D *that has many properties of a "dimension," though it is fractional; that is, it exceeds the value unity associated with the ordinary, rectifiable, curves.*

Seacoast shapes are examples of highly involved curves such that each of their portion can—in a statistical sense—be considered a reduced-scale image of the whole. This property will be referred to as "statistical self-similarity." To speak of a length for such figures is usually meaningless. Similarly (*1*), "the left bank of the Vistula, when measured with increased precision, would furnish lengths ten, hundred or even thousand times as great as the length read off the school map." More generally, geographical curves can be considered as superpositions of features of widely scattered characteristic size; as ever finer features are taken account of, the measured total length increases, and there is usually no clearcut gap between the realm of geography and details with which geography need not be concerned.

Quantities other than length are thus needed to discriminate between various degrees of complication for a geographical curve. When a curve is self-similar, it is characterized by an exponent of similarity, D, which possesses great usefulness.

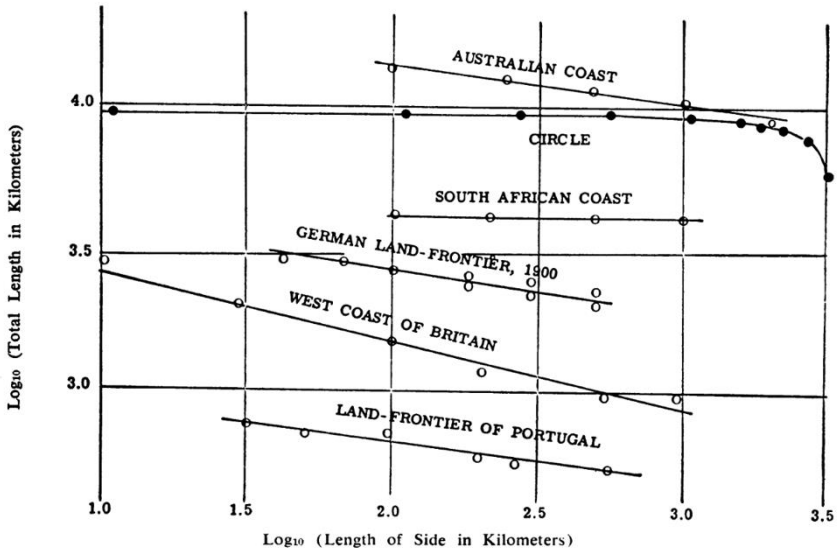

Fig. 1. Richardson's data concerning measurements of geographical curves by way of polygons which have equal sides and have their corners on the curve. For the circle, the total length tends to a limit as the side goes to zero. In all other cases, it increases as the side becomes shorter, the slope of the doubly logarithmic graph being in absolute value equal to D–1. (Reproduced from *2*, Fig. 17, by permission.)

Self-similarity methods are a potent tool in the study of chance phenomena, including geostatistics, as well as economics (*3*) and physics (*4*). In fact, many noises have dimensions D contained between 0 and 1, so that the scientist ought to consider dimension as a continuous quantity ranging from 0 to infinity.

Returning to the claim made in the first paragraph, let us review the methods used when attempting to measure the length of a seacoast. Since a geographer is unconcerned with minute details, he may choose a positive scale G as a lower limit to the length of geographically meaningful features. Then, to evaluate the length of a coast between two of its points A and B, he may draw the shortest inland curve joining A and B while staying within a distance G of the sea. Alternatively, he may draw the shortest line made of straight segments of length at most G, whose vertices are points of the coast which include A and B. There are many other possible definitions. In practice, of course, one must be content with approximations to shortest paths. We shall suppose that measurements are made by walking a pair of dividers along a map so as to count the number of equal sides of length G of an open polygon whose corners lie on the curve. If G is small enough, it does not matter whether one starts from A or B. Thus, one obtains an estimate of the length to be called $L(G)$.

Unfortunately, geographers will disagree about the value of G, while $L(G)$ depends greatly upon G. Consequently, it is necessary to know $L(G)$ for several values of G. Better still, it would be nice to have an analytic formula linking $L(G)$ with G. Such a formula, of an entirely empirical character, was proposed by Lewis F. Richardson (*2*) but unfortunately it attracted no attention. The formula is $L(G) = M\,G^{1-D}$, where M is a positive constant and D is a constant at least equal to unity. This

프랙탈 (fractals)

- 임의의 작은 규모에서 미세한 구조를 지닌 복잡한 기하학
- 자기 유사성 (self-similarity, self-affinity)
- 아름다움, 복잡성, 무한한 구조의 절묘한 조합
- 산, 구름, 해안선, 혈관망, 나무, 브로콜리 등의 자연 구조
- 컴퓨터 그래픽, 이미지 압축, 균열 구조 역학, 유체역학 (비스코스 핑거링)

- **“이상한 끌개”의 기하학적 구조**
- 로렌츠 방정식 해의 위상 공간
- 표면 무한 복소체 (infinite complex of surfaces)

Von Koch curve

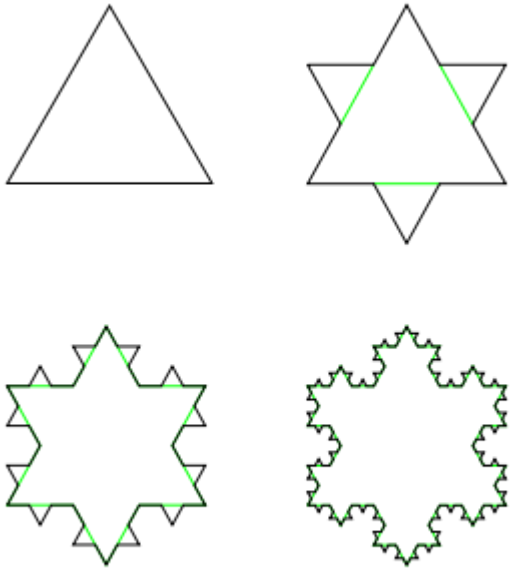

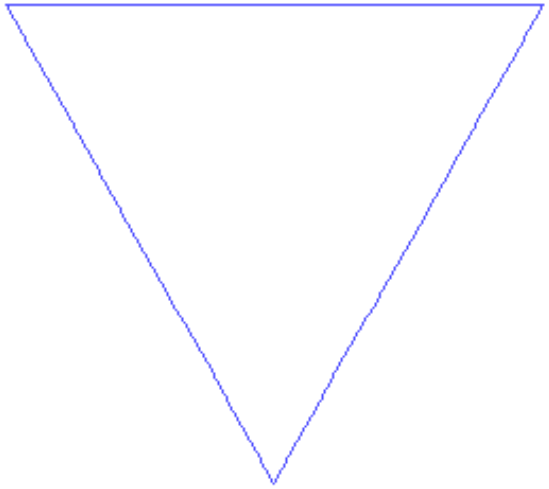

Zooming into the Koch curve

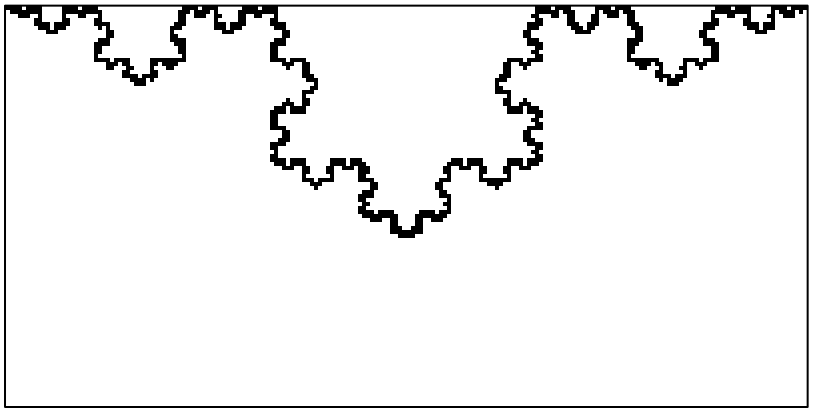

Zooming out...

the Koch Snowflake

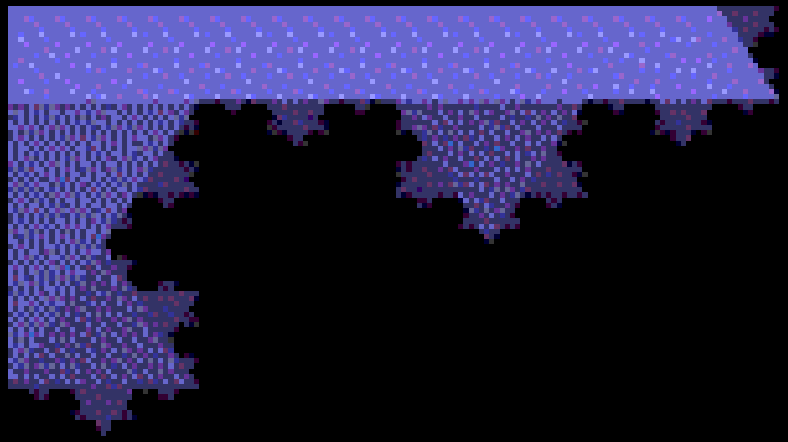

a box fractal

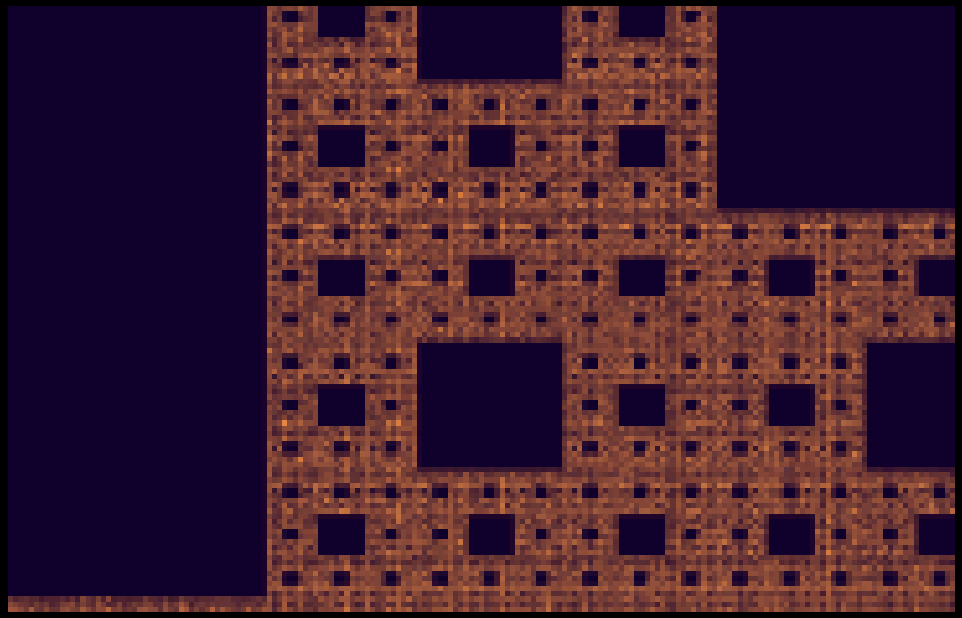

Allometric scaling law

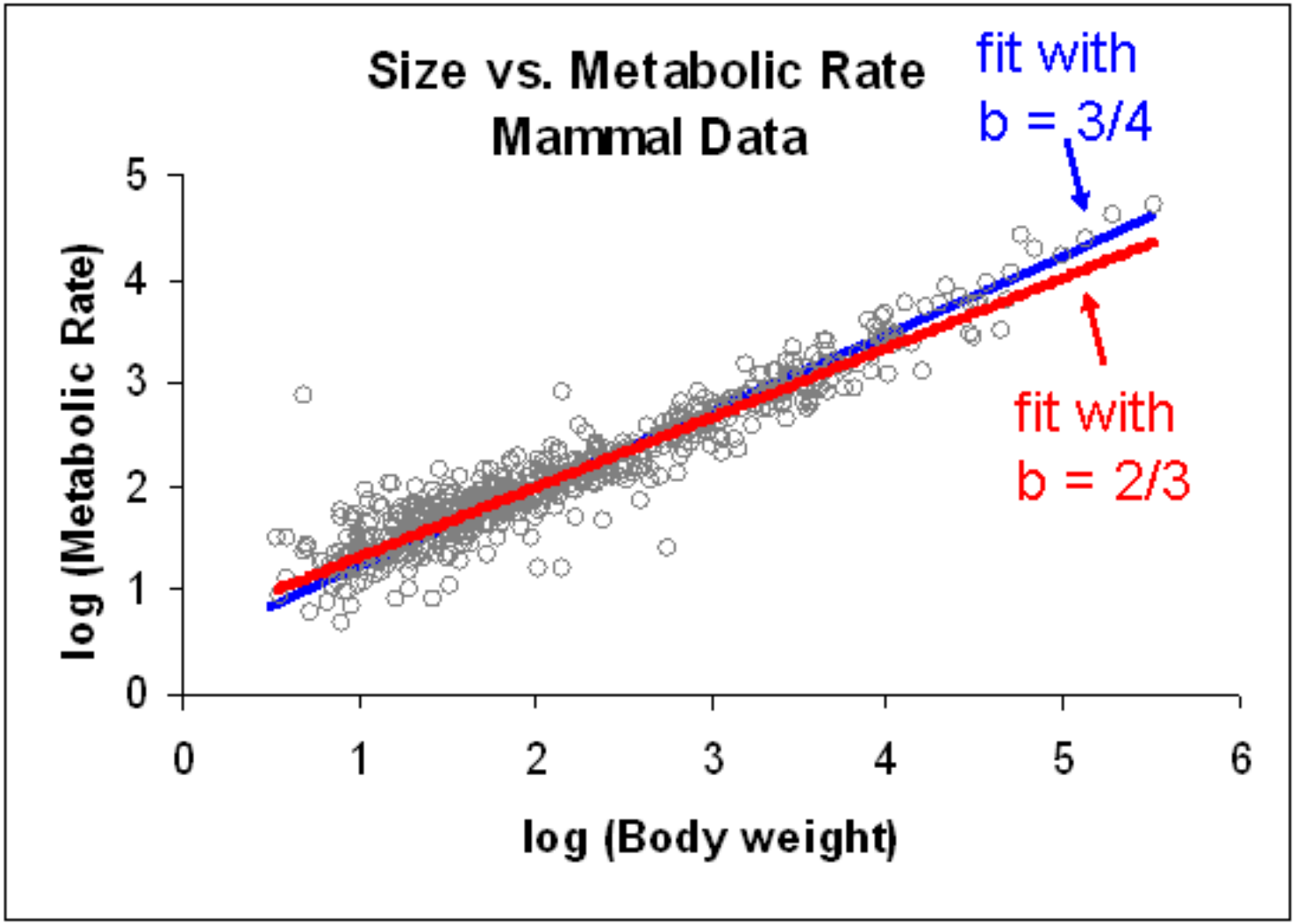

West, G. B.; Brown, J.H.; Enquist, B. J. (1997). *Science*. **276** (5309): 122-126.
doi:10.1126/science.276.5309.122

A General Model for the Origin of Allometric Scaling Laws in Biology

Geoffrey B. West, James H. Brown,* Brian J. Enquist

Allometric scaling relations, including the 3/4 power law for metabolic rates, are characteristic of all organisms and are here derived from a general model that describes how essential materials are transported through space-filling fractal networks of branching tubes. The model assumes that the energy dissipated is minimized and that the terminal tubes do not vary with body size. It provides a complete analysis of scaling relations for mammalian circulatory systems that are in agreement with data. More generally, the model predicts structural and functional properties of vertebrate cardiovascular and respiratory systems, plant vascular systems, insect tracheal tubes, and other distribution networks.

Biological diversity is largely a matter of body size, which varies over 21 orders of magnitude (*1*). Size affects rates of all biological structures and processes from cellular metabolism to population dynamics (*2*, *3*). The dependence of a biological variable Y on body mass M is typically characterized by an allometric scaling law of the form

$$Y = Y_0 M^b \qquad (1)$$

where b is the scaling exponent and Y_0 a

underlies these laws: Living things are sustained by the transport of materials through linear networks that branch to supply all parts of the organism. We develop a quantitative model that explains the origin and ubiquity of quarter-power scaling; it predicts the essential features of transport systems, such as mammalian blood vessels and bronchial trees, plant vascular systems, and insect tracheal tubes. It is based on three unifying princi-

그림 1 동물들의 대사율

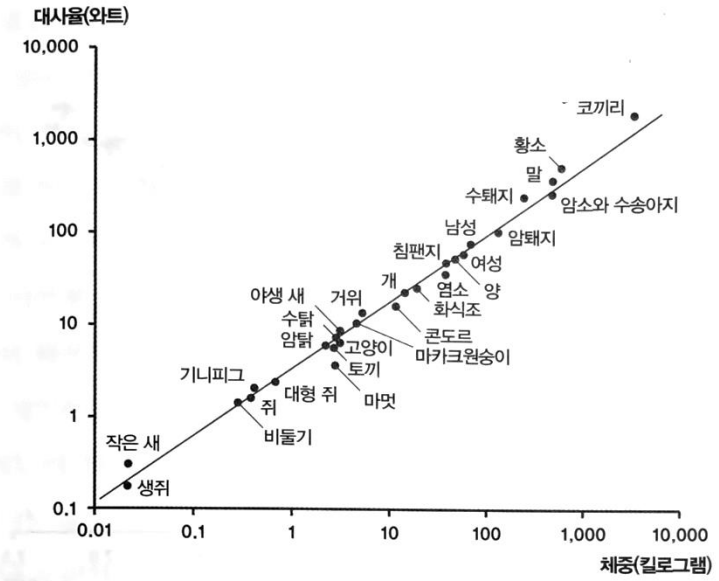

그림 2 동물들의 평생 심장 박동 수

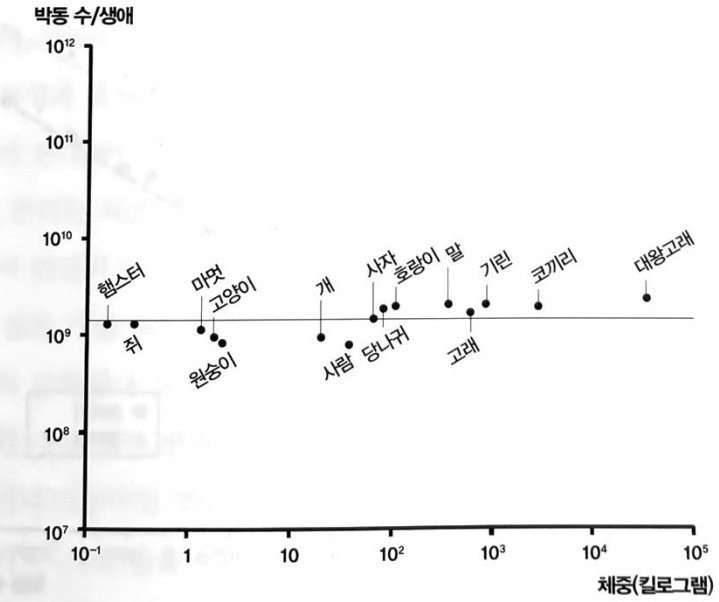

그림 9 곤충 군체의 생물량 생산률

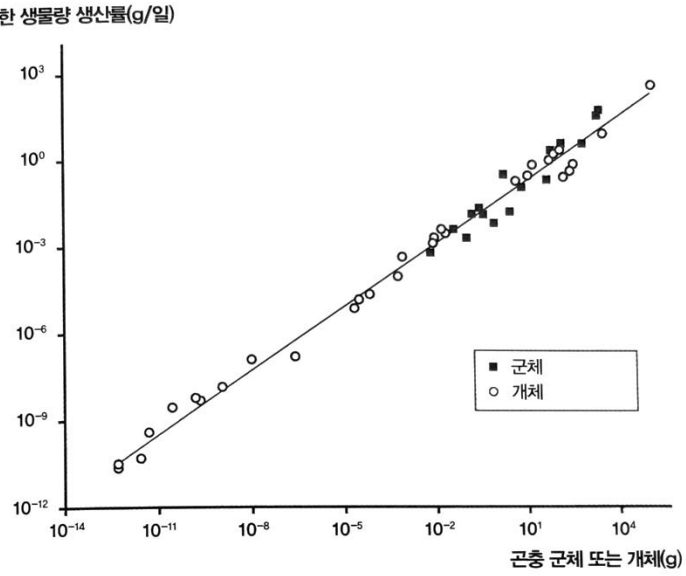

그림 10 동물들의 심장 박동 수

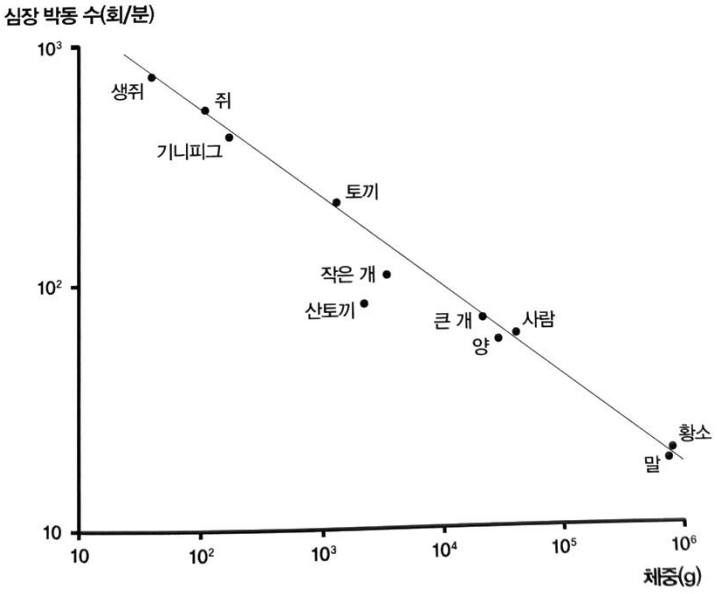

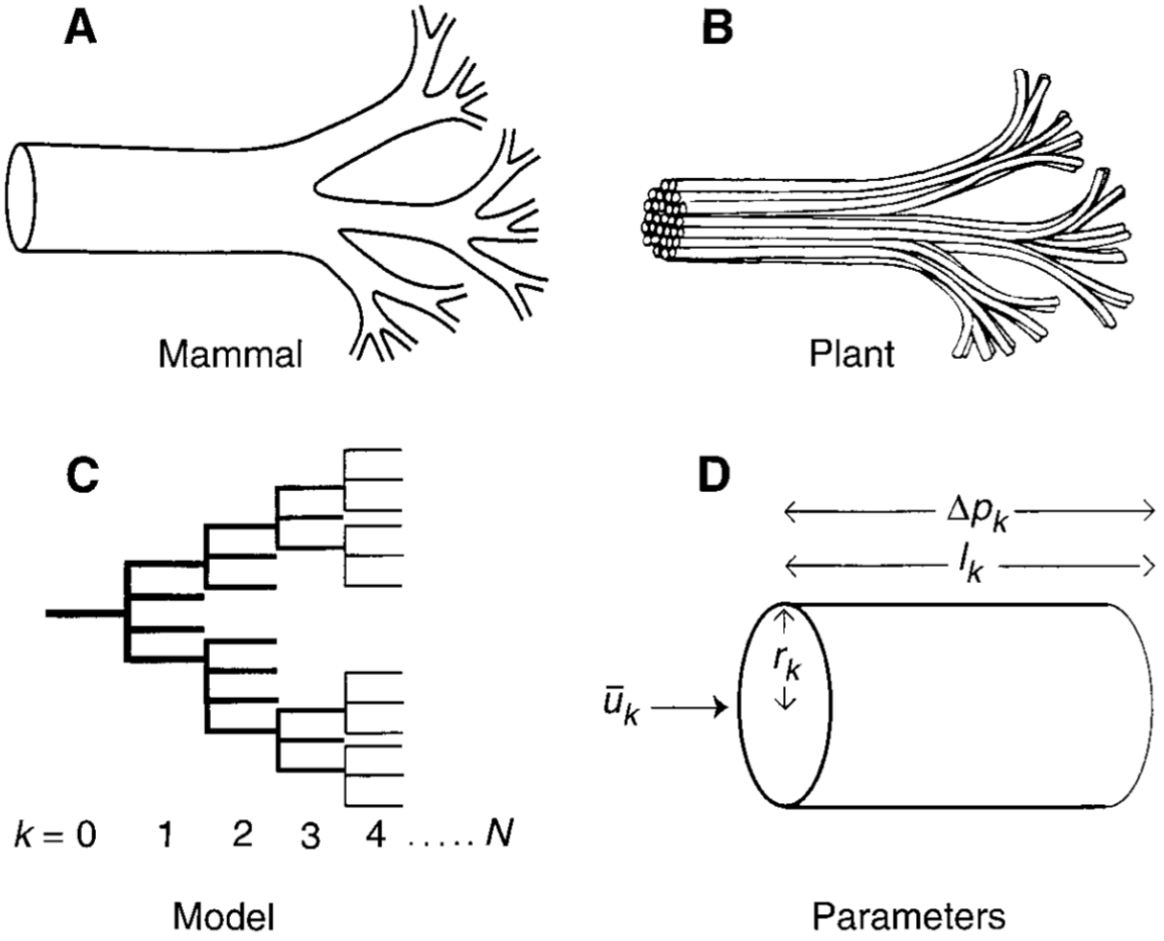

Fig. 1. Diagrammatic examples of segments of biological distribution networks: (**A**) mammalian circulatory and respiratory systems composed of branching tubes; (**B**) plant vessel-bundle vascular system composed of diverging vessel elements; (**C**) topological representation of such networks, where *k* specifies the order of the level, beginning with the aorta ($k = 0$) and ending with the capillary ($k = N$); and (**D**) parameters of a typical tube at the *k*th level.

Metabolic rate

$$B \propto \dot{Q} \propto M^a$$

Total number of branches

$$N_k = n_0 n_1 \cdots n_k$$

Volume rate of flow

$$\dot{Q}_k = \pi r_k^2 \overline{u_k}$$

Total number of capillaries

$$N_c \propto M^a$$

$$\dot{Q}_0 = N_k \dot{Q}_k = N_k \pi r_k^2 \overline{u}_k = N_c \pi r_c^2 \overline{u}_c$$ (flow conservation)

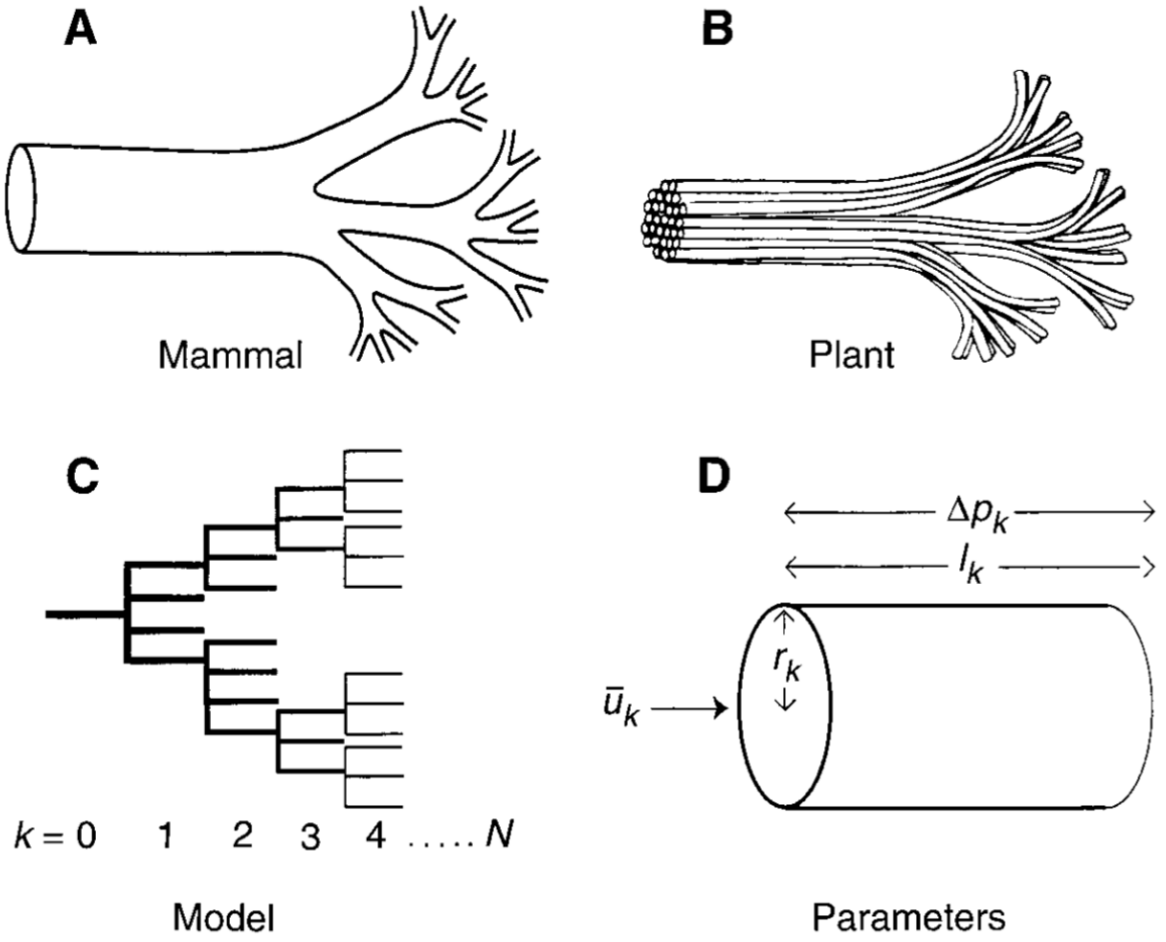

Fig. 1. Diagrammatic examples of segments of biological distribution networks: (**A**) mammalian circulatory and respiratory systems composed of branching tubes; (**B**) plant vessel-bundle vascular system composed of diverging vessel elements; (**C**) topological representation of such networks, where *k* specifies the order of the level, beginning with the aorta ($k = 0$) and ending with the capillary ($k = N$); and (**D**) parameters of a typical tube at the *k*th level.

$$N = \frac{a \ln(M/M_o)}{\ln n}$$

$$\beta_k \equiv \frac{r_{k+1}}{r_k} \qquad \gamma_k \equiv \frac{l_{k+1}}{l_k} \qquad N_c = n^N \propto M^a$$

$$n_k = n,\ \beta_k = \beta,\ \gamma_k = \gamma \qquad N_k = n_0 n_1 \cdots n_k = n^k$$

Total volume of fluid ("blood volume")

$$V_b = \sum_{k=0}^{N} N_k V_k = \sum_{k=0}^{N} \pi r_k^2 l_k n^k = \frac{(n\gamma\beta^2)^{-(N+1)} - 1}{(n\gamma\beta^2)^{-1} - 1} n^N V_c$$

$$V_b \sim \frac{V_0}{1 - n\gamma\beta^2} = \frac{V_c\,(\gamma\beta^2)^{-N}}{1 - n\gamma\beta^2} \propto M$$

$$N = \frac{a \ln(M/M_o)}{\ln n}$$

$M\,(\gamma\beta^2)^N \sim 1$ Capillaries are invariant units.

$$a = -\frac{\ln n}{\ln(\gamma\beta^2)}$$

$$\gamma = n^{-\frac{1}{3}}, \beta = n^{-\frac{1}{2}}, a = \frac{3}{4}$$

* Space-filling fractal

$$\frac{4}{3}\pi\left(\frac{l_k}{2}\right)^3 N_k \approx \frac{4}{3}\pi\left(\frac{l_{k+1}}{2}\right)^3 N_{k+1}$$

$$\gamma_k \equiv \frac{l_{k+1}}{l_k} \approx \left(\frac{N_{k+1}}{N_k}\right)^{-\frac{1}{3}} = n^{-\frac{1}{3}}$$

* Area-preserving branching

$$\pi r_k^2 = \mathrm{n}\pi r_{k+1}^2$$

$$\beta_k \equiv \frac{r_{k+1}}{r_k} = n^{-\frac{1}{2}}$$

$$\frac{4}{3}\pi\left(\frac{l_k}{2}\right)^3 N_k \approx \frac{4}{3}\pi\left(\frac{l_{k+1}}{2}\right)^3 N_{k+1} \qquad \gamma_k \equiv \frac{l_{k+1}}{l_k} \approx \left(\frac{N_{k+1}}{N_k}\right)^{-\frac{1}{3}} = n^{-\frac{1}{3}}$$

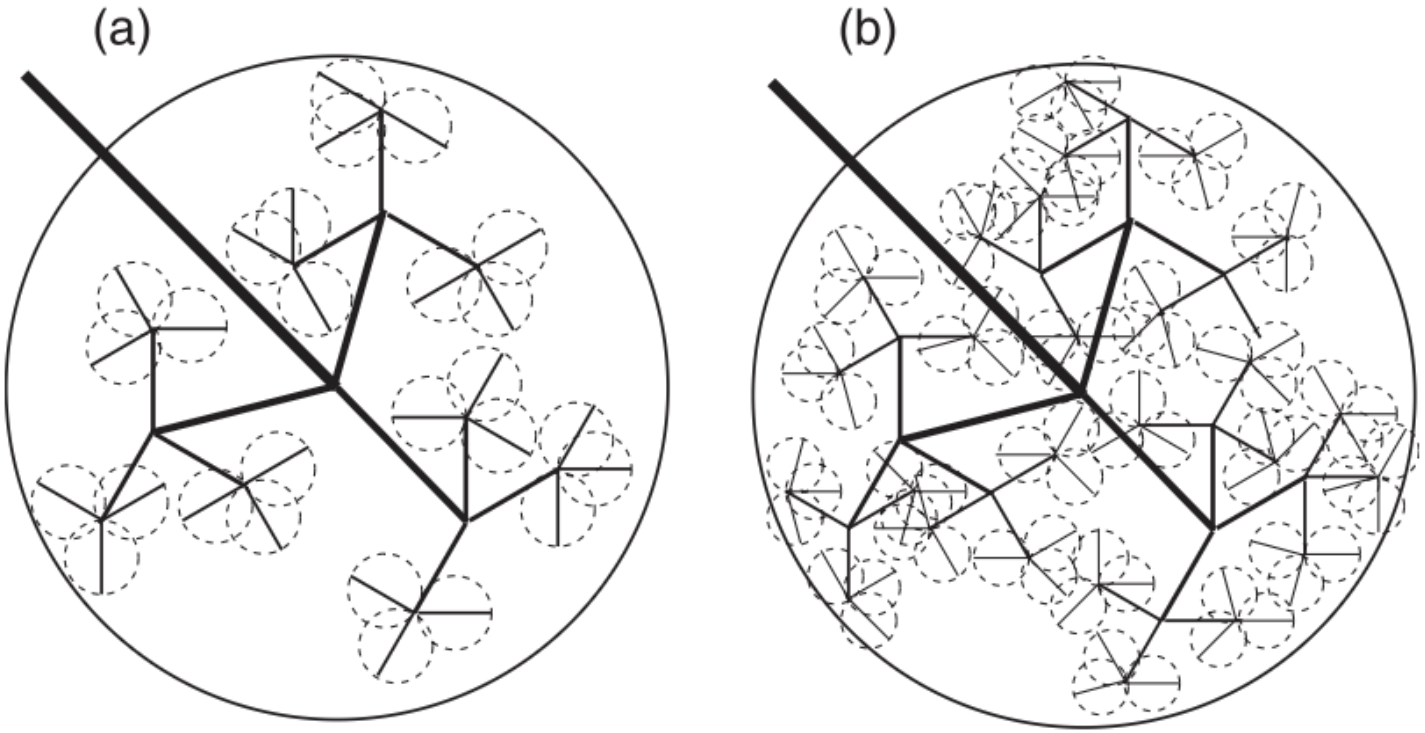

Fig. 3. Illustration of the quantity $N_k l_k^3$ at level k (a) and level $k + 1$ (b). Here $k = 4$. The quantity $N_k l_k^3$ is the sum of volumes of all circles (spheres in three dimensions) at level k.

Allometric scaling

$$\gamma = n^{-\frac{1}{3}}, \beta = n^{-\frac{1}{2}}, a = \frac{3}{4}$$

$$B \propto M^{3/4} \qquad N_c \propto M^{3/4}$$

$$r_0 = \beta^{-N} r_c = N_c^{1/2} r_c \propto M^{3/8}$$

$$l_0 = \gamma^{-N} l_c = N_c^{1/3} l_c \propto M^{1/4}$$

표 1 심혈관계

양	예측값	측정값
대동맥 반지름	3/8=0.375	0.36
대동맥 혈압	0=0.00	0.032
대동맥 혈류 속도	0.00	0.07
혈액량	1=1.00	1.00
순환 시간	1/4=0.25	0.25
순환 거리	1/4=0.25	자료 없음
심장 1회 박출량	1=1.00	1.03
심장 박동 수	−1/4=−0.25	−0.25
심장 박출량	3/4=0.75	0.74
모세혈관 수	3/4=0.75	자료 없음
수도관 용적 반지름	자료 없음	자료 없음
워머슬리 수	1/4=0.25	0.25
모세혈관 밀도	−1/12=−0.083	−0.095
혈액의 O_2 친화도	−1/12=−0.083	−0.089
총 저항	−3/4=−0.75	−0.76
대사율	3/4=0.75	0.75

표 2 호흡계

양	예측값	측정값
기관 반지름	3/8=0.375	0.39
흉막 압력	0=0.00	0.004
기관의 공기 속도	0=0.00	0.02
허파 부피	1=1.00	1.05
공기 흡입량	3/4=0.75	0.80
허파꽈리 부피	1/4=0.25	자료 없음
공기 순환량	1=1.00	1.041
호흡 빈도	−1/4=−0.25	−0.26
분산력	3/4=0.75	0.78
허파꽈리 수	3/4=0.75	자료 없음
허파꽈리 반지름	1/12=0.083	0.13
허파꽈리 면적	1/6=0.167	자료 없음
허파 면적	11/12=0.92	0.95
O_2 확산력	1=1.00	0.99
총 저항	−3/4=−0.75	−0.70
O_2 소비율	3/4=0.75	0.76

표 3 식물 관다발계의 생리적·해부학적 변수들에 대한 스케일링 지수의 예측값

양	식물 무게의 함수	줄기 반지름의 함수	
	지수	지수	
	예측값	예측값	측정값
잎 수	3/4(0.75)	2(2.00)	2.007
가지 수	3/4(0.75)	−2(−2.00)	−2.00
관 수	3/4(0.75)	2(2.00)	자료 없음
줄기 길이	1/4(0.25)	2/3(0.67)	0.652
줄기 반지름	3/8(0.375)		
통도조직 면적	7/8(0.875)	7/3(2.33)	2.13
관 반지름	1/16(0.0625)	1/6(0.167)	자료 없음
전도도	1(1.00)	8/3(2.67)	2.63
잎 전도도	1/4(0.25)	2/3(0.67)	0.727
유량		2(2.00)	자료 없음
대사율	3/4(0.75)		
압력 기울기	−1/4(−0.25)	−2/3(−0.67)	자료 없음
유체 속도	−1/8(−0.125)	−1/3(−0.33)	자료 없음
가지 저항	−3/4(−0.75)	−1/3(−0.33)	자료 없음

Growth, innovation, scaling, and the pace of life in cities

$$Y(t) = Y_0 N(t)^{\beta}.$$

Luís M. A. Bettencourt*†, José Lobo‡, Dirk Helbing§, Christian Kühnert§, and Geoffrey B. West*¶

*Theoretical Division, MS B284, Los Alamos National Laboratory, Los Alamos, NM 87545; ‡Global Institute of Sustainability, Arizona State University, P.O. Box 873211, Tempe, AZ 85287-3211; §Institute for Transport and Economics, Dresden University of Technology, Andreas-Schubert-Strasse 23, D-01062 Dresden, Germany; and ¶Santa Fe Institute, 1399 Hyde Park Road, Santa Fe, NM 87501

Edited by Elinor Ostrom, Indiana University, Bloomington, IN, and approved March 6, 2007 (received for review November 19, 2006)

Humanity has just crossed a major landmark in its history with the majority of people now living in cities. Cities have long been known to be society's predominant engine of innovation and wealth creation, yet they are also its main source of crime, pollution, and disease. The inexorable trend toward urbanization worldwide presents an urgent challenge for developing a predictive, quantitative theory of urban organization and sustainable development. Here we present empirical evidence indicating that the processes relating urbanization to economic development and knowledge creation are very general, being shared by all cities belonging to the same urban system and sustained across different nations and times. Many diverse properties of cities from patent production and personal income to electrical cable length are shown to be power law functions of population size with scaling exponents, β, that fall into distinct universality classes. Quantities reflecting wealth creation and innovation have $\beta \approx 1.2 > 1$ (increasing returns), whereas those accounting for infrastructure display $\beta \approx 0.8 < 1$ (economies of scale). We predict that the pace of social life in the city increases with population size, in quantitative agreement with data, and we discuss how cities are similar to, and differ from, biological organisms, for which $\beta < 1$. Finally, we explore possible consequences of these scaling relations by deriving growth equations, which quantify the dramatic difference between growth fueled by innovation versus that driven by economies of scale. This difference suggests that, as population grows, major innovation cycles must be generated at a continually accelerating rate to sustain growth and avoid stagnation or collapse.

population | sustainability | urban studies | increasing returns | economics of scale

The increasing concentration of people in cities presents both opportunities and challenges (9) toward future scenarios of sustainable development. On the one hand, cities make possible economies of scale in infrastructure (9) and facilitate the optimized delivery of social services, such as education, health care, and efficient governance. Other impacts, however, arise because of human adaptation to urban living (9, 10–14). They can be direct, resulting from obvious changes in land use (3) [e.g., urban heat island effects (15, 16) and increased green house gas emissions (17)] or indirect, following from changes in consumption (18) and human behavior (10–14), already emphasized in classical work by Simmel and Wirth in urban sociology (11, 12) and by Milgram in psychology (13). An important result of urbanization is also an increased division of labor (10) and the growth of occupations geared toward innovation and wealth creation (19–22). The features common to this set of impacts are that they are open-ended and involve permanent adaptation, whereas their environmental implications are ambivalent, aggravating stresses on natural environments in some cases and creating the conditions for sustainable solutions in others (9).

These unfolding complex demographic and social trends make it clear that the quantitative understanding of human social organization and dynamics in cities (7, 9) is a major piece of the puzzle toward navigating successfully a transition to sustainability. However, despite much historical evidence (19, 20) that cities are the principal engines of innovation and economic growth, a quantitative, predictive theory for understanding their dynamics and organization (23, 24) and estimating their future trajectory and stability remains elusive. Significant obstacles toward this goal are the immense diversity of human activity and organization and an enormous range of geographic factors. Nevertheless,

$$Y(t) = Y_0 N(t)^{\beta}.$$

Table 1. Scaling exponents for urban indicators vs. city size

Y	β	95% CI	Adj-R^2	Observations	Country–year
New patents	1.27	[1.25,1.29]	0.72	331	U.S. 2001
Inventors	1.25	[1.22,1.27]	0.76	331	U.S. 2001
Private R&D employment	1.34	[1.29,1.39]	0.92	266	U.S. 2002
"Supercreative" employment	1.15	[1.11,1.18]	0.89	287	U.S. 2003
R&D establishments	1.19	[1.14,1.22]	0.77	287	U.S. 1997
R&D employment	1.26	[1.18,1.43]	0.93	295	China 2002
Total wages	1.12	[1.09,1.13]	0.96	361	U.S. 2002
Total bank deposits	1.08	[1.03,1.11]	0.91	267	U.S. 1996
GDP	1.15	[1.06,1.23]	0.96	295	China 2002
GDP	1.26	[1.09,1.46]	0.64	196	EU 1999–2003
GDP	1.13	[1.03,1.23]	0.94	37	Germany 2003
Total electrical consumption	1.07	[1.03,1.11]	0.88	392	Germany 2002
New AIDS cases	1.23	[1.18,1.29]	0.76	93	U.S. 2002–2003
Serious crimes	1.16	[1.11, 1.18]	0.89	287	U.S. 2003
Total housing	1.00	[0.99,1.01]	0.99	316	U.S. 1990
Total employment	1.01	[0.99,1.02]	0.98	331	U.S. 2001
Household electrical consumption	1.00	[0.94,1.06]	0.88	377	Germany 2002
Household electrical consumption	1.05	[0.89,1.22]	0.91	295	China 2002
Household water consumption	1.01	[0.89,1.11]	0.96	295	China 2002
Gasoline stations	0.77	[0.74,0.81]	0.93	318	U.S. 2001
Gasoline sales	0.79	[0.73,0.80]	0.94	318	U.S. 2001
Length of electrical cables	0.87	[0.82,0.92]	0.75	380	Germany 2002
Road surface	0.83	[0.74,0.92]	0.87	29	Germany 2002

Data sources are shown in *SI Text*. CI, confidence interval; Adj-R^2, adjusted R^2; GDP, gross domestic product.

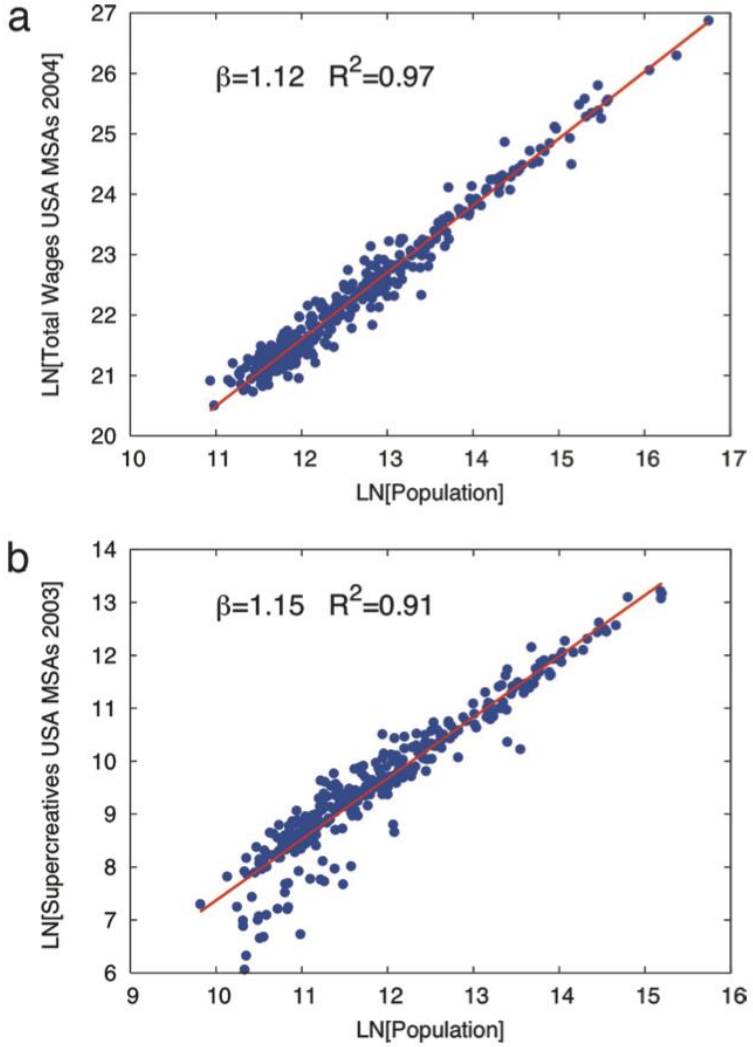

Fig. 1. Examples of scaling relationships. (*a*) Total wages per MSA in 2004 for the U.S. (blue points) vs. metropolitan population. (*b*) Supercreative employment per MSA in 2003, for the U.S. (blue points) vs. metropolitan population. Best-fit scaling relations are shown as solid lines.

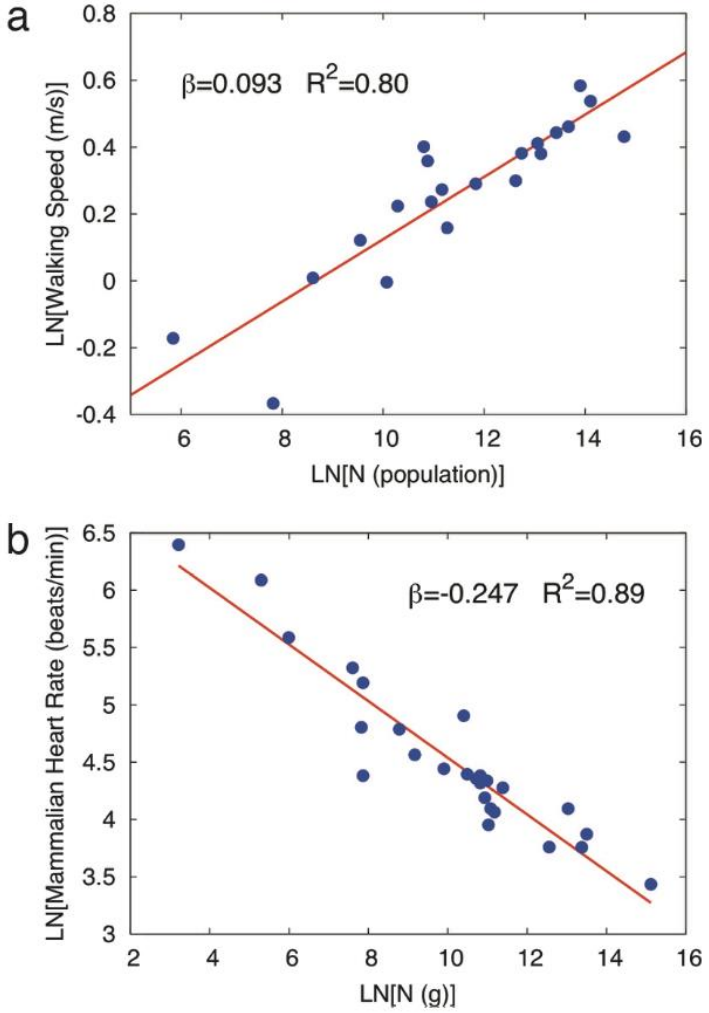

Fig. 2. The pace of urban life increases with city size in contrast to the pace of biological life, which decreases with organism size. (*a*) Scaling of walking speed vs. population for cities around the world. (*b*) Heart rate vs. the size (mass) of organisms.

The Origins of Scaling in Cities

Luís M. A. Bettencourt

Despite the increasing importance of cities in human societies, our ability to understand them scientifically and manage them in practice has remained limited. The greatest difficulties to any scientific approach to cities have resulted from their many interdependent facets, as social, economic, infrastructural, and spatial complex systems that exist in similar but changing forms over a huge range of scales. Here, I show how all cities may evolve according to a small set of basic principles that operate locally. A theoretical framework was developed to predict the average social, spatial, and infrastructural properties of cities as a set of scaling relations that apply to all urban systems. Confirmation of these predictions was observed for thousands of cities worldwide, from many urban systems at different levels of development. Measures of urban efficiency, capturing the balance between socioeconomic outputs and infrastructural costs, were shown to be independent of city size and might be a useful means to evaluate urban planning strategies.

Cities exist, in recognizable but changing forms, over an enormous range of scales (*1*), from small towns with just a few people to the gigantic metropolis of Tokyo, with more than 35 million inhabitants. Many parallels have been suggested between cities and other complex systems, from river networks (*2*) and biological organisms (*3*–*6*) to insect colonies (*1*, *7*) and ecosystems (*8*). The central flaw of all these arguments is their emphasis on analogies of form rather than function, which limit their ability to help us understand and plan cities.

Recently, our increasing ability to collect and share data on many aspects of urban life has begun to supply us with better clues to the properties of cities, in terms of general statistical patterns of land use, urban infrastructure, and rates of socioeconomic activity (*6*, *9*–*13*). These empirical observations have been summarized across several disciplines, from geography to economics, in terms of how different urban quantities (such as the area of roads or wages paid) depend on city size, usually measured by its population, N.

Santa Fe Institute, 1399 Hyde Park Road, Santa Fe, NM 87501, USA.

E-mail: bettencourt@santafe.edu

The evidence from many empirical studies over the past 40 years points to there being no special size to cities, so that most urban properties, Y, vary continuously with population size and are well described mathematically on average by power-law scaling relations of the form $Y = Y_0 N^{\beta}$, where Y_0 and β are constants in N. The surprise, perhaps, is that cities of different sizes do have very different properties. Specifically, one generally observes that rates of social quantities (such as wages or new inventions) increase per capita with city size (*11*, *12*) (superlinear scaling, $\beta = 1 + \delta > 1$, with $\delta \simeq 0.15$), whereas the volume occupied by urban infrastructure per capita (roads, cables, etc.) decreases (sublinear scaling, $\beta = 1 - \delta < 1$) (Fig. 1). Thus, these data summarize familiar expectations that larger cities are not only more expensive and congested, but also more exciting and creative when compared to small towns.

These empirical results also suggest that, despite their apparent complexity, cities may actually be quite simple: Their average global properties may be set by just a few key parameters (*12*, *13*). However, the origin of these observed scaling relations and an explanation for the interdependences between spatial, infrastructural, and social facets of the city have remained a mystery.

Here, I develop a unified and quantitative framework to understand, at a theoretical level, how cities operate and how these interdependencies arise. Consider first the simplest model of a city with circumscribing land area A and

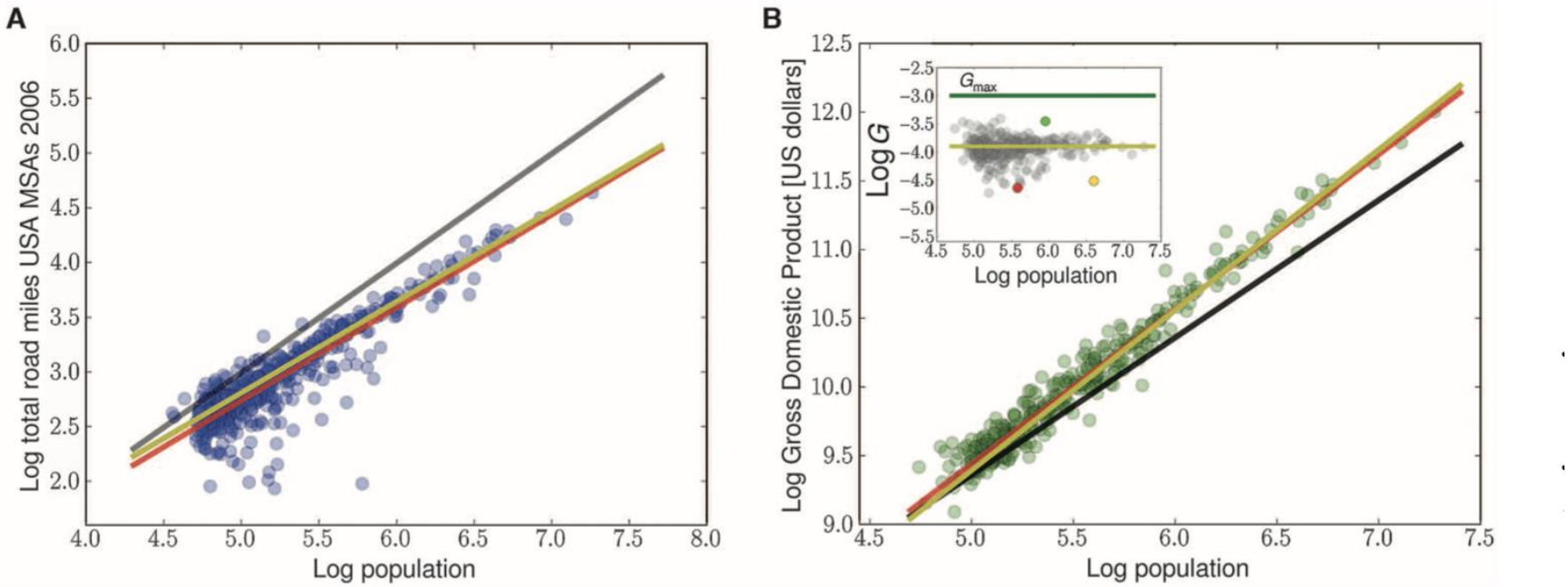

Fig. 1. Scaling of urban infrastructure and socioeconomic output. (A) Total lane miles (volume) of roads in U.S. metropolitan areas (MSAs) in 2006 (blue dots). Data for 415 urban areas were obtained from the Office of Highway Policy Information from the Federal Highway Administration (*14*). Lines show the best fit to a scaling relation $Y(N) = Y_0 N^{\beta}$(red), with $\beta = 0.849 \pm 0.038$ [95% confidence interval (CI), $R^2 = 0.65$]; the theoretical prediction, $\beta = 5/6$ (yellow); and linear scaling $\beta = 1$ (black). **(B)** Gross metropolitan product of MSAs in 2006 (green dots). Data obtained for 363 MSAs from U.S. Bureau of Economic Analysis (*14*). Lines describe best fit (red) to data, $\beta = 1.126 \pm 0.023$ (95% CI, $R^2 = 0.96$); the theoretical prediction, $\beta = 7/6$ (yellow); and proportional scaling, $\beta = 1$ (black). The two best-fit parameters in each scaling relation were estimated by means of ordinary least-squares minimization to the linear relation between logarithmically transformed variables (*14*). The inset shows the estimate of G for 313 U.S. MSAs and the conservation law $\frac{d \ln G}{d \ln N} = 0$ ($R^2 = 0.003$). G is measured as the product of gross domestic product and road volume, both per capita. As predicted by the theory, observed values of G for different cities cluster around its most likely value (mode, yellow line), which gives an estimate of the optimum G^*, and are bounded by the maximum $G_{max} \simeq 8G^*$(green line); see also Fig. 2B. Several metropolitan areas, such as Bridgeport, Connecticut (green circle); Riverside, California (yellow circle); or Brownsville, Texas (red circle), are outliers, suggesting that they are suboptimal in terms of their transportation efficiency or amount of social mixing.

Table 1. Urban indicators and their scaling relations. Columns show measured exponent ranges (see table S3 for details). Also shown are predicted values for $D = 2$, $H = 1$ (the simplest theoretical expectation) and for general D, H. Agglomeration effects vanish as $H \to 0$ (*14*). The larger range for the observed land-area exponent is likely the result of different definitions of the city in space and distinct measurement types. See table S3 and supplementary text for specific values of observed exponents, discussion, and additional data sources.

Urban scaling relations	Observed exponent range	Model ($D = 2$, $H = 1$)	Model D, H
Land area $A = aN^{\alpha}$	[0.56,1.04]	$\alpha = \frac{2}{3}$	$\alpha = \frac{D}{D+H}$
Network volume $A_n = A_0 N^{\nu}$	[0.74,0.92]	$\nu = \frac{5}{6}$	$\nu = 1 - \delta$
Network length $L_n = L_0 N^{\lambda}$	[0.55,0.78]	$\lambda = \frac{2}{3}$	$\lambda = \alpha$
Interactions per capita $\bar{I}_i = I_0 N^{\delta}$	[0.00,0.25]	$\delta = \frac{1}{6}$	$\delta = \frac{H}{D(D+H)}$
Socioeconomic rates $Y = Y_0 N^{\beta}$	[1.01,1.33]	$\beta = \frac{7}{6}$	$\beta = 1 + \delta$
Network power dissipation $W = W_0 N^{\omega}$	[1.05,1.17]	$\omega = \frac{7}{6}$	$\omega = 1 + \delta$
Average land rents $P_L = P_0 N^{\delta_L}$	[0.46,0.52]	$\delta_L = \frac{1}{2}$	$\delta_L = 1 - \alpha + \delta$

Scaling laws between population and facility densities

Jaegon Um[a,1], Seung-Woo Son[b,1], Sung-Ik Lee[c], Hawoong Jeong[b,2], and Beom Jun Kim[d,2]

[a]Department of Physics, Pohang University of Science and Technology, Pohang 790-784, Korea; [b]Department of Physics, Institute for the BioCentury, Korea Advanced Institute of Science and Technology, Daejeon 305-701, Korea; [c]National Creative Research Initiative Center for Superconductivity, Department of Physics, Sogang University, Seoul, 121-742, Korea; and [d]BK21 Physics Research Division and Department of Energy Science, Sungkyunkwan University, Suwon 440-746, Korea

Edited by H. Eugene Stanley, Boston University, Boston, MA, and approved June 24, 2009 (received for review February 20, 2009)

When a new facility like a grocery store, a school, or a fire station is planned, its location should ideally be determined by the necessities of people who live nearby. Empirically, it has been found that there exists a positive correlation between facility and population densities. In the present work, we investigate the ideal relation between the population and the facility densities within the framework of an economic mechanism governing microdynamics. In previous studies based on the global optimization of facility positions in minimizing the overall travel distance between people and facilities, it was shown that the density of facility D and that of population ρ should follow a simple power law $D \sim \rho^{2/3}$. In our empirical analysis, on the other hand, the power-law exponent α in $D \sim \rho^{\alpha}$ is not a fixed value but spreads in a broad range depending on facility types. To explain this discrepancy in α, we propose a model based on economic mechanisms that mimic the competitive balance between the profit of the facilities and the social opportunity cost for populations. Through our simple, microscopically driven model, we show that commercial facilities driven by the profit of the facilities have $\alpha = 1$, whereas public facilities driven by the social opportunity cost have $\alpha = 2/3$. We simulate this model to find the optimal positions of facilities on a real U.S. map and show that the results are consistent with the empirical data.

optimal positioning | social opportunity cost | microdynamics model

between population and the number of facilities, looks natural, but the empirical data do not support this argument. For example, in the case of public service facilities, the exponents have been observed to be 2/3. Although the exponent $\alpha = 2/3$ is derived analytically by minimizing the total travel distance between people and facilities from the global optimization scheme (5, 10, 11), the theory has failed to explain $\alpha = 1$ in the same approach, and only a phenomenological reformulation of the theory has been tried (5).

Generally, commercial facilities like small stores have to attract large numbers of people to make a profit. If they cannot do this, such stores will need to close and move to a place with larger population. On the other hand, public facilities such as fire stations and public schools need to be built in positions where they are as close as possible to their clients, because the consumed travel time or spatial distance yields the social opportunity cost by depriving visitors of time for producing other products or services. For example, public schools that exist in big cities require students who live in nearby small towns or villages to commute for a long period of time. To reduce the social opportunity cost caused by such a long-distance commute, new schools should be built in places where the population is sparse but not negligible. Therefore, one can expect that the public facilities should be more evenly distributed spatially than commercial ones. This inference is consistent with the global optimization of facility positioning to minimize the total

Table 1. Summary of the exponents

US facility	α (SE)	R^2
Ambulatory hospital	1.13(1)	0.93
Beauty care	1.08(1)	0.86
Laundry	1.05(1)	0.90
Automotive repair	0.99(1)	0.92
Private school	0.95(1)	0.82
Restaurant	0.93(1)	0.89
Accommodation	0.89(1)	0.70
Bank	0.88(1)	0.89
Gas station	0.86(1)	0.94
Death care	0.79(1)	0.80
* Fire station	0.78(3)	0.93
* Police station	0.71(6)	0.75
Public school	0.69(1)	0.87
SK facility	**α (SE)**	**R^2**
Bank	1.18(2)	0.96
Parking place	1.13(2)	0.91
* Primary clinic	1.09(2)	1.00
* Hospital	0.96(5)	0.97
* University/college	0.93(9)	0.89
Market place	0.87(2)	0.90
* Secondary school	0.77(3)	0.98
* Primary school	0.77(3)	0.97
Social welfare org.	0.75(2)	0.84
* Police station	0.71(5)	0.94
Government office	0.70(1)	0.93
* Fire station	0.60(4)	0.93
* Public health center	0.09(5)	0.19

Summary of the values of α in $D \sim \rho^{\alpha}$ for various facilities in the US and SK. The coefficient of determination R^2 is obtained through the least-squares analysis. The value for each facility type is obtained from information in the county level, except for the asterisk(*)-marked values, which are from the state level (US) and the province level (SK). The numbers in parentheses are the standard errors in the last digits.

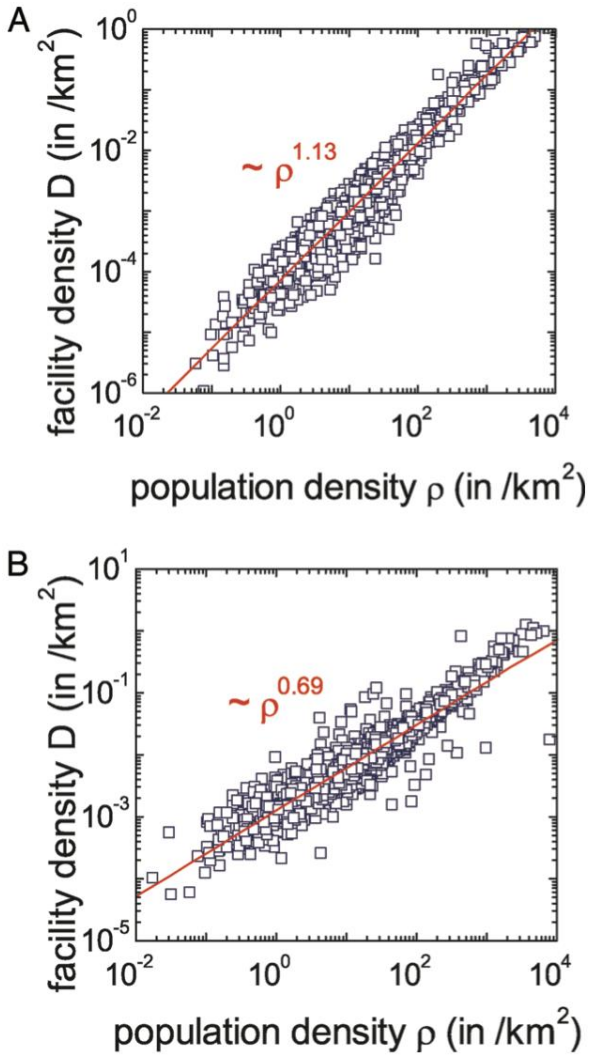

Fig. 1. Scatter plots of population and facility density obtained from empirical data. (*A*) Facility density *D* versus population density ρ for ambulatory hospitals in the US. (*B*) *D* versus ρ for the public schools in the US. For ambulatory hospital the exponent is 1.13 close to 1, which shows clearly a different distribution from the exponent 0.69 for public schools. The public school shows roughly 2 regimes of different exponents around $\rho \sim 100/\text{km}^2$. The region above 100/km^2 of population density shows the exponent as ≈1, and the region below 100/km^2 shows 2/3. The population density 100/km^2 corresponds to the cross-over point of the facility density 0.03/km^2, which means that 1 school covers about 33 km^2. If we assume the geometry is nearly a circle, the radius of the attending distance is ≈3 km. For attending distances <3 km, public school distribution also shows similar behaviors to those of the private schools.

Simple calculation of α

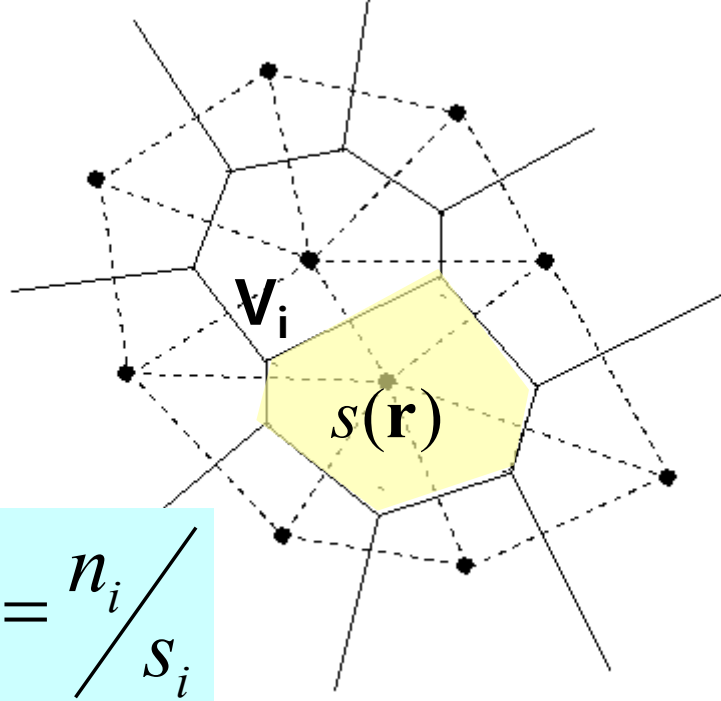

*value of facility $v_i \equiv n_i \langle r_i \rangle^{\beta}$

in one Voronoi cell, $\langle r_i \rangle \sim s_i^{1/2}$, $\rho_i = n_i / s_i$

At stationary state... $v_i \approx const.$ $D_i = \frac{1}{s_i} \sim \rho_i^{2/(\beta+2)}$

$$\therefore \; D \sim \rho^{\alpha}, \; \alpha = \frac{2}{\beta+2}$$

$$\begin{cases} \beta = 1 \rightarrow \alpha = 2/3 \\ \beta = 0 \rightarrow \alpha = 1 \end{cases}$$

Simulation Model (local rule)

* Value/Profit of the facilities

$$v_i \equiv n_i \langle r_i \rangle^{\beta}$$

(i) Remove the facility with the lowest v_i
(ii) Construct new facility near the facility with highest v_i

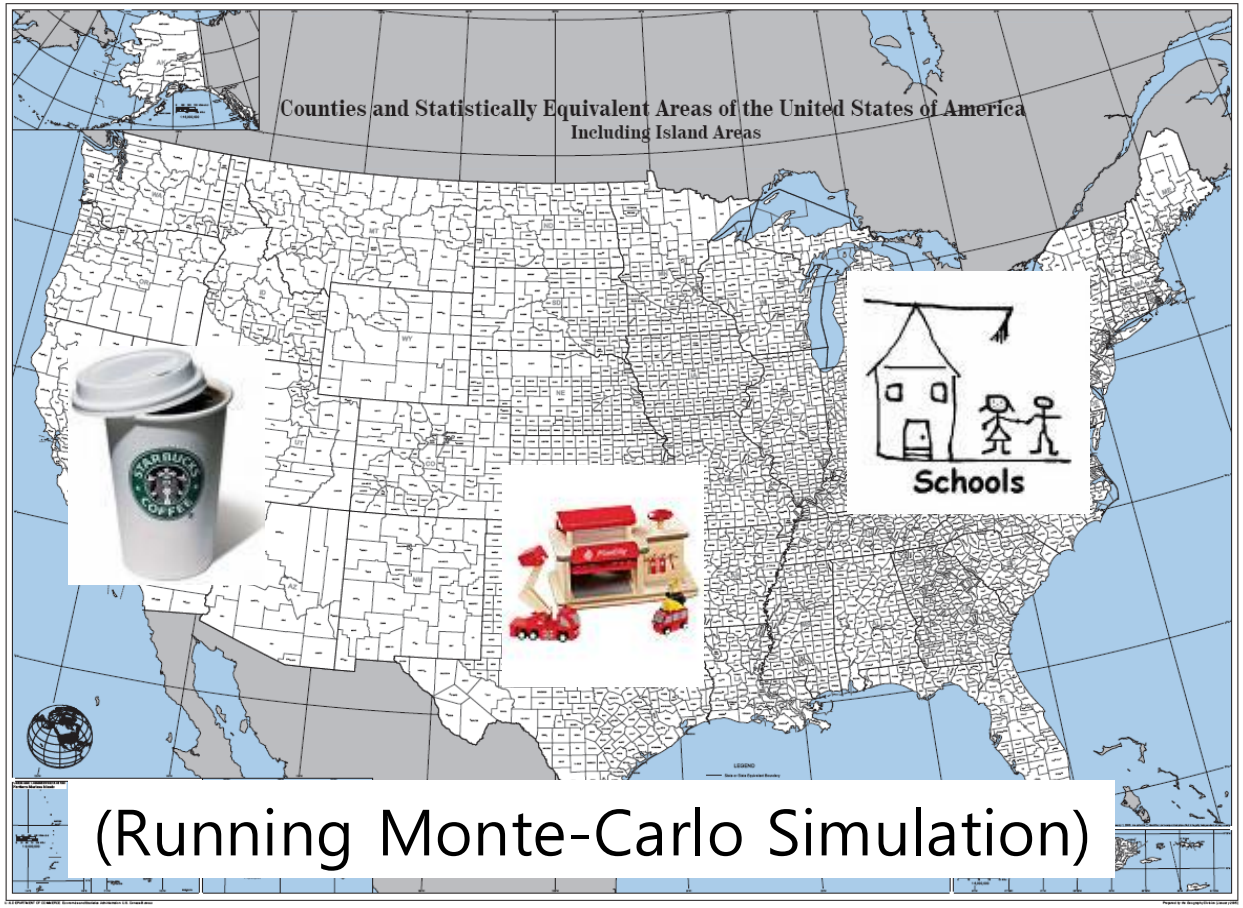

private 0 β 1 public

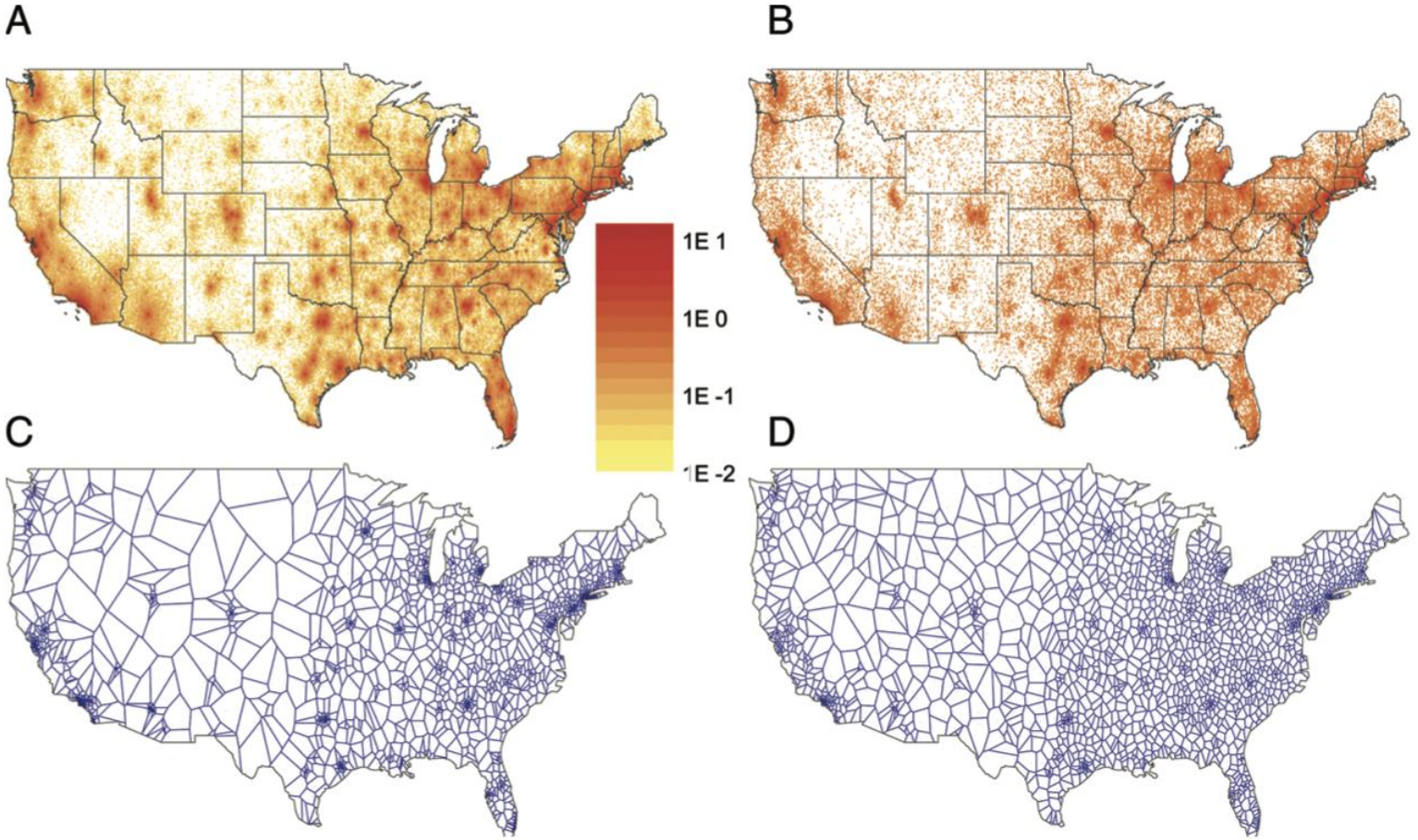

Fig. 2. Distribution of public and private facilities. Density plot for ambulatory hospitals (*A*) and public schools (*B*) in the US. Voronoi cell diagram from model simulation for commercial (*C*) and public facilities (*D*). Note that the spatial distribution in *B* and *D* for public facilities is more uniform than that in *A* and *C* for commercial facilities.

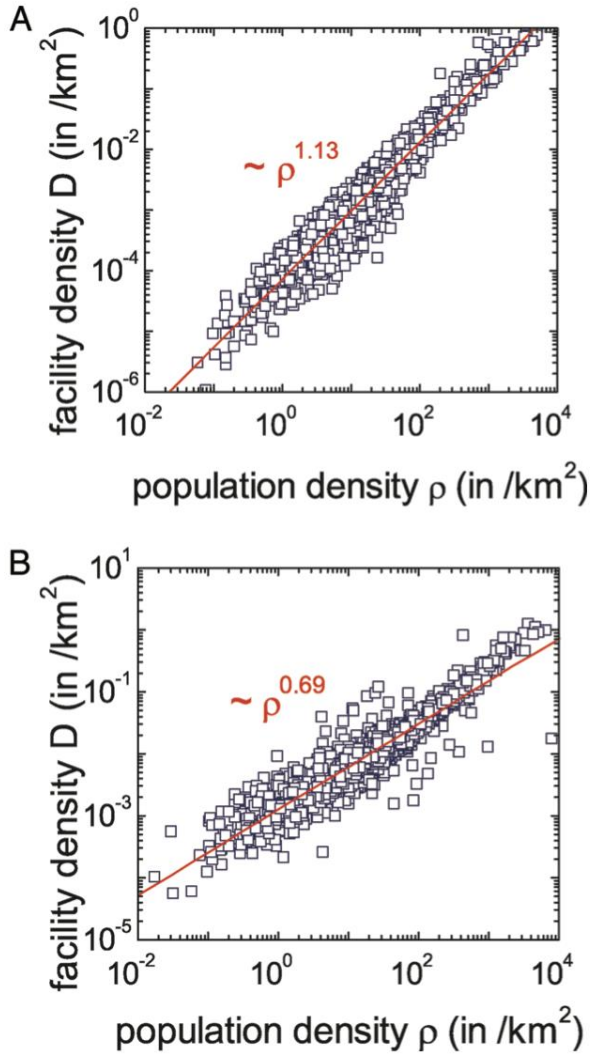

Fig. 1. Scatter plots of population and facility density obtained from empirical data. (*A*) Facility density *D* versus population density ρ for ambulatory hospitals in the US. (*B*) *D* versus ρ for the public schools in the US. For ambulatory hospital the exponent is 1.13 close to 1, which shows clearly a different distribution from the exponent 0.69 for public schools. The public school shows roughly 2 regimes of different exponents around $\rho \sim 100/\text{km}^2$. The region above $100/\text{km}^2$ of population density shows the exponent as ≈ 1, and the region below $100/\text{km}^2$ shows 2/3. The population density $100/\text{km}^2$ corresponds to the cross-over point of the facility density $0.03/\text{km}^2$, which means that 1 school covers about 33 km^2. If we assume the geometry is nearly a circle, the radius of the attending distance is ≈ 3 km. For attending distances <3 km, public school distribution also shows similar behaviors to those of the private schools.

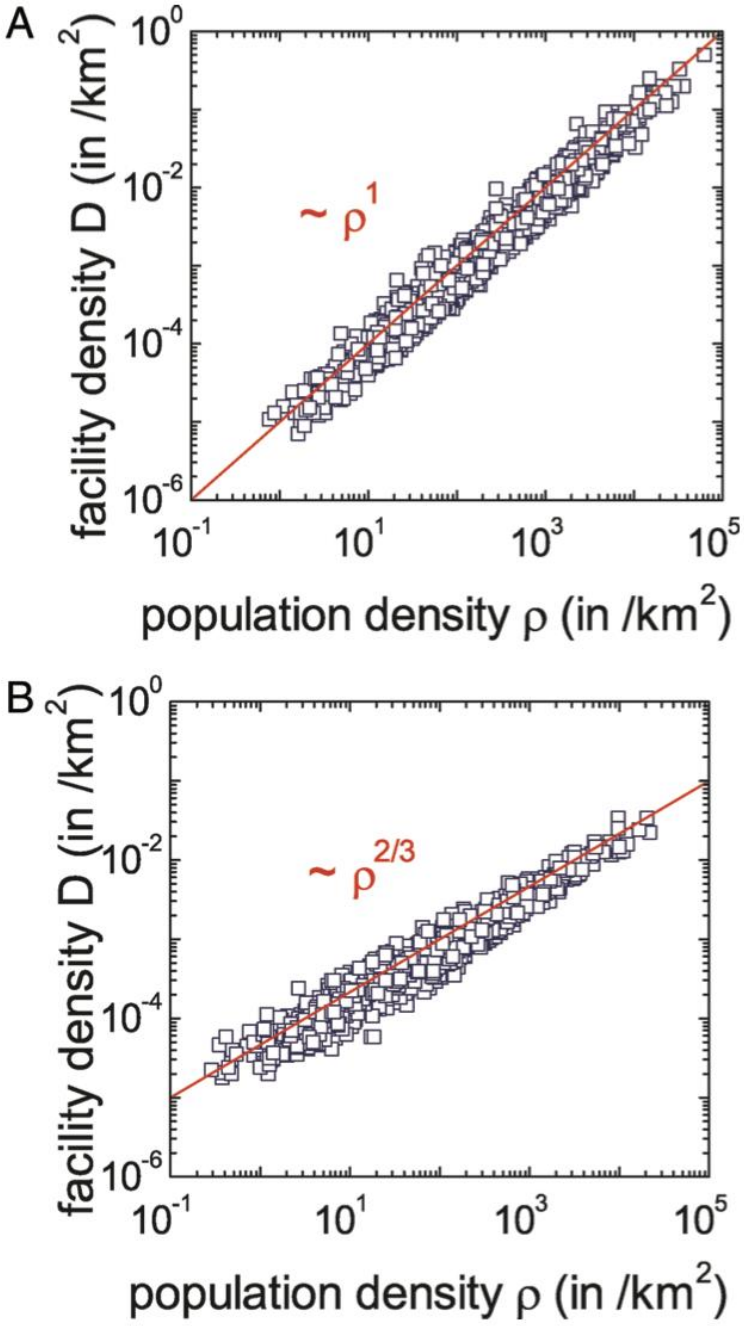

Fig. 3. Simulation results. (*A*) Facility density *D* versus population density ρ for the commercial facility. (*B*) *D* versus ρ for the public facility.

Table 1. Summary of the exponents

US facility	α (SE)	R^2
Ambulatory hospital	1.13(1)	0.93
Beauty care	1.08(1)	0.86
Laundry	1.05(1)	0.90
Automotive repair	0.99(1)	0.92
Private school	0.95(1)	0.82
Restaurant	0.93(1)	0.89
Accommodation	0.89(1)	0.70
Bank	0.88(1)	0.89
Gas station	0.86(1)	0.94
Death care	0.79(1)	0.80
* Fire station	0.78(3)	0.93
* Police station	0.71(6)	0.75
Public school	0.69(1)	0.87
SK facility	**α (SE)**	**R^2**
Bank	1.18(2)	0.96
Parking place	1.13(2)	0.91
* Primary clinic	1.09(2)	1.00
* Hospital	0.96(5)	0.97
* University/college	0.93(9)	0.89
Market place	0.87(2)	0.90
* Secondary school	0.77(3)	0.98
* Primary school	0.77(3)	0.97
Social welfare org.	0.75(2)	0.84
* Police station	0.71(5)	0.94
Government office	0.70(1)	0.93
* Fire station	0.60(4)	0.93
* Public health center	0.09(5)	0.19

Summary of the values of α in $D \sim \rho^{\alpha}$ for various facilities in the US and SK. The coefficient of determination R^2 is obtained through the least-squares analysis. The value for each facility type is obtained from information in the county level, except for the asterisk(*)-marked values, which are from the state level (US) and the province level (SK). The numbers in parentheses are the standard errors in the last digits.

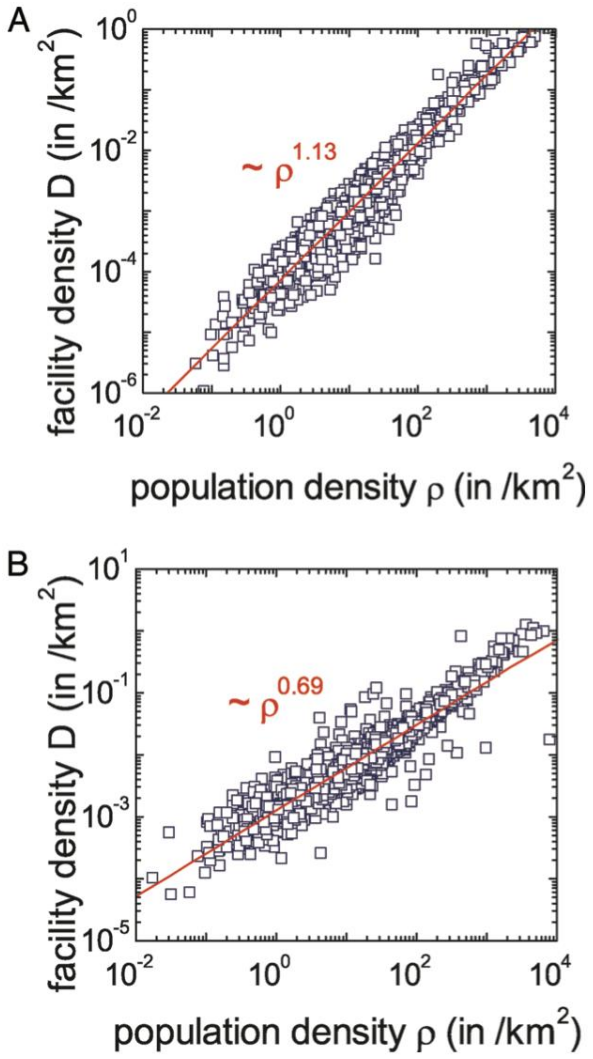

Fig. 1. Scatter plots of population and facility density obtained from empirical data. (*A*) Facility density *D* versus population density ρ for ambulatory hospitals in the US. (*B*) *D* versus ρ for the public schools in the US. For ambulatory hospital the exponent is 1.13 close to 1, which shows clearly a different distribution from the exponent 0.69 for public schools. The public school shows roughly 2 regimes of different exponents around $\rho \sim 100/\text{km}^2$. The region above 100/km^2 of population density shows the exponent as ≈1, and the region below 100/km^2 shows 2/3. The population density 100/km^2 corresponds to the cross-over point of the facility density 0.03/km^2, which means that 1 school covers about 33 km^2. If we assume the geometry is nearly a circle, the radius of the attending distance is ≈3 km. For attending distances <3 km, public school distribution also shows similar behaviors to those of the private schools.

과제

- 각 팀이 하나 이상의 실세계 또는 시뮬레이션 데이터를 골라서 power-law scaling이 나타나는지 분석해 보세요.
- 데이터는 물리 실험 (avalache 크기, 균열 길이 분포 등), 생물학/생태 (종 풍부도, 질량–대사율 관계 등), 사회/도시 (도시 규모와 인프라/경제 지표, 소득 분포 등), 그리고 네트워크 시뮬레이션 데이터 (네트워크 percolation / Ising / sandpile 에서 클러스터나 avalanche 크기 분포 등) 가운데에서 자유롭게 선택하세요.
- 선택한 데이터에 대해 히스토그램과 PDF/CCDF, log–log 플롯을 그려서 파워법칙 후보 구간을 찾아보고, 그 구간에서 직선 피팅으로 지수를 추정해 보세요.
- 가능하다면 지수분포나 로그정규분포와도 비교해 보면서, "정말 power-law라고 부를 만한가, 아니면 cutoff가 있는 파워법칙이나 단순 heavy-tail인가"를 정성적으로 토론하고 관련 모델을 제시해 보세요.
- 각 팀이 자기 데이터셋과 관련된 논문을 최소 두 편 이상 찾아서, 그 분야에서 어떤 스케일링 법칙이 보고되어 있는지, 전형적인 지수 값이 얼마인지, 그리고 그 지수를 어떻게 해석하고 있는지(임계현상, 보편성, 자기조직화 임계, 최적화 메커니즘 등) 함께 토의하세요.

표 1 심혈관계

양	예측값	측정값
대동맥 반지름	3/8=0.375	0.36
대동맥 혈압	0=0.00	0.032
대동맥 혈류 속도	0.00	0.07
혈액량	1=1.00	1.00
순환 시간	1/4=0.25	0.25
순환 거리	1/4=0.25	자료 없음
심장 1회 박출량	1=1.00	1.03
심장 박동 수	−1/4=−0.25	−0.25
심장 박출량	3/4=0.75	0.74
모세혈관 수	3/4=0.75	자료 없음
수도관 용적 반지름	자료 없음	자료 없음
워머슬리 수	1/4=0.25	0.25
모세혈관 밀도	−1/12=−0.083	−0.095
혈액의 O_2 친화도	−1/12=−0.083	−0.089
총 저항	−3/4=−0.75	−0.76
대사율	3/4=0.75	0.75

표 2 호흡계

양	예측값	측정값
기관 반지름	3/8=0.375	0.39
흉막 압력	0=0.00	0.004
기관의 공기 속도	0=0.00	0.02
허파 부피	1=1.00	1.05
공기 흡입량	3/4=0.75	0.80
허파꽈리 부피	1/4=0.25	자료 없음
공기 순환량	1=1.00	1.041
호흡 빈도	−1/4=−0.25	−0.26
분산력	3/4=0.75	0.78
허파꽈리 수	3/4=0.75	자료 없음
허파꽈리 반지름	1/12=0.083	0.13
허파꽈리 면적	1/6=0.167	자료 없음
허파 면적	11/12=0.92	0.95
O_2 확산력	1=1.00	0.99
총 저항	−3/4=−0.75	−0.70
O_2 소비율	3/4=0.75	0.76

표 3 식물 관다발계의 생리적·해부학적 변수들에 대한 스케일링 지수의 예측값

양	식물 무게의 함수	줄기 반지름의 함수	
	지수	지수	
	예측값	예측값	측정값
잎 수	3/4(0.75)	2(2.00)	2.007
가지 수	3/4(0.75)	−2(−2.00)	−2.00
관 수	3/4(0.75)	2(2.00)	자료 없음
줄기 길이	1/4(0.25)	2/3(0.67)	0.652
줄기 반지름	3/8(0.375)		
통도조직 면적	7/8(0.875)	7/3(2.33)	2.13
관 반지름	1/16(0.0625)	1/6(0.167)	자료 없음
전도도	1(1.00)	8/3(2.67)	2.63
잎 전도도	1/4(0.25)	2/3(0.67)	0.727
유량		2(2.00)	자료 없음
대사율	3/4(0.75)		
압력 기울기	−1/4(−0.25)	−2/3(−0.67)	자료 없음
유체 속도	−1/8(−0.125)	−1/3(−0.33)	자료 없음
가지 저항	−3/4(−0.75)	−1/3(−0.33)	자료 없음

$$Y(t) = Y_0 N(t)^{\beta}.$$

Table 1. Scaling exponents for urban indicators vs. city size

Y	β	95% CI	Adj-R^2	Observations	Country–year
New patents	1.27	[1.25,1.29]	0.72	331	U.S. 2001
Inventors	1.25	[1.22,1.27]	0.76	331	U.S. 2001
Private R&D employment	1.34	[1.29,1.39]	0.92	266	U.S. 2002
"Supercreative" employment	1.15	[1.11,1.18]	0.89	287	U.S. 2003
R&D establishments	1.19	[1.14,1.22]	0.77	287	U.S. 1997
R&D employment	1.26	[1.18,1.43]	0.93	295	China 2002
Total wages	1.12	[1.09,1.13]	0.96	361	U.S. 2002
Total bank deposits	1.08	[1.03,1.11]	0.91	267	U.S. 1996
GDP	1.15	[1.06,1.23]	0.96	295	China 2002
GDP	1.26	[1.09,1.46]	0.64	196	EU 1999–2003
GDP	1.13	[1.03,1.23]	0.94	37	Germany 2003
Total electrical consumption	1.07	[1.03,1.11]	0.88	392	Germany 2002
New AIDS cases	1.23	[1.18,1.29]	0.76	93	U.S. 2002–2003
Serious crimes	1.16	[1.11, 1.18]	0.89	287	U.S. 2003
Total housing	1.00	[0.99,1.01]	0.99	316	U.S. 1990
Total employment	1.01	[0.99,1.02]	0.98	331	U.S. 2001
Household electrical consumption	1.00	[0.94,1.06]	0.88	377	Germany 2002
Household electrical consumption	1.05	[0.89,1.22]	0.91	295	China 2002
Household water consumption	1.01	[0.89,1.11]	0.96	295	China 2002
Gasoline stations	0.77	[0.74,0.81]	0.93	318	U.S. 2001
Gasoline sales	0.79	[0.73,0.80]	0.94	318	U.S. 2001
Length of electrical cables	0.87	[0.82,0.92]	0.75	380	Germany 2002
Road surface	0.83	[0.74,0.92]	0.87	29	Germany 2002

Data sources are shown in *SI Text*. CI, confidence interval; Adj-R^2, adjusted R^2; GDP, gross domestic product.

Table 1. Summary of the exponents

US facility	α (SE)	R^2
Ambulatory hospital	1.13(1)	0.93
Beauty care	1.08(1)	0.86
Laundry	1.05(1)	0.90
Automotive repair	0.99(1)	0.92
Private school	0.95(1)	0.82
Restaurant	0.93(1)	0.89
Accommodation	0.89(1)	0.70
Bank	0.88(1)	0.89
Gas station	0.86(1)	0.94
Death care	0.79(1)	0.80
* Fire station	0.78(3)	0.93
* Police station	0.71(6)	0.75
Public school	0.69(1)	0.87
SK facility	**α (SE)**	**R^2**
Bank	1.18(2)	0.96
Parking place	1.13(2)	0.91
* Primary clinic	1.09(2)	1.00
* Hospital	0.96(5)	0.97
* University/college	0.93(9)	0.89
Market place	0.87(2)	0.90
* Secondary school	0.77(3)	0.98
* Primary school	0.77(3)	0.97
Social welfare org.	0.75(2)	0.84
* Police station	0.71(5)	0.94
Government office	0.70(1)	0.93
* Fire station	0.60(4)	0.93
* Public health center	0.09(5)	0.19

Summary of the values of α in $D \sim \rho^{\alpha}$ for various facilities in the US and SK. The coefficient of determination R^2 is obtained through the least-squares analysis. The value for each facility type is obtained from information in the county level, except for the asterisk(*)-marked values, which are from the state level (US) and the province level (SK). The numbers in parentheses are the standard errors in the last digits.

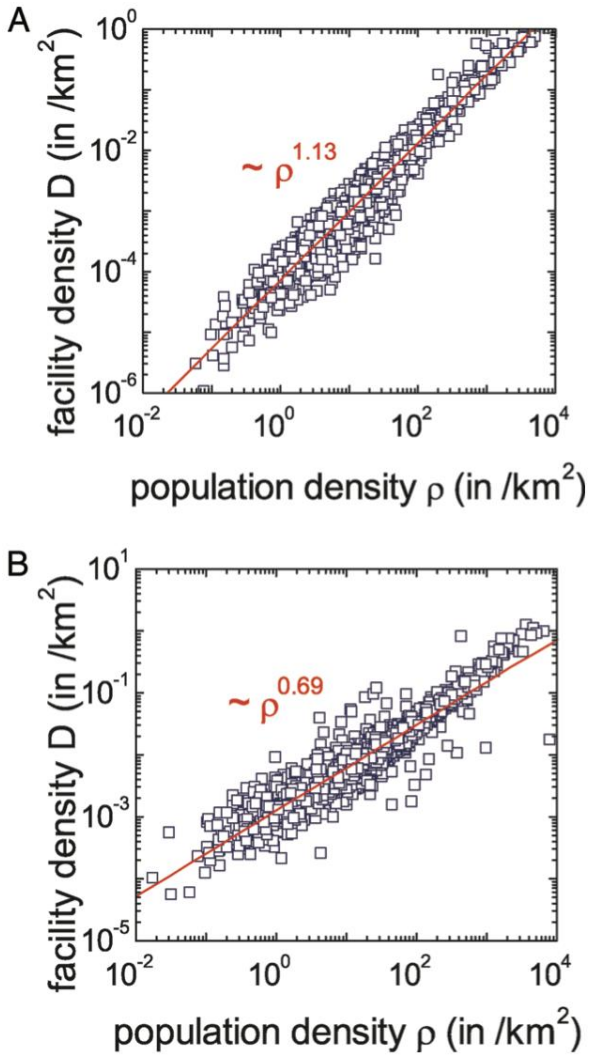

Fig. 1. Scatter plots of population and facility density obtained from empirical data. (*A*) Facility density *D* versus population density ρ for ambulatory hospitals in the US. (*B*) *D* versus ρ for the public schools in the US. For ambulatory hospital the exponent is 1.13 close to 1, which shows clearly a different distribution from the exponent 0.69 for public schools. The public school shows roughly 2 regimes of different exponents around $\rho \sim 100/\text{km}^2$. The region above 100/km^2 of population density shows the exponent as ≈1, and the region below 100/km^2 shows 2/3. The population density 100/km^2 corresponds to the cross-over point of the facility density 0.03/km^2, which means that 1 school covers about 33 km^2. If we assume the geometry is nearly a circle, the radius of the attending distance is ≈3 km. For attending distances <3 km, public school distribution also shows similar behaviors to those of the private schools.

Exploring the relationship between the spatial distribution of roads and universal pattern of travel-route efficiency in urban road networks

Minjin Lee et al. (2023)

Chaos, Solitons and Fractals 174, 113770 (2023).

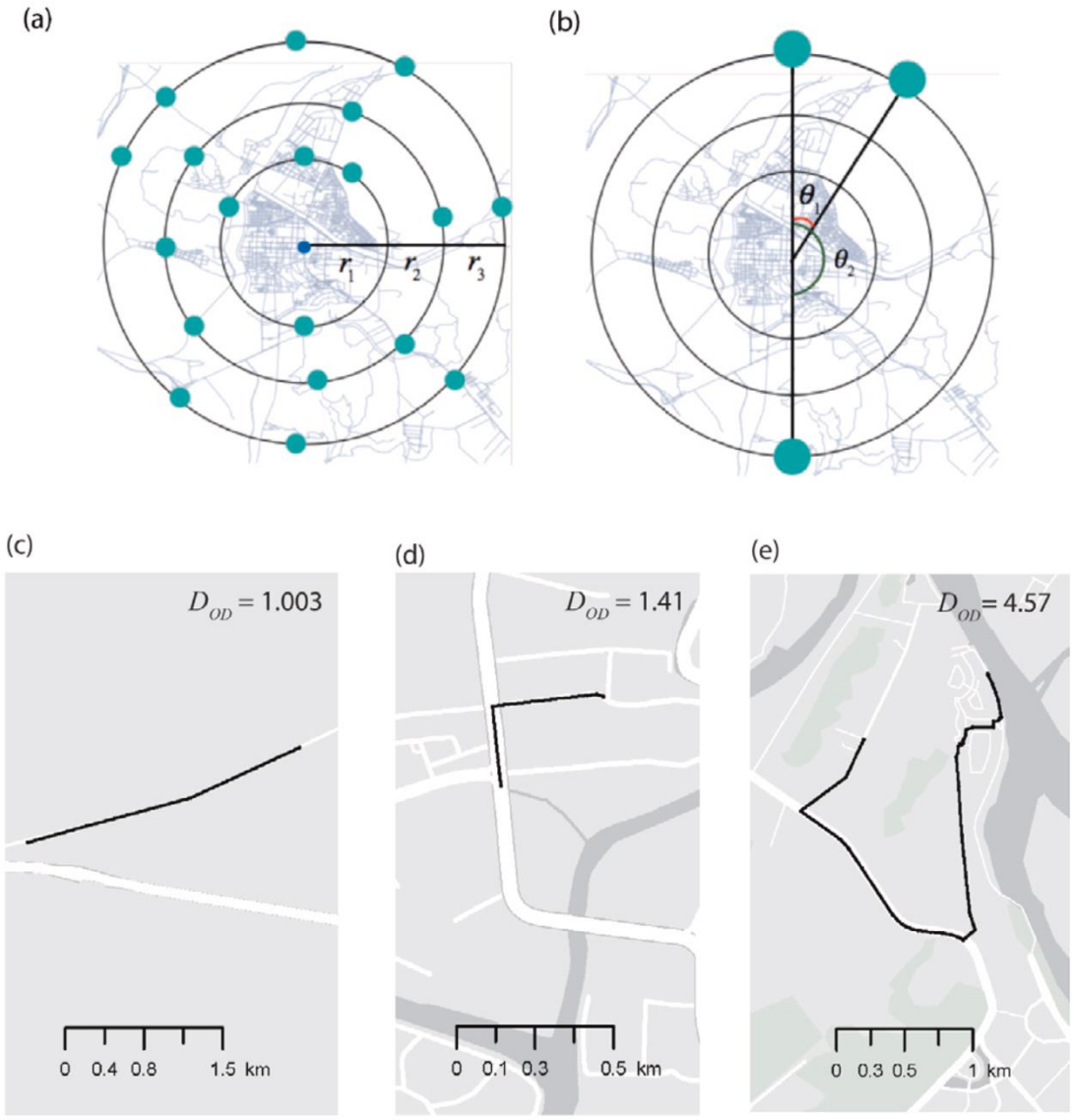

Fig. 1. Sampling of OD pairs and examples of the different detour indices D_{OD}. (a) The OD points are randomly selected on a circle with a given radius r_n. For example, one point at r_1 and another point at r_2 are not regarded as an OD pair. (b) The angular distance θ_{OD} is defined as the included angle between two lines connecting the OD points to the city center. (c)–(e) Examples of travel routes with different D_{OD}s.

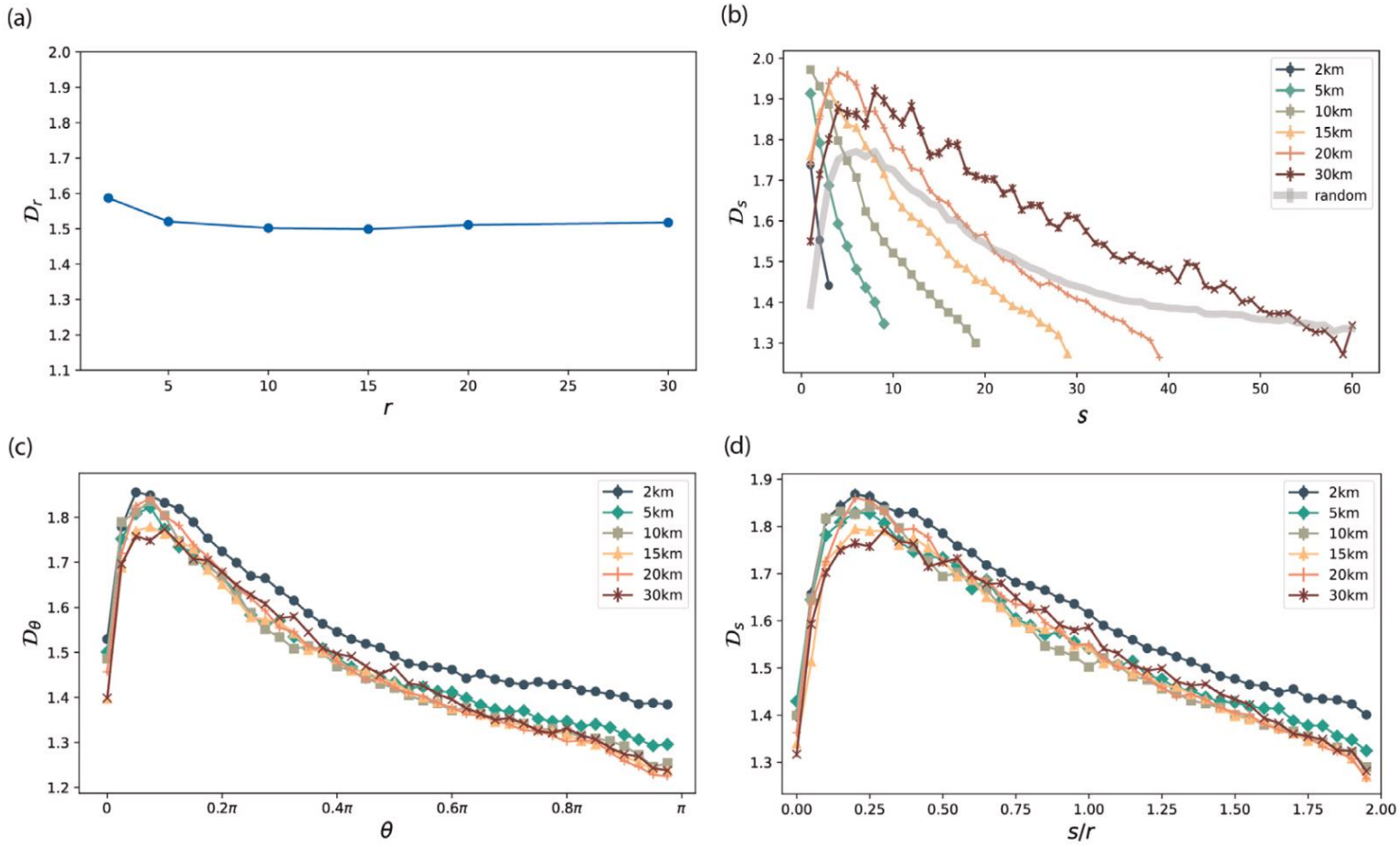

Fig. 3. Average detour index versus the respective spatial variable for 70 cities. (a) $\mathcal{D}_r$ [Eq. (2)] with respect to the radius r from the city center, (b) $\mathcal{D}_s$ [Eq. (3)] with respect to the Euclidean distance s, and (c) $\mathcal{D}_\theta$ [Eq. (4)] with respect to the angular distance θ, respectively. The radius-fixed sampling provides various curves for different radii (from 2 km to 30 km) in $\mathcal{D}_s$ and $\mathcal{D}_\theta$. $\mathcal{D}_\theta$ collapses nicely, indicating that (d) $\mathcal{D}_s$ collapses to a single curve with a scaling factor of r, which can be easily estimated using the trigonometric identity. For comparison, $\mathcal{D}_s$ in the case of random sampling is plotted in panel (b), but the radius is not defined in this sampling, so scaling cannot be performed in panel (d). The error bars represent the standard error and are approximately the size of the symbols.

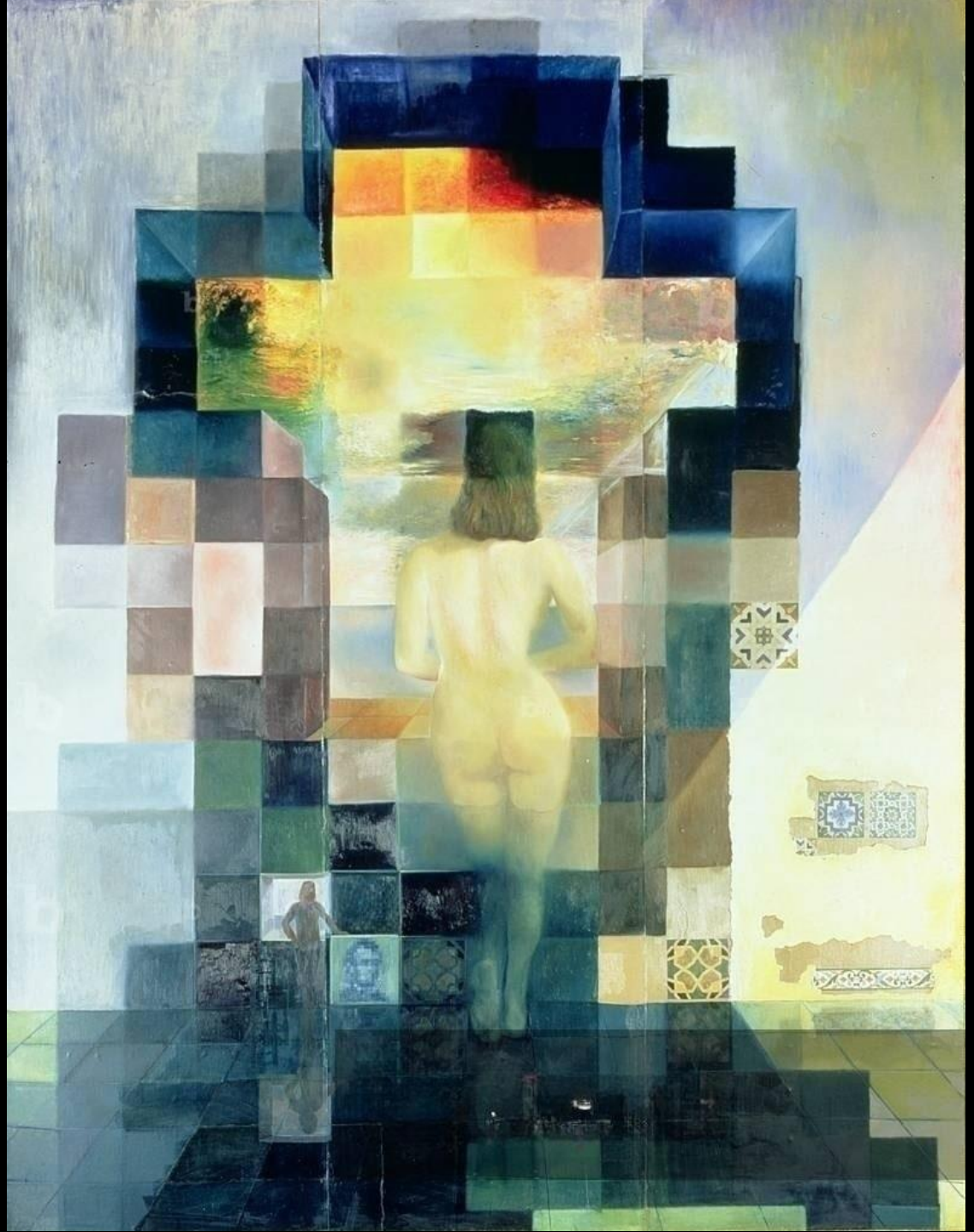

Gala Contemplating
the Mediterranean Sea,
1976 by Salvador Dali

Large-Scale Quantitative Analysis of Painting Arts

Daniel Kim[1], Seung-Woo Son[2] & Hawoong Jeong[3,4]

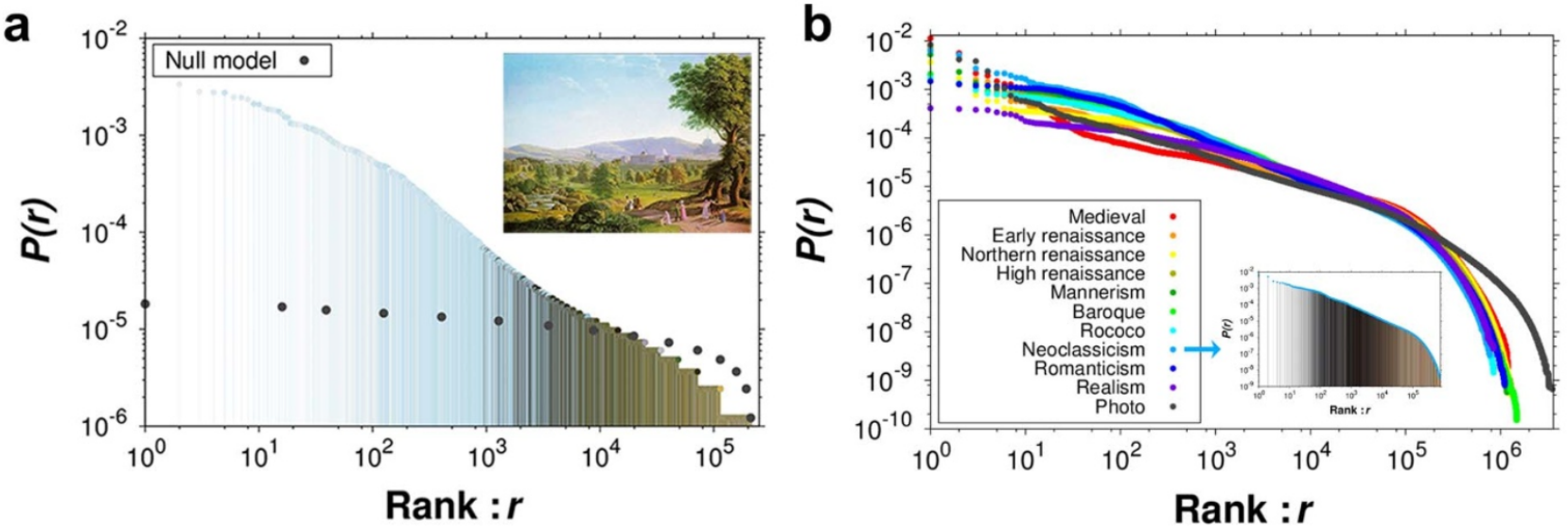

Figure 1 | **Rank-ordered color-usage distributions for an image and periods.** (a) Fraction distribution of each color in a descending rank order for the art work of German painter Johann Erdmann Hummel (1769-1852), "*Schloss Wilhelmshöhe with the Habichtswald*" (This image is out of copyright.). The horizontal axis indicates the rank of a color in frequency and the vertical axis denotes the proportion of a color in an image. The most (least) used color is located at the leftmost (rightmost) position on the horizontal axis. The black dots represent color choices from the same palette uniformly at random. (b) Rank-ordered color-usage distributions (RCDs) of the 10 periods and photographs. Note that the distribution of photographs clearly shows a different tail. Inset: RCD for the neoclassicism period. The displayed color corresponds to its rank. Note that the fraction is normalized by the image size and the number of paintings in each period.

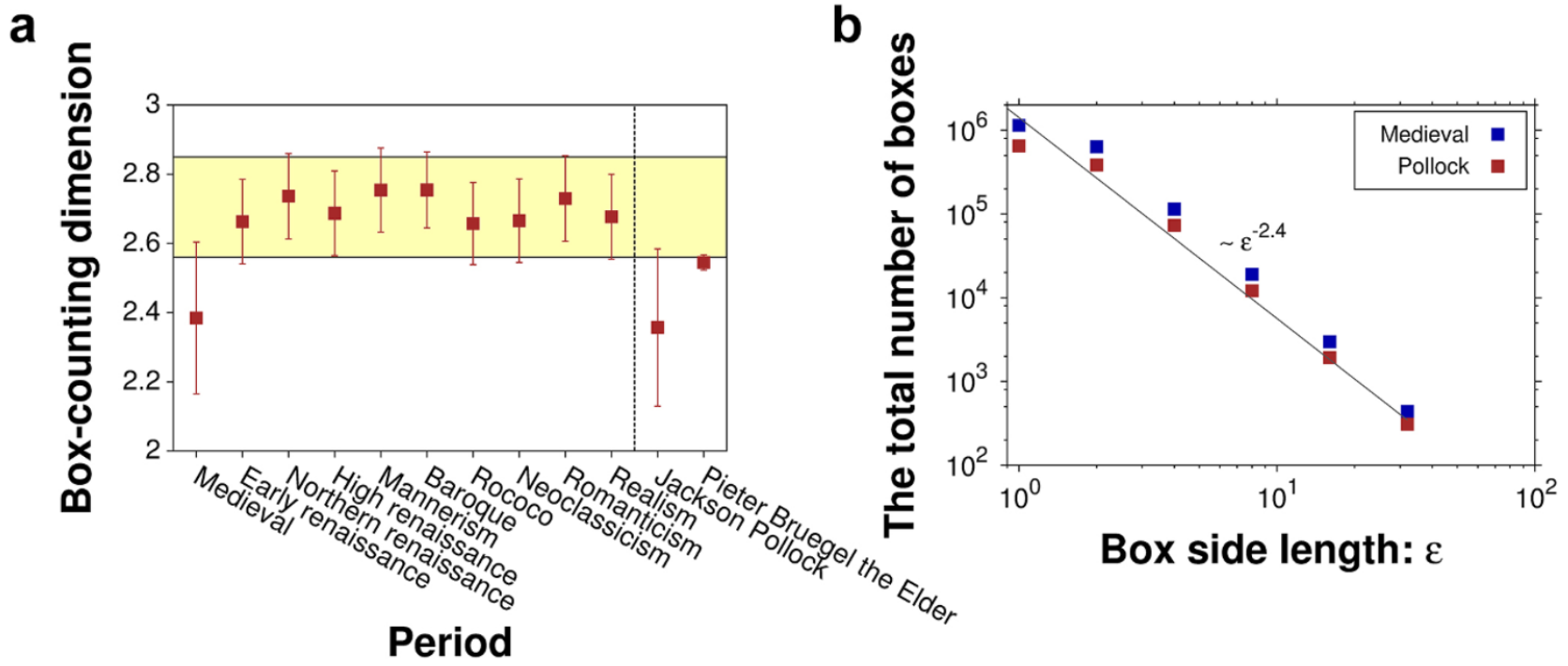

Figure 2 | Box-counting dimension and its tendency. (a) The results of box-counting dimension over the 10 artistic periods display a significant difference of the medieval period from the other periods. Error bars indicate the standard deviation. (b) The number of boxes to cover the color space versus box size. The fractal dimension in the color space of Jackson Pollock's drip paintings is measured around 2.35, similar to that of medieval paintings (see also Figure S5 in the supplement), but dissimilar to that of another iconoclastic artist Pieter Bruegel the Elder.

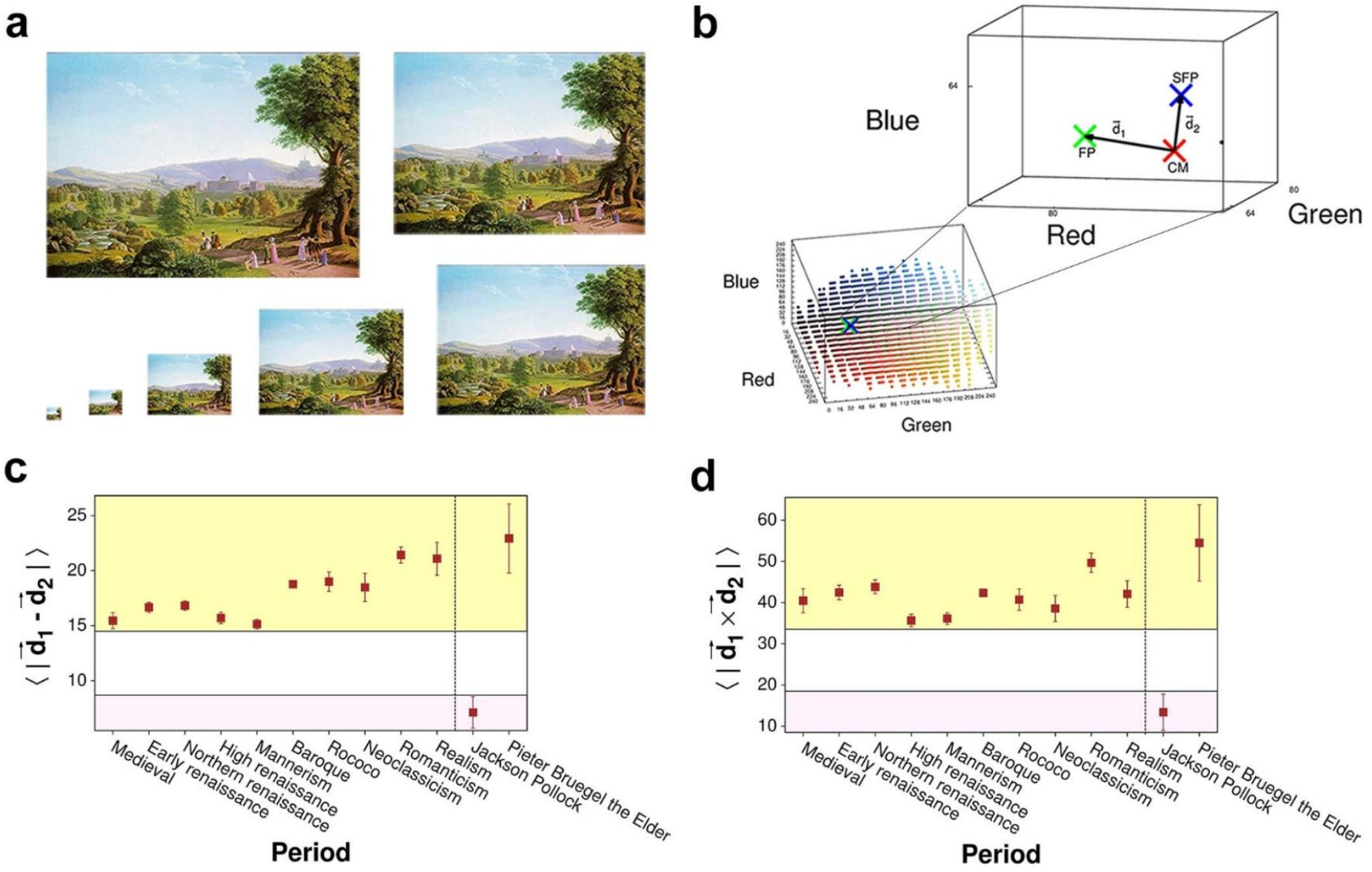

Figure 3 | Spatial renormalization of original and shuffled images. (a) An example of transforming an image into a fixed point. (Figure 1a also contains the image which is out of copyright.) (b) An illustrative example of the center of mass (CM), the fixed point (FP), and the shuffled fixed point (SFP) in RGB color space. (c) Norm of difference of $\boldsymbol{d}_1$ and $\boldsymbol{d}_2$ over 10 periods and comparison with Pollock's drip paintings and Pieter Bruegel the Elder's paintings. (d) Norm of cross product of $\boldsymbol{d}_1$ and $\boldsymbol{d}_2$ over 10 periods and comparison with Pollock's drip paintings and Pieter Bruegel the Elder's paintings.


PopulouSCAPE
- NIGHT FLIGHT OVER AN URBANIZING WORLD -
WHAT' S NEW
■ PROFILE
■ FLIGHT ROUTE
■ EXHIBITION
■ CONTACT US
■PopulouSCAPE DVD 絶賛発売中 愛・地球博で上映されたあの感動巨篇が遂にDVD化！
オンライン購入はこちら Amazon.co.jp | Spiral Online Store | 南洋堂書店WEBショップ
発行:スパイラル／株式会社ワコールアートセンター 発売:新風舎 制作:Team PopulouSCAPE
定価 2,400円（本体 2,286円＋税） ISBN4-289-01285-X
＊書店からもご注文いただけます。
Lagos
Kano
Kasuna
Ibadan
KINSHASA

FLIGHT ROUTE

－我々は強く結ばれつつある．インターネットの利用者は 10 億人を超え，知の連繋が広がっている．我々は，その連繋の向こう側にポピュラスケープという風景を見出すだろう．

－国際航空旅客数は年間 2 億 7100 万人．ムンバイからフランクフルトへは 12 万人が飛行し，都市を固く結んでいる．年間 5668 万人が利用するヨーロッパの空港は，都市化する世界の拠点となる．

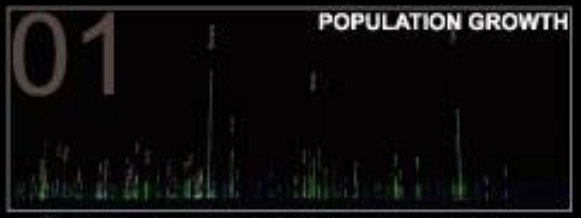

－現在，世界人口の半数が都市に住んでいる．ポピュラスケープには，そのうちの 20 億人が住む．人口 5 万人以上の 8375 都市が描かれる．都市人口は 50 年間で 3 倍に増え，今も 1 日 17 万人の都市人口増加がある．都市は，未来への鍵である．

－ 複数の都市が都市圏を形成し，地域の成長の核となっている．増加する人口を支え，貧困を緩和し，環境破壊の抑止力を与えるのは，都市である．都市化がはらむ問題への答えとなりうるのは，都市自身なのだ．

－ 数え切れないほどの我々の都市，その一つ一つに，創造の神話がある．都市の名前が，それをおしえてくれる．

FLIGHT ROUTE

* Thanks to :

Populouscape Team.

http://www.populouscape.com/

* Special thanks to...

伊藤香織（いとう かおり）/ データディレクター

- Data Director / Kaori ITO

– 1971 年東京生まれ．東京理科大学建築学科専任講師．東京大学空間情報科学研究センター客員研究員．博士（工学）．地理データと人間活動データを収集・統合し，モデル化によって膨大なデータに形を与えた．

& Soo-Jin Lee 이수진 (KAIST 문화기술대학원).

Homogeneous function (동차함수)

A function $f(x)$ of one variable $x > 0$ is a homogeneous function if

$$f(\lambda^a x) = \lambda f(x) \quad \text{for all } \lambda > 0,$$

and it is a power law with exponent $1/a$ if

$$f(x) = x^{1/a} f(1),$$

where $f(1)$ is the value of the function at $x = 1$.

K. Christensen and R. Moloney, “Complexity and Criticality” (2005).

Homogeneous f(x), power law

$$f(\lambda^a x) = \lambda f(x)$$

choose $\lambda^a = 1/x$

$$f(x) = \frac{1}{\lambda} f(1)$$
$$= x^{1/a} f(1)$$

power law

$$f(x) = x^{1/a} f(1)$$

$$f(\lambda^a x) = (\lambda^a x)^{1/a} f(1)$$
$$= \lambda x^{1/a} f(1)$$
$$= \lambda f(x)$$

homogeneous

$$f(\lambda^a x) = \lambda f(x)$$

$$\frac{f(\lambda^a x)}{f(x)} = \lambda$$

$$a = -\frac{1}{2}$$

$$\lambda = 100$$

$$\lambda^a = \frac{1}{10}$$

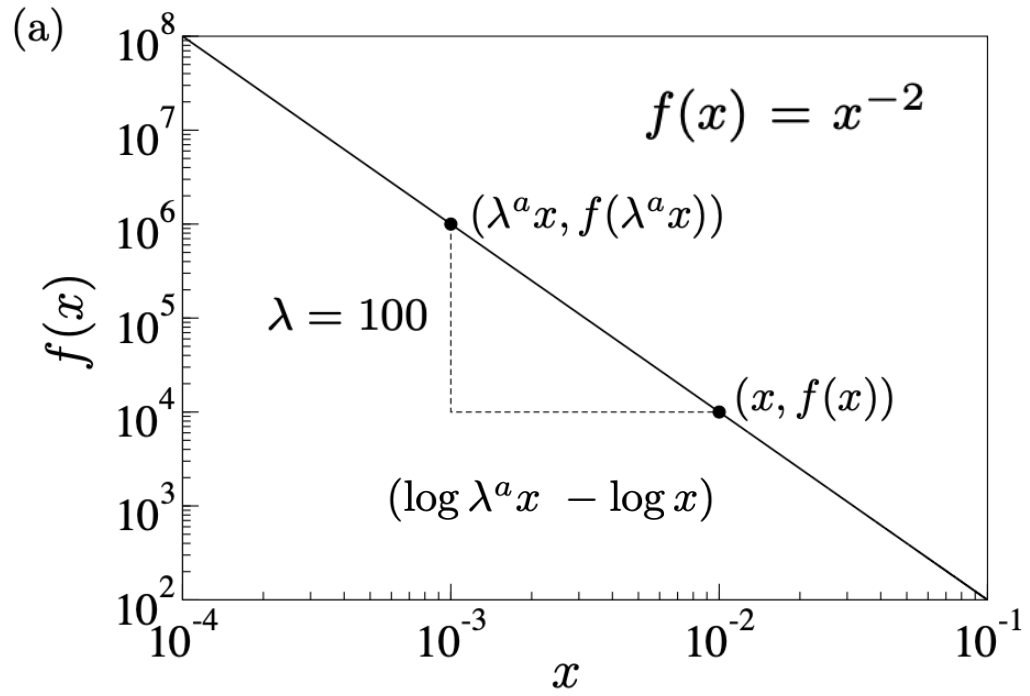

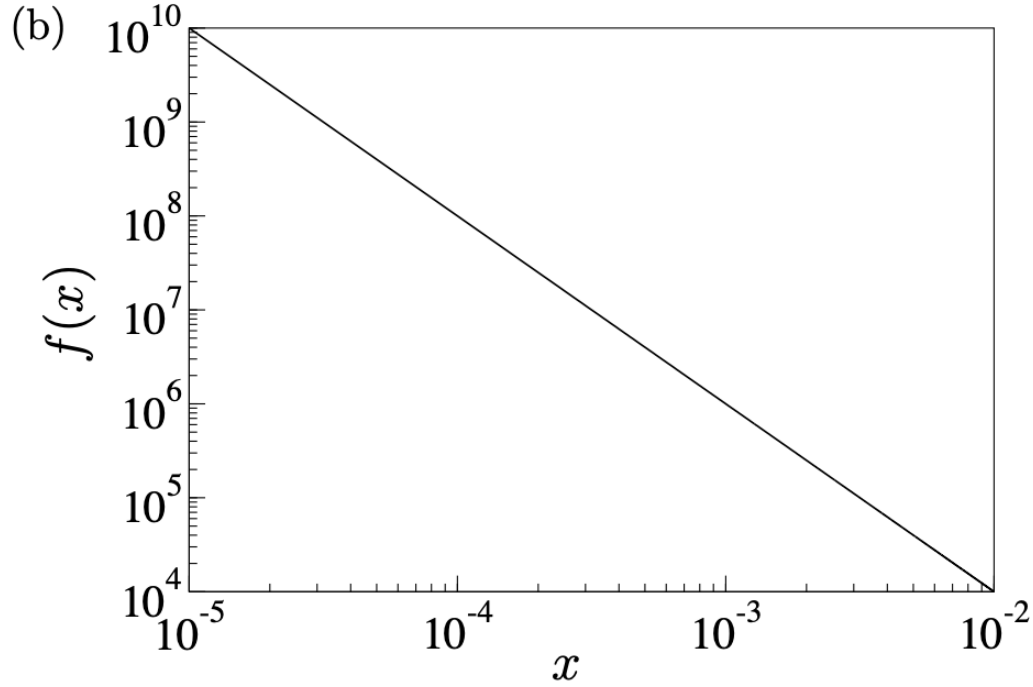

Two variables function f(x, y)

A function $f(x, y)$ of two variables is a generalised homogeneous function if

$$f\left(\lambda^a x, \lambda^b y\right) = \lambda f(x, y) \quad \text{for all } \lambda > 0,$$

and it satisfies a scaling form with exponent $1/a$ if

$$f(x, y) = |x|^{1/a} \mathcal{G}_{\pm}\left(y/|x|^{b/a}\right),$$

where $\mathcal{G}_{\pm}\left(y/|x|^{b/a}\right) = f\left(\pm 1, y/|x|^{b/a}\right)$ is the value of the function f at $x = \pm 1$ and the rescaled variable $y/|x|^{b/a}$. The function $\mathcal{G}_{\pm}$ is the so-called scaling function.

Generalised homogeneous function

$$f\left(\lambda^a x, \lambda^b y\right) = \lambda f(x, y)$$

$$\lambda^a = \frac{1}{|x|}, \quad \lambda = \frac{1}{|x|^{1/a}}$$

$$\begin{aligned} f(x, y) &= \frac{1}{\lambda} f\left(\pm 1, \lambda^b y\right) \\ &= |x|^{1/a} f\left(\pm 1, y/|x|^{b/a}\right) \\ &= |x|^{1/a} \mathcal{G}_{\pm}\left(y/|x|^{b/a}\right) \end{aligned}$$

scaling form

Scaling function form

$$f(x,y) = |x|^{1/a}\mathcal{G}_{\pm}\left(y/|x|^{b/a}\right)$$

$$\begin{aligned} f\left(\lambda^a x, \lambda^b y\right) &= \left(\lambda^a |x|\right)^{1/a} \mathcal{G}\left(\lambda^b y/(\lambda^a |x|)^{b/a}\right) \\ &= \lambda |x|^{1/a} \mathcal{G}\left(y/|x|^{b/a}\right) \\ &= \lambda f(x,y) \end{aligned}$$

generalised homogeneous function

$$\frac{f\left(\lambda^a x, \lambda^b y\right)}{f(x,y)} = \lambda$$

Ex)

$$f(x,y) = x^3 + y^2$$

$$a = 1/3, b = 1/2$$

$$\lambda = 27$$

$$\lambda^a = 3, \lambda^b \approx 5.2$$

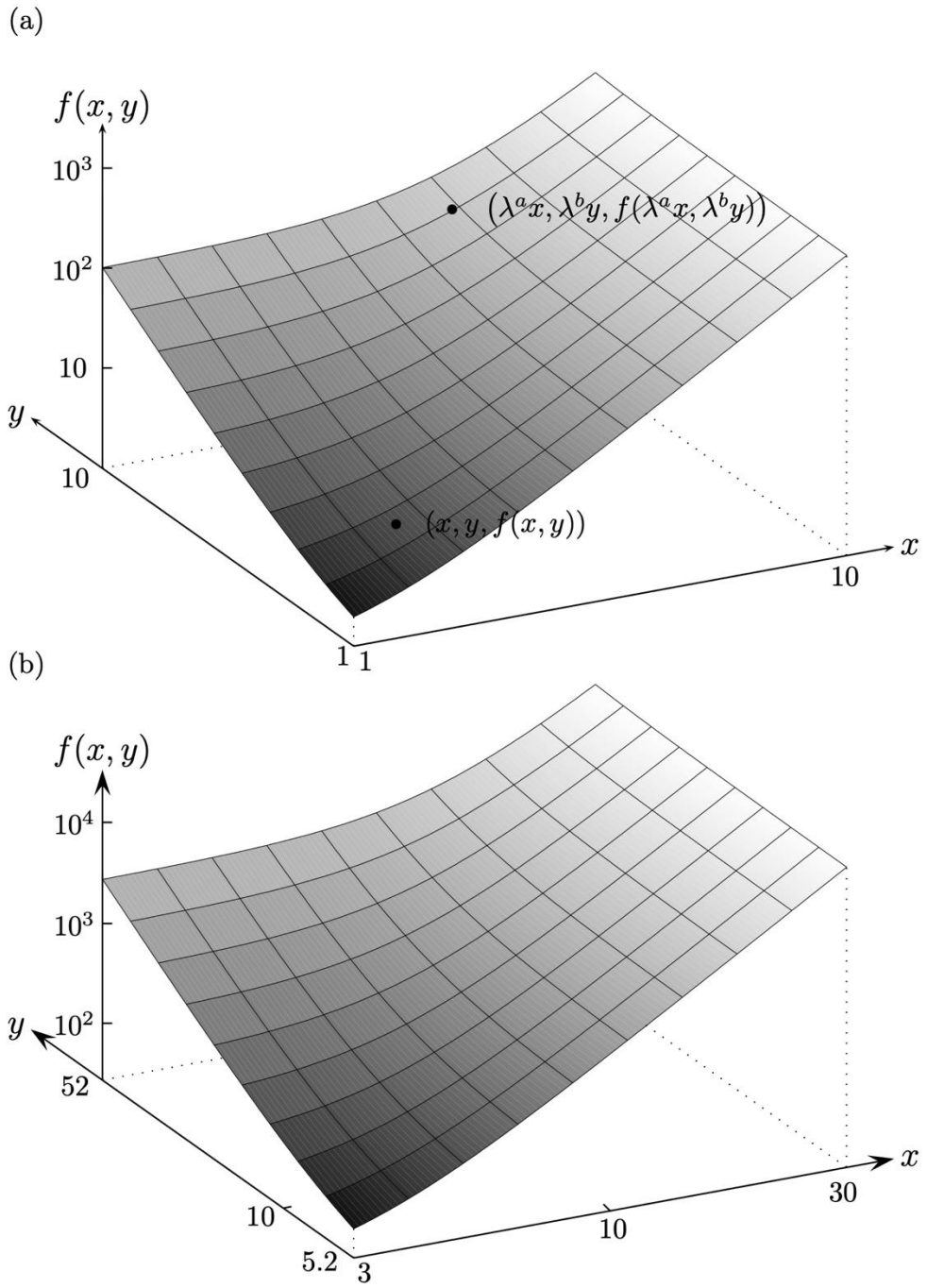

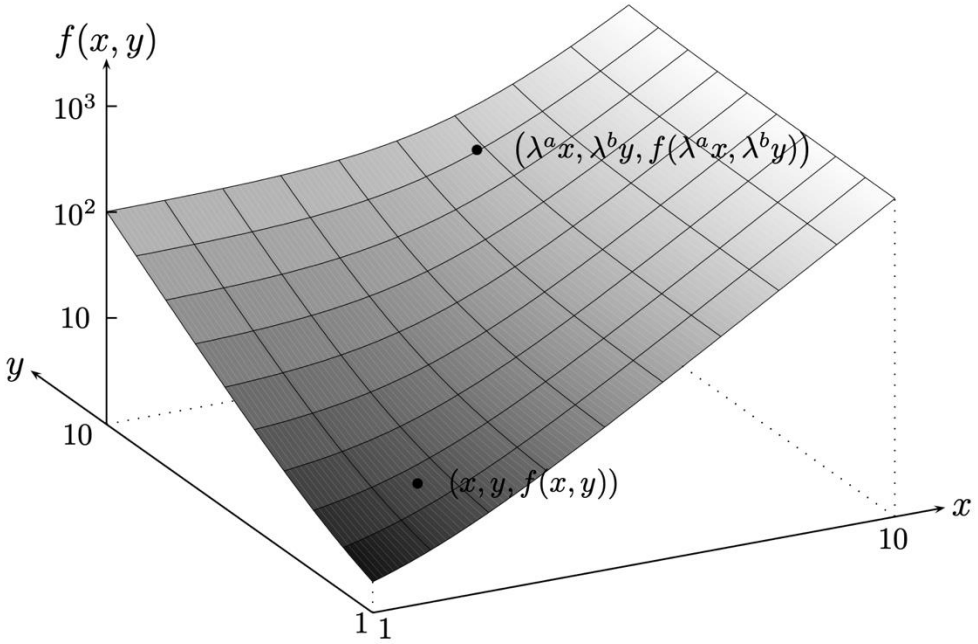

Ex)

$$f(x,y) = x^3 + y^2$$

$$x^{-3} f(x,y) = 1 + y^2/x^3$$

$$x^{-3} f(x,y) = 1 + \left(y/x^{3/2}\right)^2$$

$$f(x,y) = |x|^{1/a} \mathcal{G}_{\pm}\left(y/|x|^{b/a}\right)$$

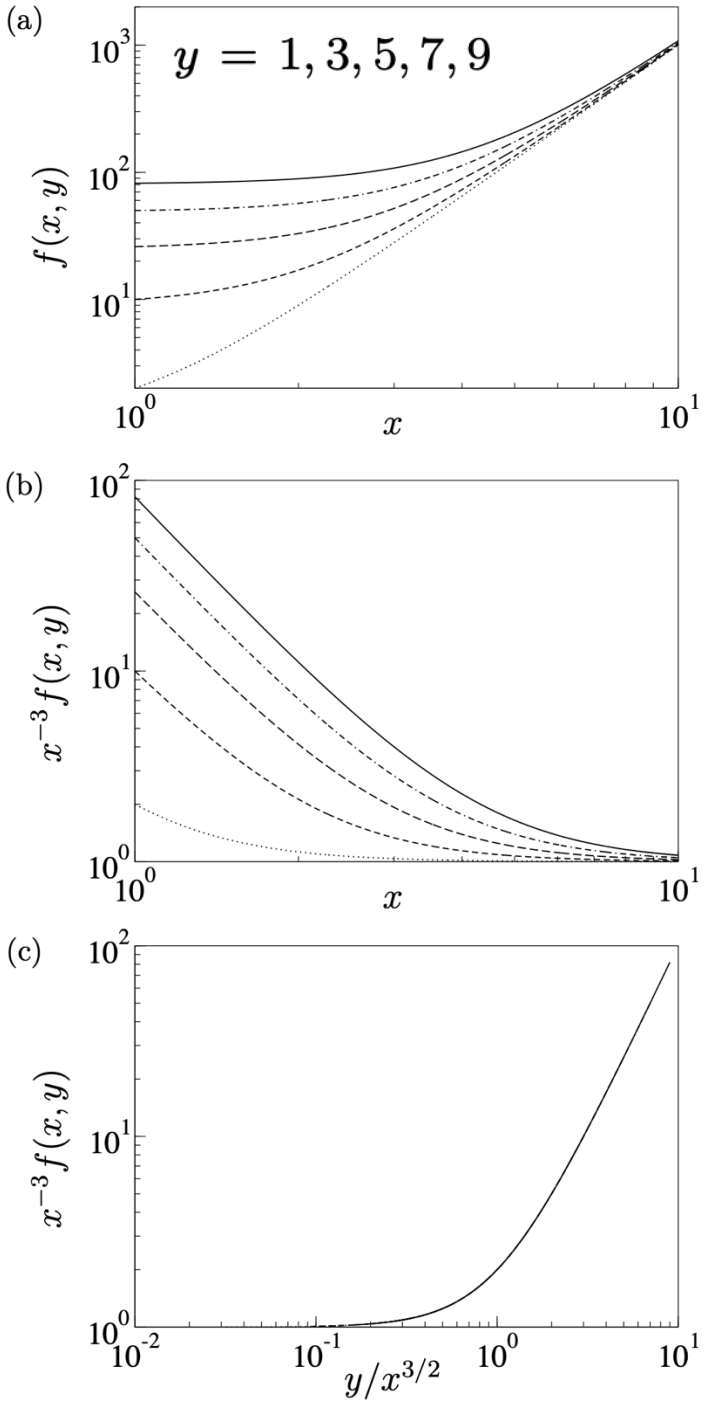

Fractals

$$M(\ell) \propto \ell^D$$

$$D = \lim_{\ell \to \infty} \frac{\log M(\ell)}{\log \ell}$$

$n = 0$ $n = 1$ $n = 2$ $n = 3$

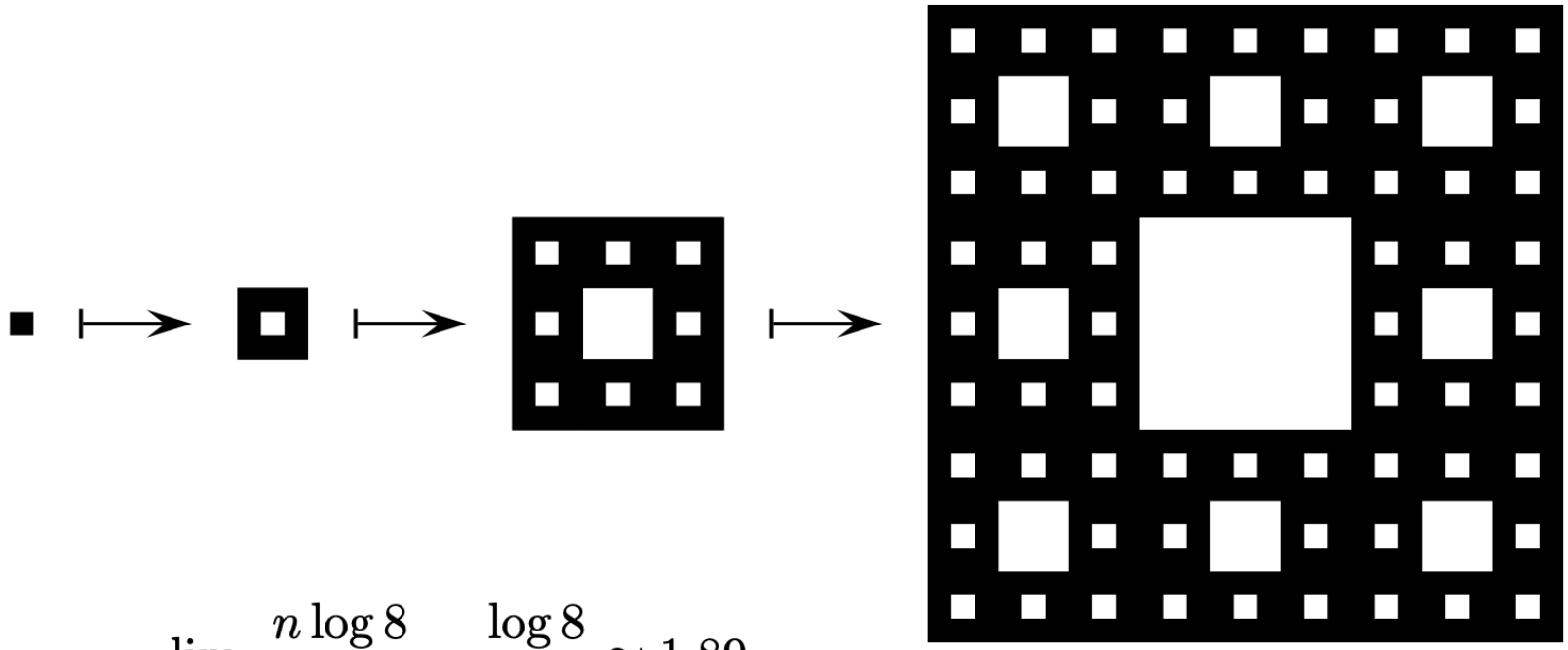

$$D_{\text{black}} = \lim_{n \to \infty} \frac{n \log 8}{n \log 3} = \frac{\log 8}{\log 3} \approx 1.89$$

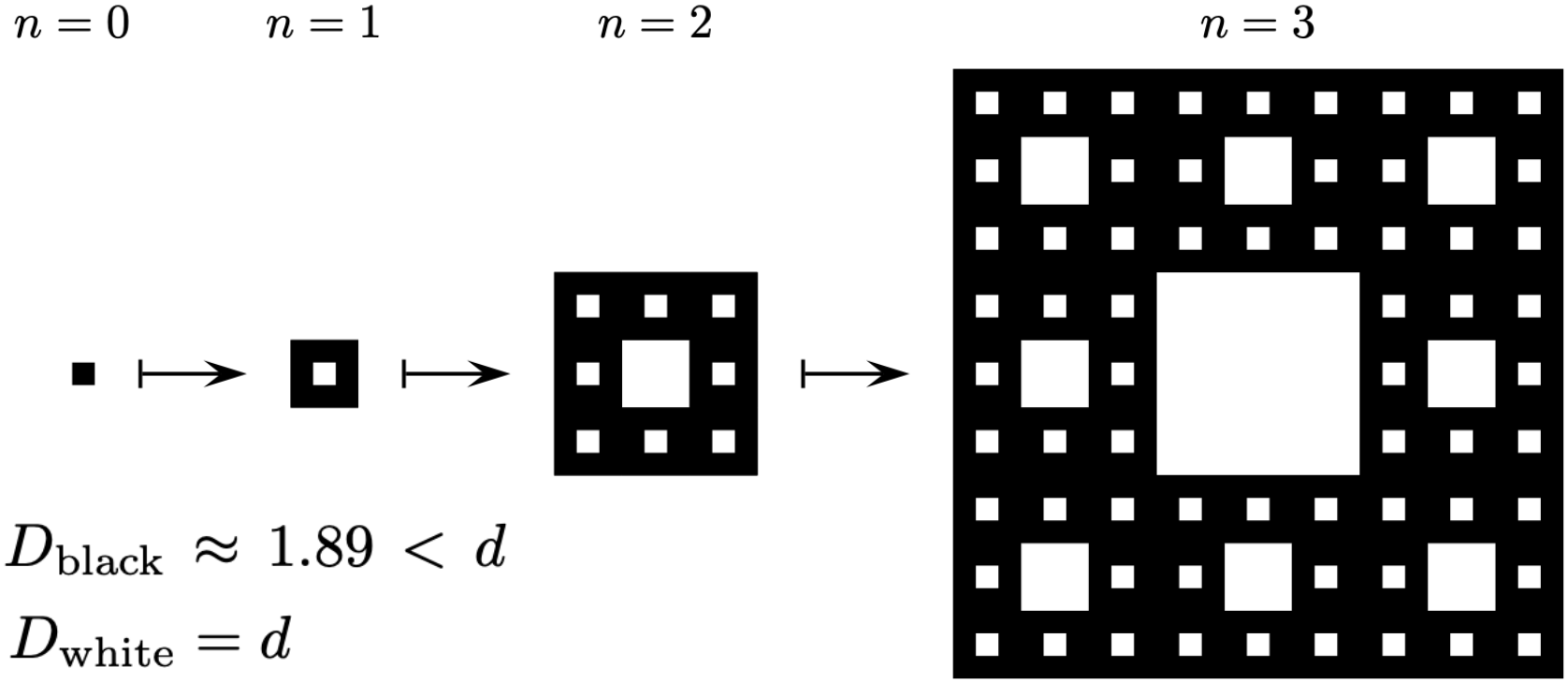

$$D_{\text{black}} \approx 1.89 < d$$

$$D_{\text{white}} = d$$

Table D.1 At iteration n, the linear size $\ell = 3^n$ with a total number of 9^n unit squares of which 8^n are black. The remaining $9^n - 8^n$ unit squares are white.

Iteration	n	0	1	2	3
Linear size ℓ	3^n	1	3	9	27
Total number of unit squares	9^n	1	9	81	729
Number of black unit squares	8^n	1	8	64	512
Number of white unit squares	$9^n - 8^n$	0	1	17	217

Density or prosity

$$\rho(\ell) = \frac{M(\ell)}{\ell^d} \propto \ell^{D-d}$$

$$\rho_{\text{black}} \propto \ell^{-0.11}$$

$$\rho_{\text{white}} \propto \ell^0 = \text{constant}$$

$n = 0$ $n = 1$ $n = 2$ $n = 3$

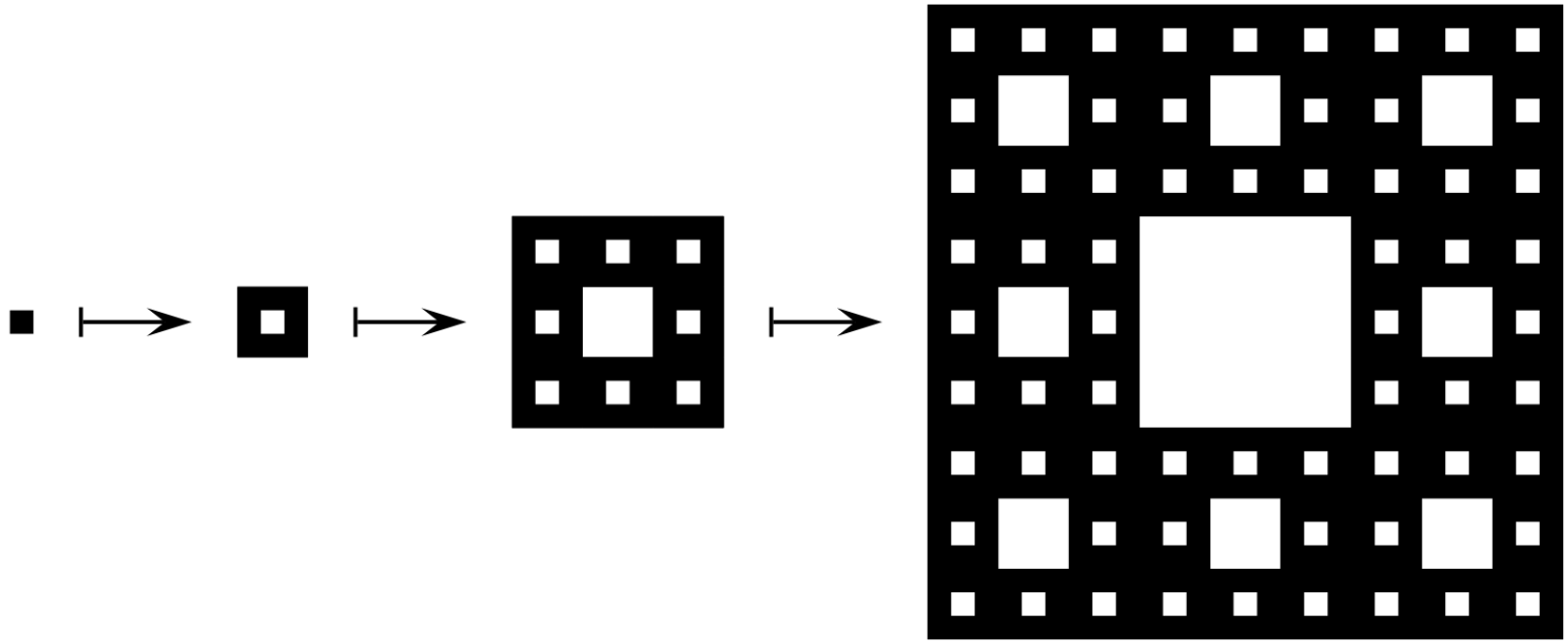

Q.

3차원(d = 3) 다공성 프랙탈 물질 내부의 서로 연결된 구멍들 안에 기름이 존재하는 유전(oil reservoir)을 생각하자. 부피가 0.001 m^3, 0.008 m^3, 0.064 m^3 인 세 샘플에서 측정된 기름의 밀도는 각각 250 kg/m^3, 177 kg/m^3, 125 kg/m^3 이다. 부피가 10^3 km^3 인 유전에서 회수할 수 있는 기름의 양은 얼마인가?

$$\rho(\ell) = \frac{M(\ell)}{\ell^d} \propto \ell^{D-d}$$

$$\frac{\rho_{\text{oil}}(\ell_2)}{\rho_{\text{oil}}(\ell_1)} = \left(\frac{\ell_2}{\ell_1}\right)^{D_{\text{oil}}-d}$$

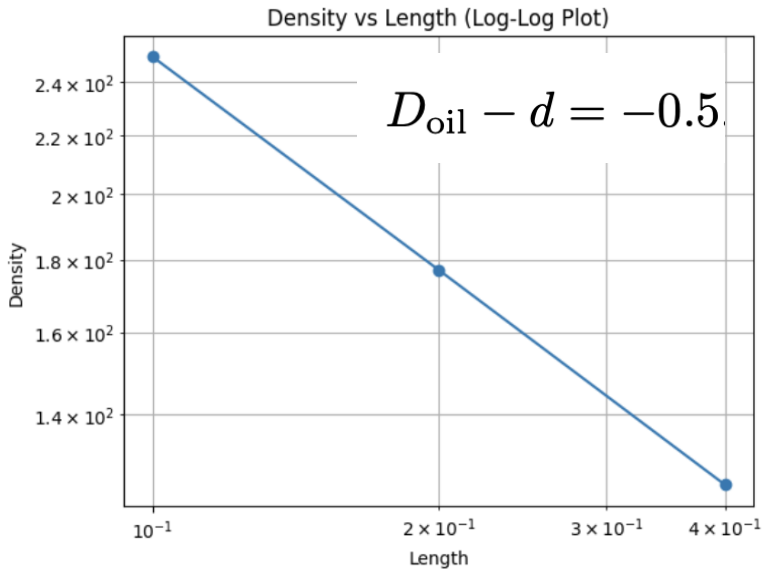

$$\rho_{\text{oil}}(\ell_2) = \left(\frac{\ell_2}{\ell_1}\right)^{D_{\text{oil}}-d} \rho_{\text{oil}}(\ell_1)$$

$$= 100000^{-0.5}\ 250\ \text{kg m}^{-3}$$

$$\approx 0.79\ \text{kg m}^{-3}$$

What is Percolation?

사전적 의미(?)

percolation n
1 여과; 삼출, 삼투
2 퍼컬레이션 ((퍼컬레이터로 커피 끓이기))

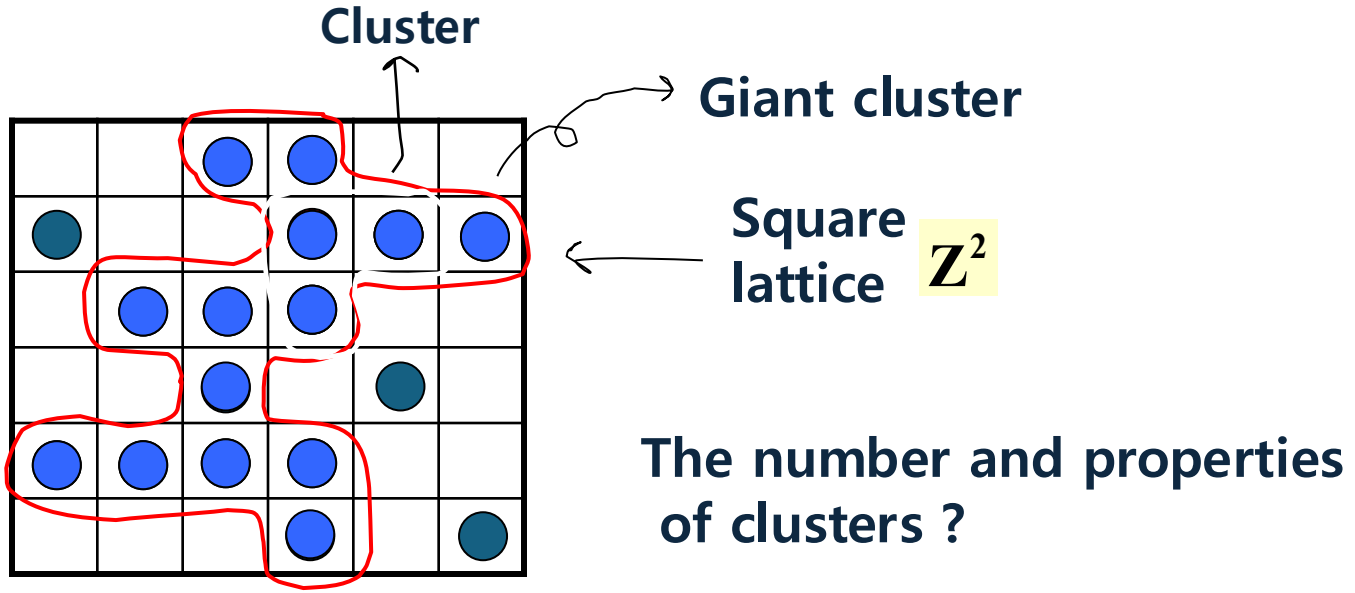

Percolation - First discussed by Hammersley in 1957

A fun example

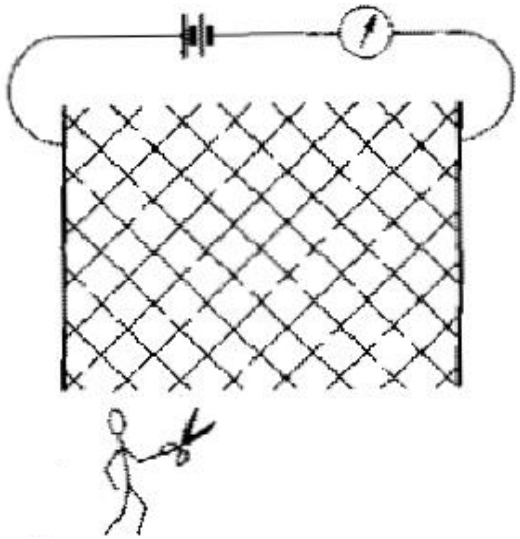

Let's consider a 2D network as shown in left figure. The communication network, represented by a very large square-lattice network of interconnections, is attacked by a crazed saboteur who, armed with wire cutters, proceeds to cut the connecting links at random.

Q. What fraction of the links (or bonds) must be cut in order to electrically isolate the two boundary bars?

A. 50%

Threshold concentration

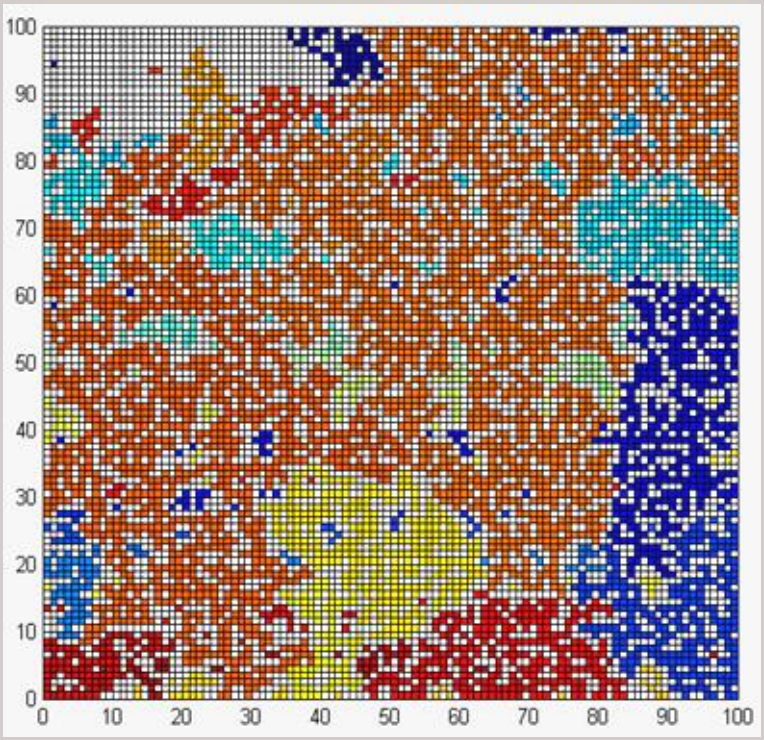

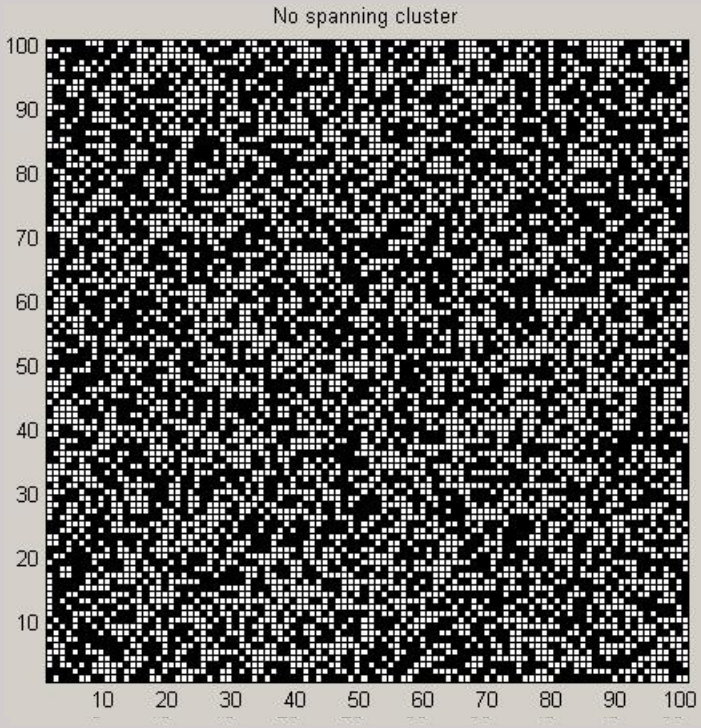

P = 0.6

P = 0.5

- **Threshold concentration (p_c) = 0.5927** (2D square site)

Percolation thresholds

Table 1. Selected percolation thresholds for various lattices. 'Site' refers to site percolation and 'bond' to bond percolation. In all cases, only nearest neighbours form clusters, and no correlations are allowed between different sites or bonds. If the result is not exact (see text), the error probably affects only the last decimal.

Lattice	Site	Bond
Honeycomb	0·6962	0·65271
Square	0·592746	0·50000
Triangular	0·500000	0·34729
Diamond	0·43	0·388
Simple cubic	0·3116	0·2488
BCC	0·246	0·1803
FCC	0·198	0·119
$d = 4$ hypercubic	0·197	0·1601
$d = 5$ hypercubic	0·141	0·1182
$d = 6$ hypercubic	0·107	0·0942
$d = 7$ hypercubic	0·089	0·0787

In finite systems as simulated on a computer one does not have in general a sharply defined threshold; any effective threshold values obtained numerically or experimentally need to be extrapolated carefully to infinite system size.

Thermodynamic limit - physicist

Mathematically exact ?

Exact percolation threshold P_c

Bethe lattice (with z branch) = $\frac{1}{z-1}$

1 D chain = 1

square bond percolation = 1/2

triangular site percolation = 1/2

triangular bond percolation = $2\sin(\frac{\pi}{18})$

honeycomb bond percolation = $1-2\sin(\frac{\pi}{18})$

honeycomb site percolation $\leq$ $1/\sqrt{2}$

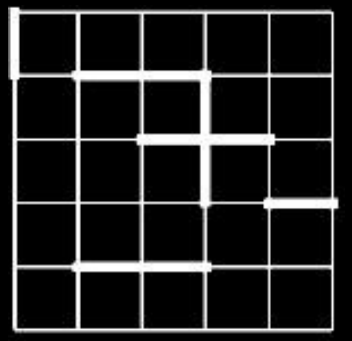

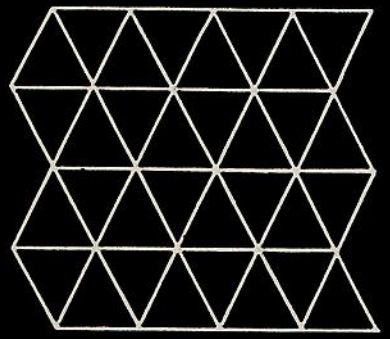

For square site percolation and 3D percolation, no plausible guess for exact result.

Percolation Phase Transition

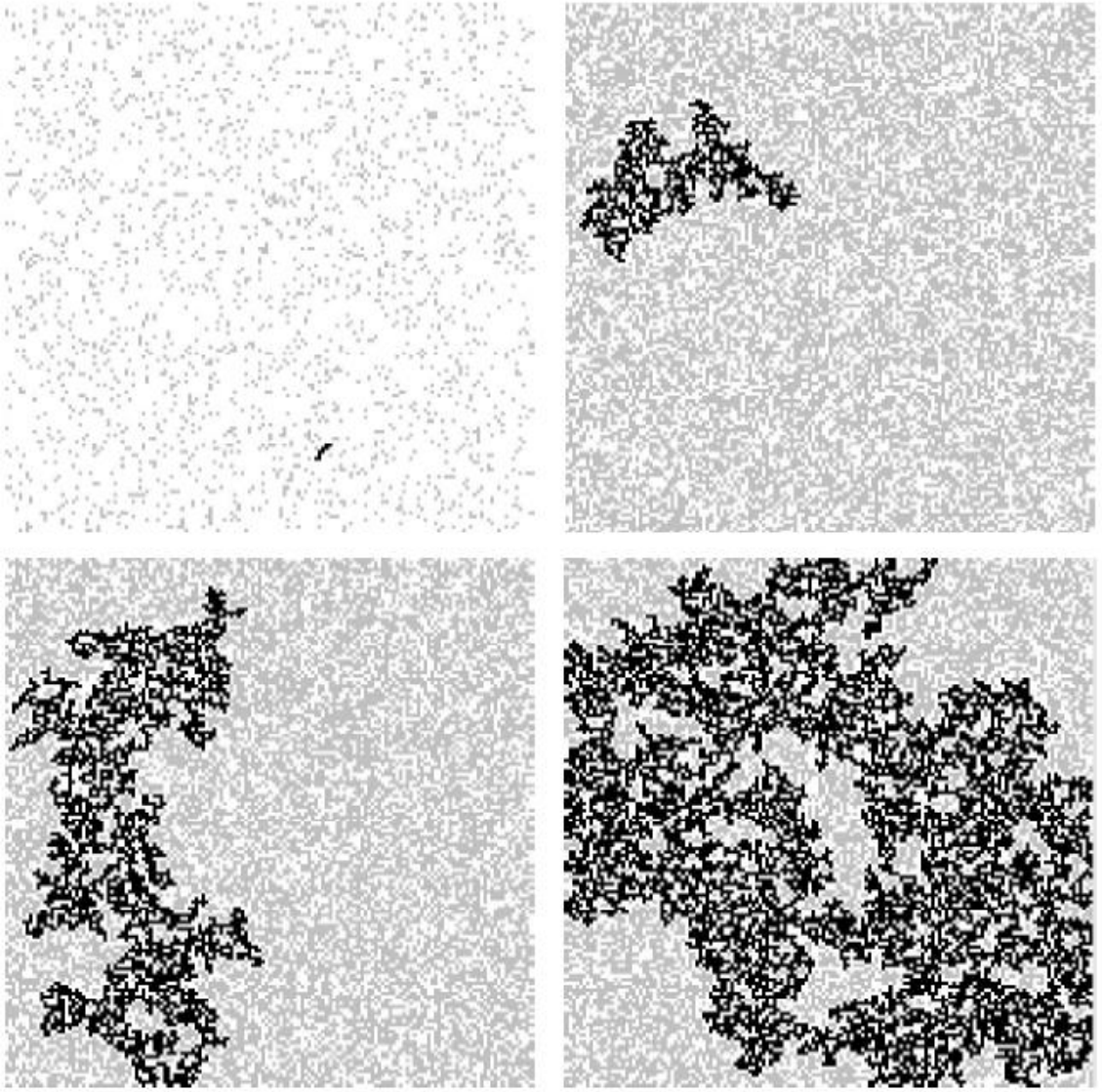

K. Christensen and R. Moloney, “Complexity and Criticality” (2005).

Percolation Theory

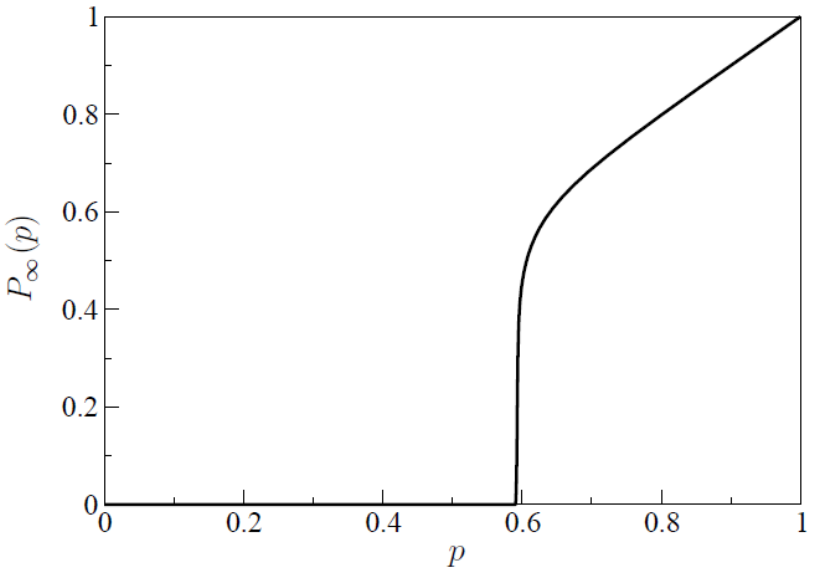

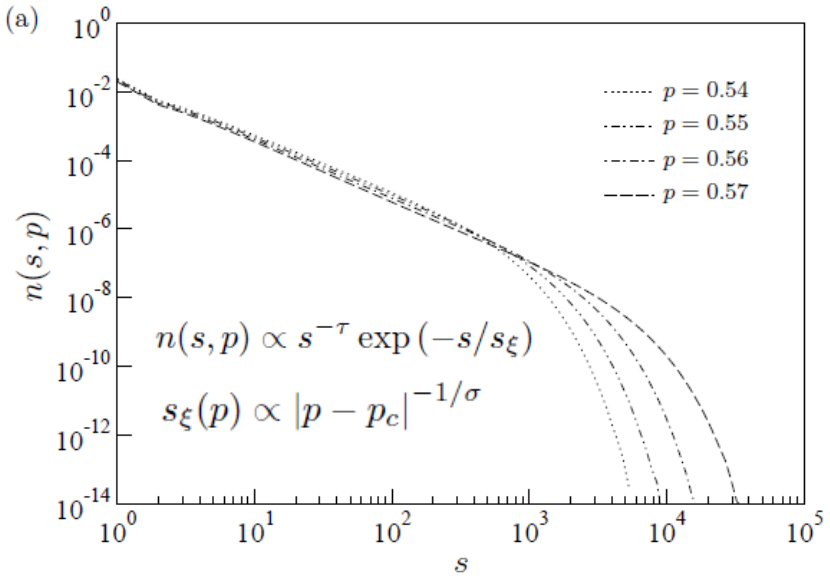

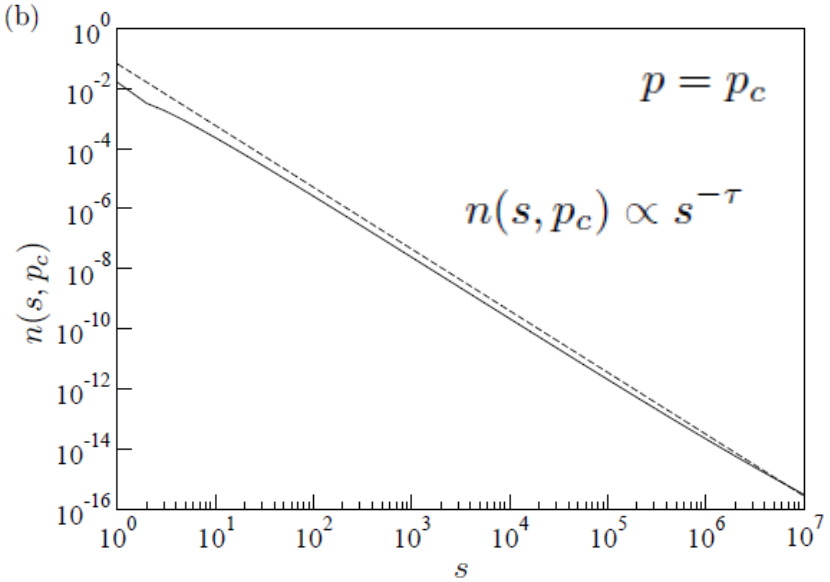

P_∞ : probability that any given site belongs to the infinite (giant) cluster

$$P_\infty(p) \propto (p - p_c)^\beta \quad \text{for } p \to p_c^+$$

n_s : density of clusters of size s

number of clusters of size s per lattice site

$$\sum_{s=1}^{\infty} s n(s,p) = p \quad \text{for } p < 1$$

1st moment of cluster size

Percolation Theory

n_s : density of clusters of size s

number of clusters of size s per lattice site

$$\sum_s n_s s = p \quad (p < p_c)$$

1st moment of cluster size

For $p \ll p_c$ $\quad n_s \propto e^{-cs} \quad c = f(p)$

For $p = p_c$ $\quad n_s \propto s^{-\tau}$

$$n_s \propto s^{-\tau} e^{-cs} \qquad c \propto |p - p_c|^{1/\sigma} \quad (p \to p_c)$$

P_∞ : probability that any given site belongs to the infinite cluster

$$P_\infty + \sum_s s n_s = p$$

$$P_\infty = 0 \quad (p < p_c)$$

$$P_\infty \propto |p - p_c|^{\beta} \qquad p = p_c + \varepsilon$$

Susceptibility

2nd moment of cluster size

$$\chi(p) = \frac{\sum_{s=1}^{\infty} s^2 n(s,p)}{\sum_{s=1}^{\infty} s n(s,p)}$$: average cluster size S

(percolation susceptibility)

$$\chi(p) \propto |p - p_c|^{-\gamma} \quad \text{for } p \to p_c$$

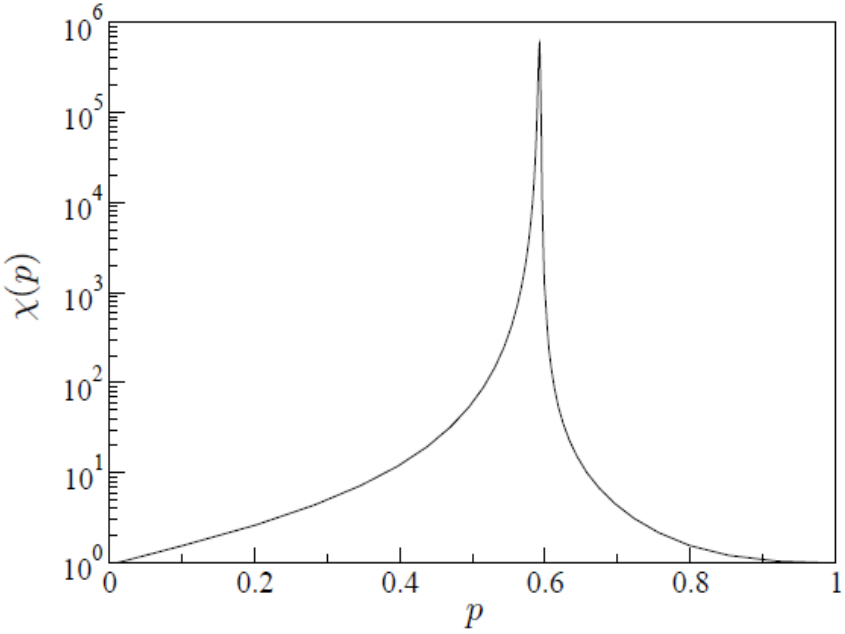

$$\chi(p) = \frac{\sum_{s=1}^{\infty} s^2 n(s,p)}{\sum_{s=1}^{\infty} s n(s,p)}$$

$$\propto \sum_{s=1}^{\infty} s^{2-\tau} \exp\left(-s/s_\xi\right)$$

$$\approx \int_1^{\infty} s^{2-\tau} \exp\left(-s/s_\xi\right)\, ds$$

$$= \int_{1/s_\xi}^{\infty} (u s_\xi)^{2-\tau} \exp(-u) s_\xi \, du \quad \text{with } u = s/s_\xi$$

$$= s_\xi^{3-\tau} \int_{1/s_\xi}^{\infty} u^{2-\tau} \exp(-u)\, du,$$

$$n(s,p) \propto s^{-\tau} \exp\left(-s/s_\xi\right)$$

$$s_\xi(p) \propto |p - p_c|^{-1/\sigma}$$

$$\chi(p) = s_\xi^{3-\tau}\, \Gamma(3-\tau)$$

$$\propto |p - p_c|^{-(3-\tau)/\sigma}$$

$$\propto |p - p_c|^{-\gamma}$$

$$\gamma = \frac{3-\tau}{\sigma}$$

Susceptibility

2nd moment of cluster size

$$\chi(p) = \frac{\sum_{s=1}^{\infty} s^2 n(s,p)}{\sum_{s=1}^{\infty} s n(s,p)}$$: average cluster size S

(percolation susceptibility)

$$\chi(p) \propto |p - p_c|^{-\gamma} \quad \text{for } p \to p_c$$

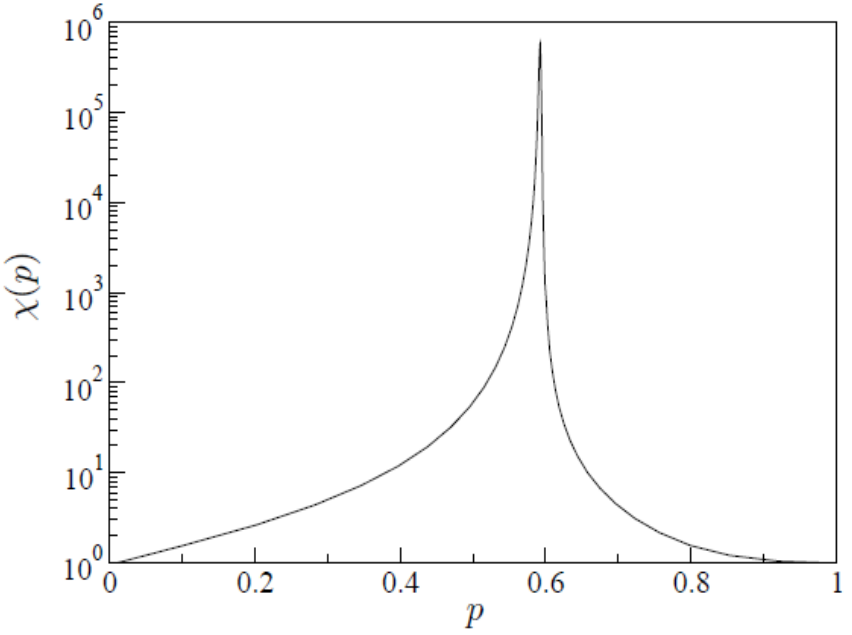

correlation length

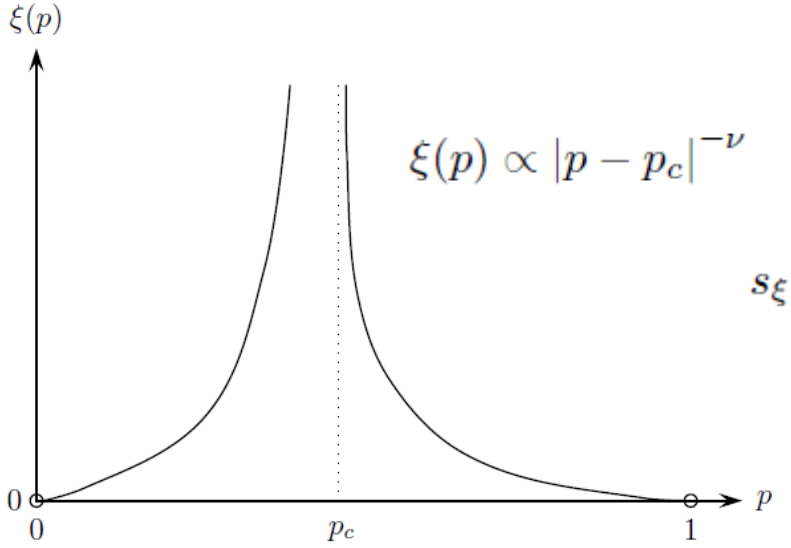

$$\xi(p) \propto |p - p_c|^{-\nu}$$

$$s_\xi \propto \xi^D$$

$$\propto |p - p_c|^{-D\nu} \quad \text{for } p \to p_c$$

$$\propto |p - p_c|^{-1/\sigma} \quad \text{for } p \to p_c$$

$$D = \frac{1}{\nu\sigma}$$

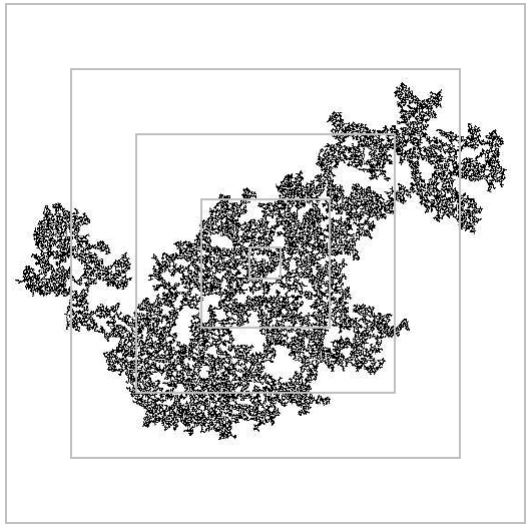

Percolation Theory

$$S = \frac{\sum_s s^2 n_s}{\sum_s s n_s} \propto \sum_s s^2 n_s$$: average cluster size S (Percolation susceptibility)

2nd moment of cluster size

$$\propto C_- |p - p_c|^{-\gamma} \qquad (p < p_c)$$

$$\propto C_+ |p - p_c|^{-\gamma'} \qquad (p > p_c)$$

$$\gamma = \gamma' \;\; ; \quad R = \frac{C_-}{C_+} \qquad \text{universal}$$

Percolation specific heat

Consider the Gibbs free energy as the singular part of the zeroth moment of cluster size distribution.

$$G_S(p) = \left[\sum_s n_s(p) \right]_{\text{sing}}$$

zeroth moment of cluster size

$$M_0 = \sum_s s^0 n_s = \sum_s n_s \propto |p - p_c|^{2-\alpha}$$

Percolation correlation length $\xi \propto |p - p_c|^{-\gamma}$

Critical Percolation Thresholds

Table 1.1 The critical occupation probabilities for various lattice types and dimensions in site and bond percolation. The current best estimates for the critical occupation probabilities, which are not known exactly, are given in decimal form. The second column lists the coordination number, z (the number of nearest neighbours) for a given lattice.

Lattice	z	Site percolation	Bond percolation
$d = 1$ line	2	1	1
$d = 2$ hexagonal	3	0.6971^{a}	$1 - 2\sin(\pi/18)^{b,c}$
square	4	0.59274621^{d}	$1/2^{b,e}$
triangular	6	$1/2^{b}$	$2\sin(\pi/18)^{b,c}$
$d = 3$ diamond	4	0.4301^{f}	0.3893^{a}
simple cubic	6	0.3116080^{g}	0.2488126^{h}
body-centred cubic	8	0.2459615^{g}	0.1802875^{h}
face-centred cubic	12	0.1992365^{g}	0.1201635^{h}
$d = 4$ hypercubic	8	0.196889^{i}	0.160130^{i}
$d = 5$ hypercubic	10	0.14081^{i}	0.118174^{i}
$d = 6$ hypercubic	12	0.1090^{j}	0.09420^{k}
$d = 7$ hypercubic	14	0.08893^{l}	0.078685^{k}
Bethe	z	$1/(z-1)^{m}$	$1/(z-1)^{m}$

K. Christensen and R. Moloney, “Complexity and Criticality” (2005

Universal Critical Exponents

Exponent: Quantity	$d=1$	$d=2$	$d=3$	$d=4$	$d=5$	$d\geq 6$	Bethe
$\beta:\ P_\infty(p)\propto(p-p_c)^\beta$	0 (dis)	5/36	0.4181(8)	0.657(9)	0.830(10)	1	1
$\gamma:\ \chi(p)\propto\lvert p-p_c\rvert^{-\gamma}$	1	43/18	1.793(3)	1.442(16)	1.185(5)[a]	1	1
$\nu:\ \xi(p)\propto\lvert p-p_c\rvert^{-\nu}$	1	4/3[b]	0.8765(16)	0.689(10)[c]	0.569(5)	1/2	1/2
$\sigma:\ s_\xi(p)\propto\lvert p-p_c\rvert^{-1/\sigma}$	1	36/91	0.4522(8)[d]	0.476(5)	0.496(4)	1/2	1/2
$\tau:\ n(s,p)\propto s^{-\tau}\mathcal{G}(s/s_\xi)$	2	187/91	2.18906(6)[d]	2.313(3)[e]	2.412(4)[e]	5/2	5/2
$D:\ s_\xi\propto\xi^D$	1	91/48[b]	2.523(6)	3.05(5)	3.54(4)	4	4

$$\beta=\frac{\tau-2}{\sigma} \qquad \gamma=\frac{3-\tau}{\sigma} \qquad D=\frac{1}{\nu\sigma} \qquad D-d=-\frac{\beta}{\nu}$$

Scaling Relations!

K. Christensen and R. Moloney, “Complexity and Criticality” (2005).

Scaling function

$$n(s,p) \propto s^{-\tau}\mathcal{G}(s/s_\xi) \quad \text{for } p \to p_c, s \gg 1,$$

$$s_\xi(p) \propto |p - p_c|^{-1/\sigma} \quad \text{for } p \to p_c,$$

$$\mathcal{G}(s/s_\xi) \propto s^\tau n(s,p) \quad s \gg 1$$

(a)

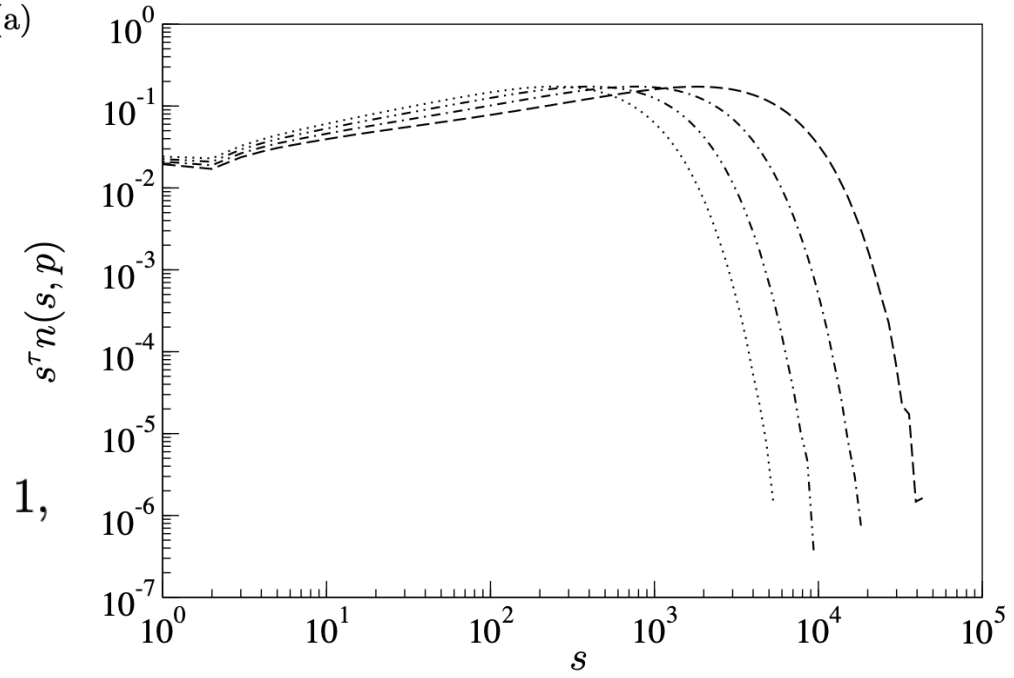

(b)

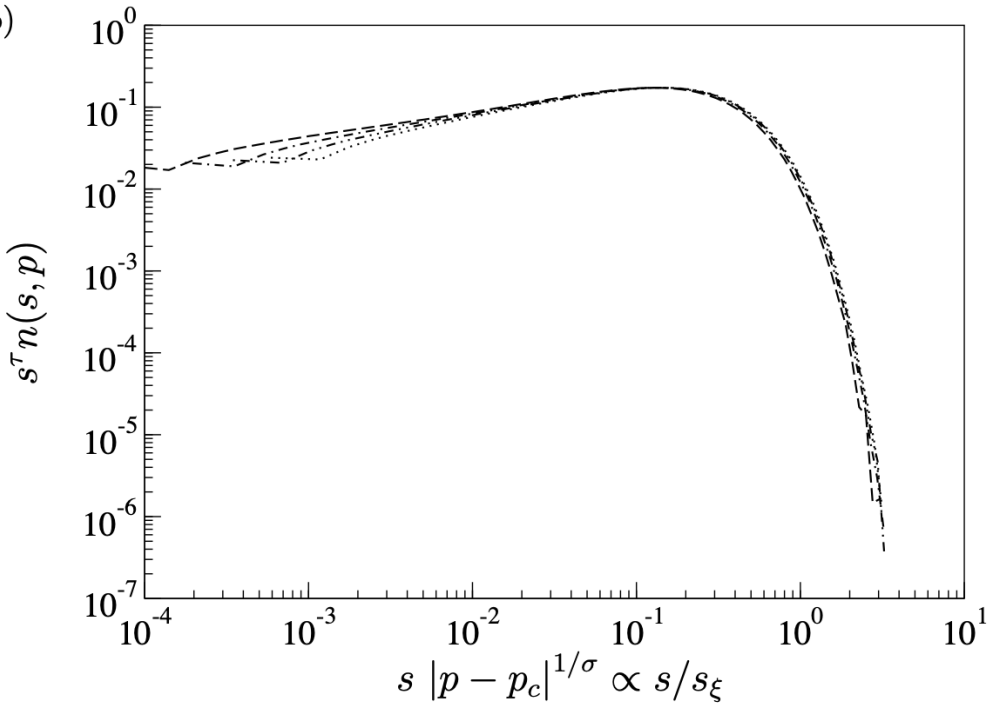

$P_\infty(p) \propto (p - p_c)^\beta \quad \text{for } p \to p_c^+$

$P_\infty + \sum_s sn_s = p$

$$P_\infty(p) = p - \sum_{s=1}^{\infty} sn(s,p)$$

$$= p_c - \sum_{s=1}^{\infty} sn(s,p) + (p - p_c)$$

$$= \sum_{s=1}^{\infty} sn(s,p_c) - \sum_{s=1}^{\infty} sn(s,p) + (p - p_c)$$

$$P_\infty(p) = \sum_{s=1}^{\infty} [sn(s,p_c) - sn(s,p)] + (p - p_c)$$

$$\propto \sum_{s=1}^{\infty} s^{1-\tau} [\mathcal{G}(0) - \mathcal{G}(s/s_\xi)] + (p - p_c).$$

$$P_\infty(p) \propto \int_1^\infty s^{1-\tau}[\mathcal{G}(0) - \mathcal{G}(s/s_\xi)]\, ds + (p - p_c)$$

$$\propto \int_{1/s_\xi}^\infty (u s_\xi)^{1-\tau}[\mathcal{G}(0) - \mathcal{G}(u)] s_\xi\, du + (p - p_c) \quad \text{with } u = s/s_\xi$$

$$\propto s_\xi^{2-\tau} \int_{1/s_\xi}^\infty u^{1-\tau}[\mathcal{G}(0) - \mathcal{G}(u)]\, du + (p - p_c)$$

$$P_\infty(p) \propto s_\xi^{2-\tau} \int_0^\infty u^{1-\tau}[\mathcal{G}(0) - \mathcal{G}(u)]\, du + (p - p_c)$$

$$\propto (p - p_c)^{(\tau-2)/\sigma} \int_0^\infty u^{1-\tau}[\mathcal{G}(0) - \mathcal{G}(u)]\, du + (p - p_c)$$

$$P_\infty(p) \propto (p - p_c)^{(\tau-2)/\sigma} \propto (p - p_c)^\beta \qquad \beta = \frac{\tau - 2}{\sigma}$$

(a)

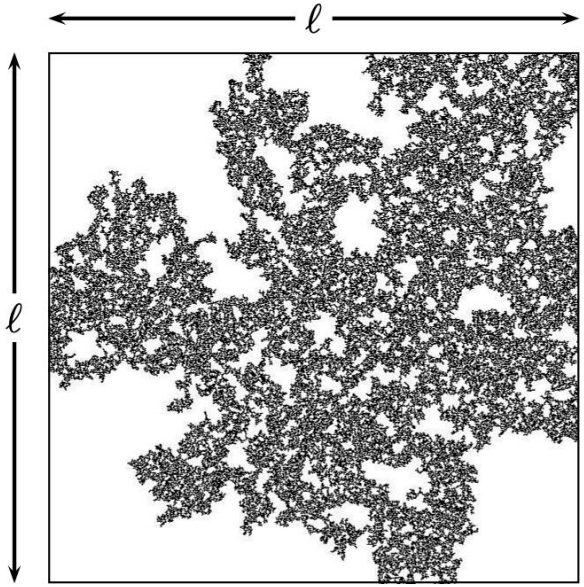

$$P_\infty(p;\ell) = \frac{M_\infty(p;\ell)}{\ell^2}$$

$$M_\infty(p_c;\ell) \propto \ell^D \qquad D = 91/48 \approx 1.90$$

(b)

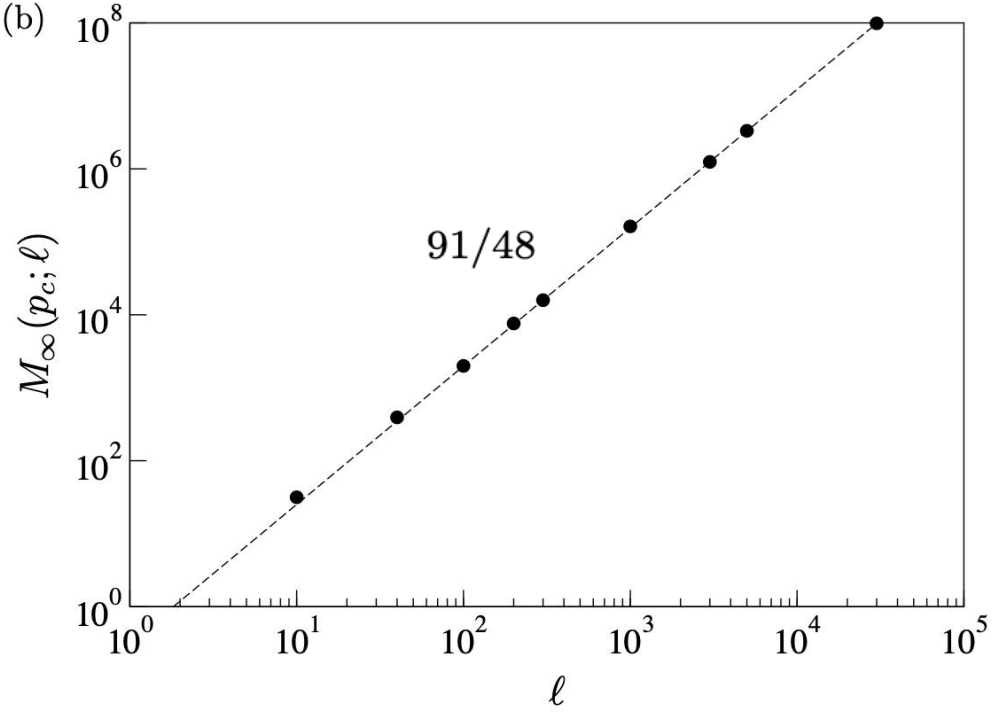

$$P_\infty(p_c;\ell) = \frac{M_\infty(p_c;\ell)}{\ell^2} \propto \ell^{D-d}$$

Self-similarity

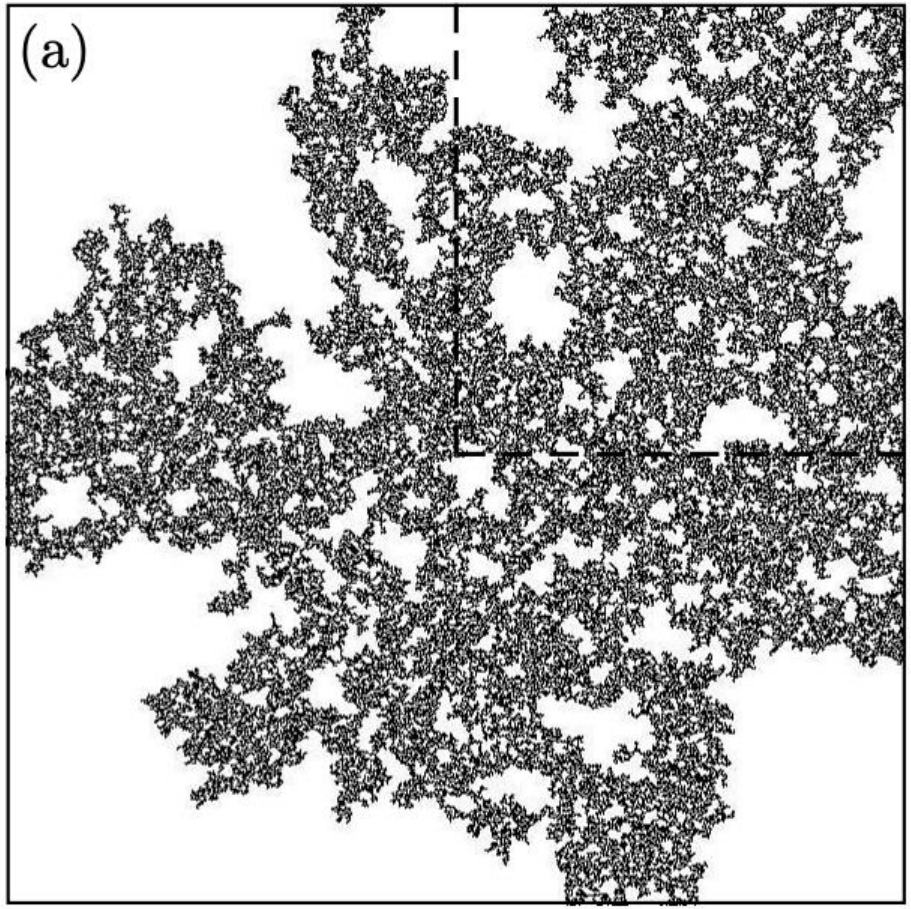

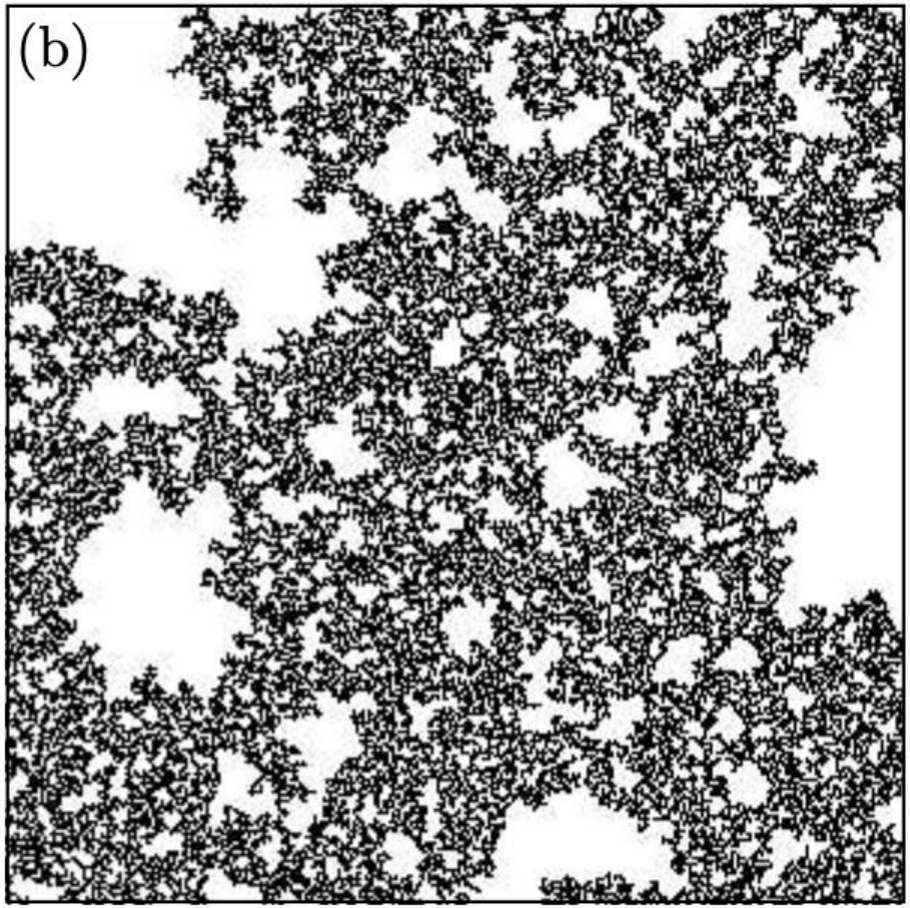

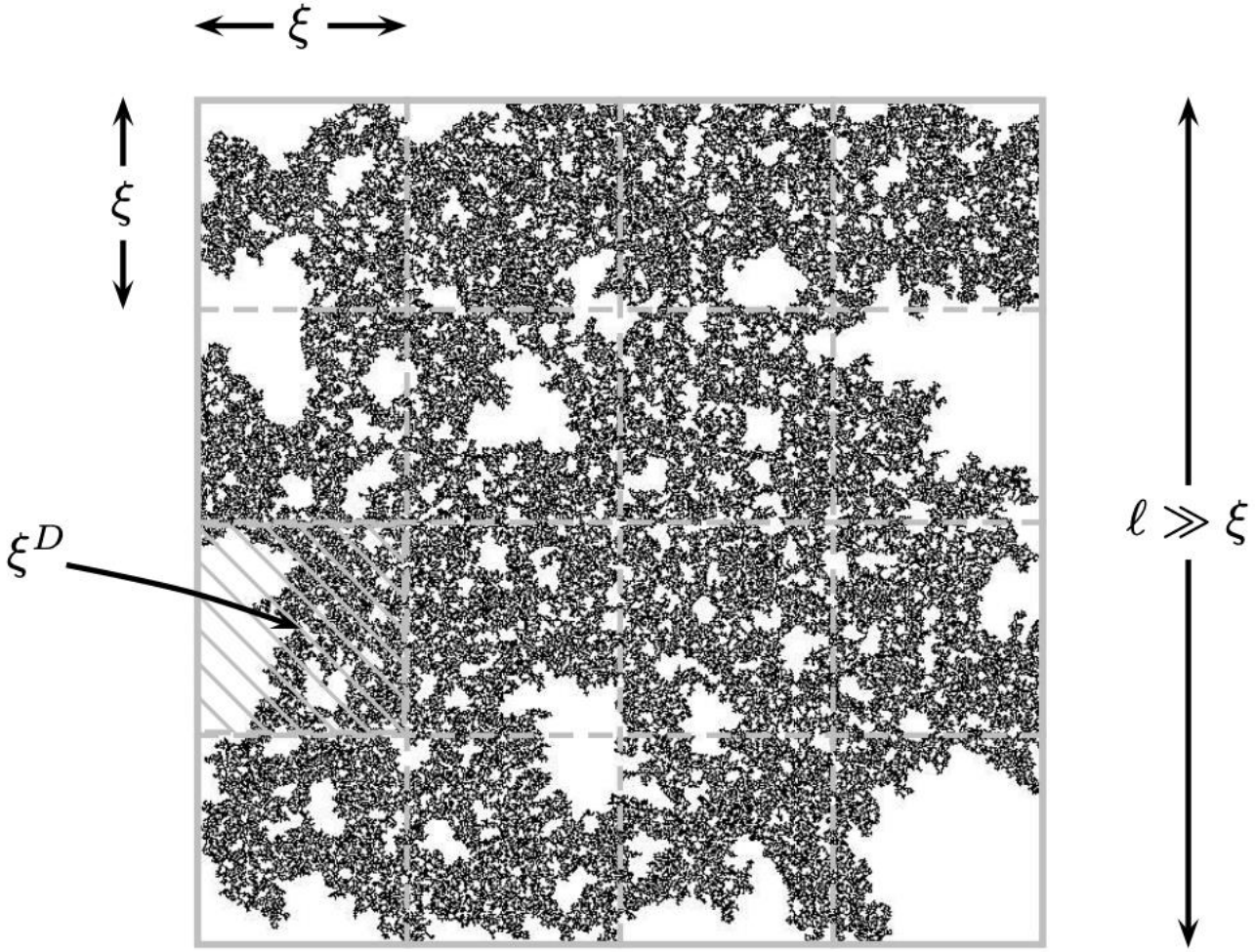

$$M_\infty(\xi;\ell) \propto (\ell/\xi)^d \xi^D \quad \text{for } \ell \gg \xi$$
$$= \xi^{D-d}\ell^d \quad \text{for } \ell \gg \xi$$

$$P_\infty(p_c;\ell) = \frac{M_\infty(p_c;\ell)}{\ell^2} \propto \ell^{D-d}$$

$$\begin{aligned} M_\infty(\xi;\ell) &= P_\infty(p;\ell)\ell^d \\ &= P_\infty(p)\ell^d && \text{for } \ell \gg \xi \\ &\propto (p-p_c)^\beta \ell^d && \text{for } \ell \gg \xi, p \to p_c^+ \\ &\propto \xi^{-\beta/\nu}\ell^d && \text{for } \ell \gg \xi, p \to p_c^+ \end{aligned}$$

$$\xi(p) \propto |p-p_c|^{-\nu}$$

$$\begin{aligned} M_\infty(\xi;\ell) &\propto (\ell/\xi)^d \xi^D && \text{for } \ell \gg \xi \\ &= \xi^{D-d}\ell^d && \text{for } \ell \gg \xi \end{aligned}$$

$$D - d = -\frac{\beta}{\nu}$$

$$M_\infty(\xi;\ell) \propto \begin{cases} \ell^D & \text{for } \ell \ll \xi \\ \ell^D (\ell/\xi)^{d-D} & \text{for } \ell \gg \xi \end{cases}$$

$$P_\infty(\xi;\ell) = \frac{M_\infty(\xi;\ell)}{\ell^d} \propto \begin{cases} \ell^{D-d} & \text{for } \ell \ll \xi \\ \xi^{D-d} & \text{for } \ell \gg \xi \end{cases}$$

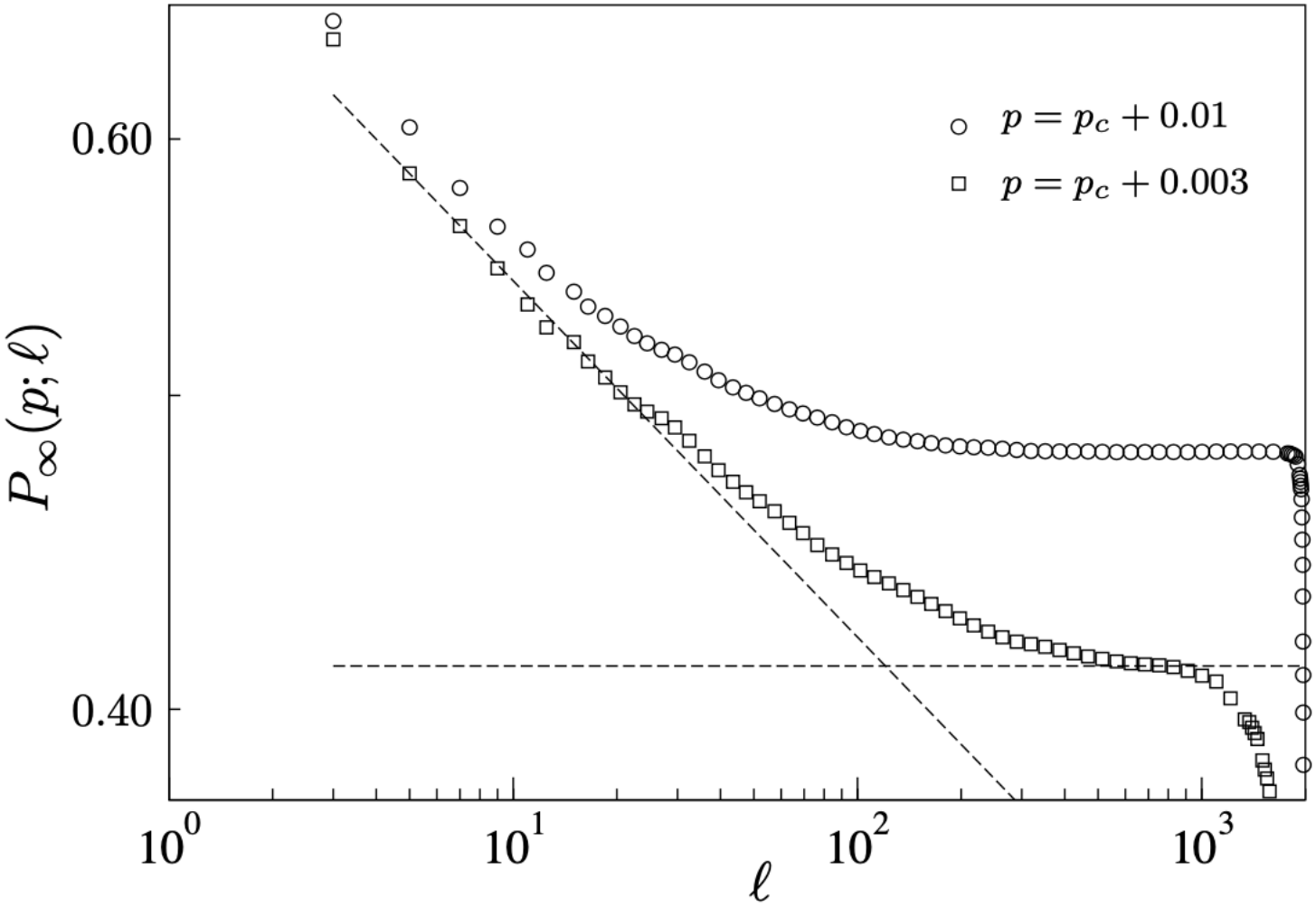

Scaling Relations

Near $p = p_c$

$$\beta = \frac{\tau - 2}{\sigma} \qquad \gamma = \frac{3 - \tau}{\sigma} \qquad 2 - \alpha = \frac{\tau - 1}{\sigma} = 2\beta + \gamma \qquad D = d - \frac{\beta}{\nu}$$

Exact results on a Bethe Lattice (Cayley tree)

$$p_c = \frac{1}{z - 1}\,, \quad \tau = \frac{5}{2}\,, \quad \sigma = \frac{1}{2}\,, \quad \gamma = 1\,, \quad \beta = 1$$

Finite size scaling

$$\xi(p) \propto |p - p_c|^{-\nu}$$

$$P_\infty(p) \propto (p - p_c)^\beta \propto \xi^{-\beta/\nu} \quad \text{for } p \to p_c^+$$

$$P_\infty(\xi; \ell) = \frac{M_\infty(\xi; \ell)}{\ell^d} \propto \begin{cases} \ell^{D-d} & \text{for } \ell \ll \xi \\ \xi^{D-d} & \text{for } \ell \gg \xi \end{cases}$$

$$D - d = -\frac{\beta}{\nu}$$

$$P_\infty(p; L) \propto \begin{cases} \xi^{-\beta/\nu} & \text{for } L \gg \xi \\ L^{-\beta/\nu} & \text{for } 1 \ll L \ll \xi \end{cases}$$

$$P_\infty(p;L) \propto \begin{cases} \xi^{-\beta/\nu} & \text{for } L \gg \xi \\ L^{-\beta/\nu} & \text{for } 1 \ll L \ll \xi \end{cases}$$

$$\xi(p) \propto |p - p_c|^{-\nu}$$

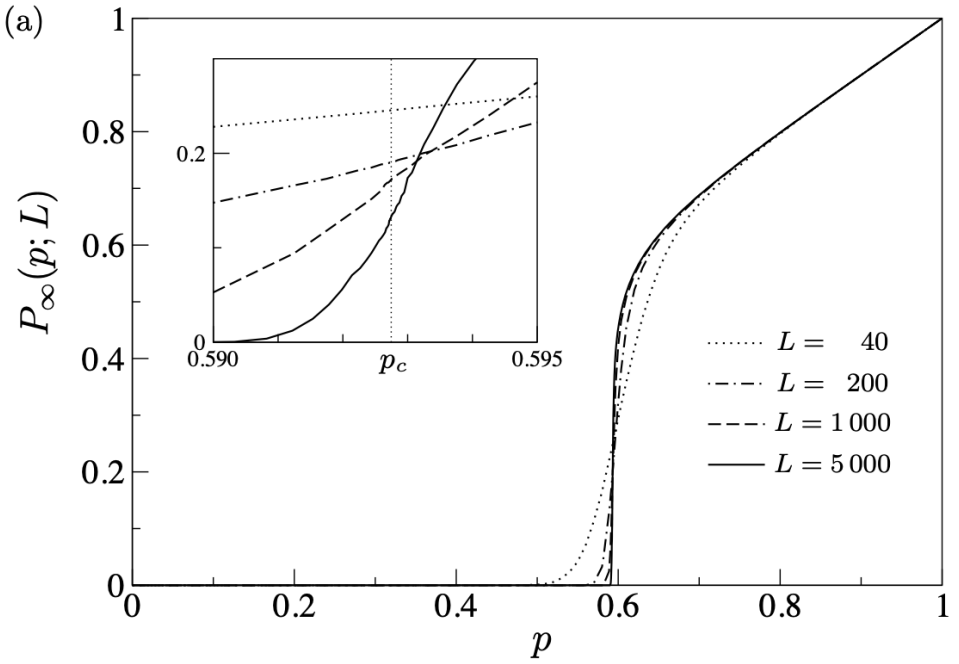

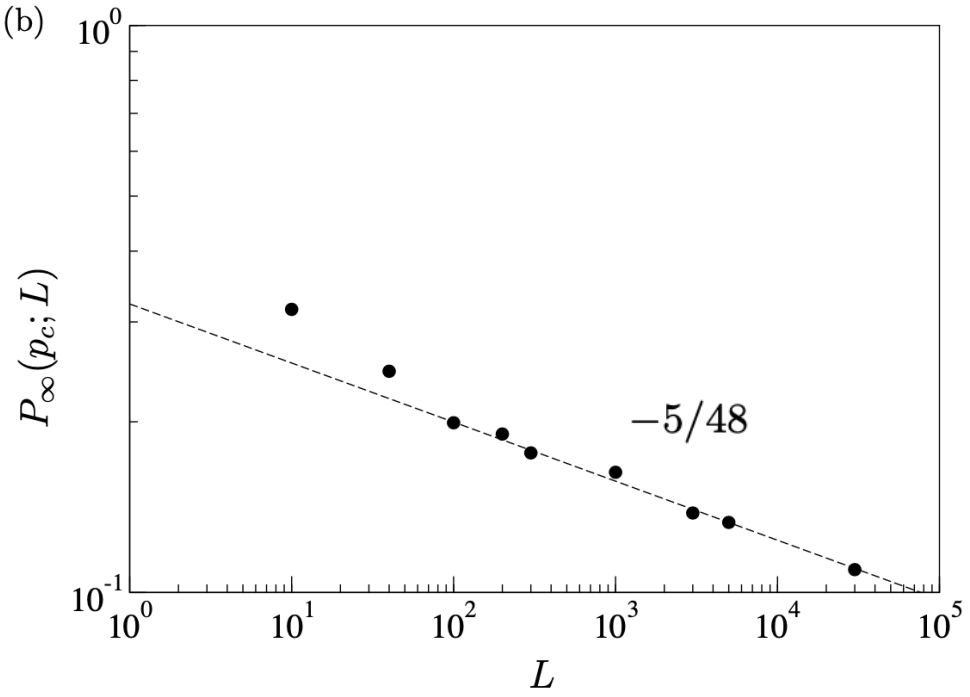

$$\chi(p) \propto |p - p_c|^{-\gamma} \quad \text{for } p \to p_c$$
$$\propto \xi^{\gamma/\nu} \quad \text{for } p \to p_c$$

$$\xi(p) \propto |p - p_c|^{-\nu}$$

$$\chi(p; L) \propto \begin{cases} \xi^{\gamma/\nu} & \text{for } L \gg \xi \\ L^{\gamma/\nu} & \text{for } 1 \ll L \ll \xi \end{cases}$$

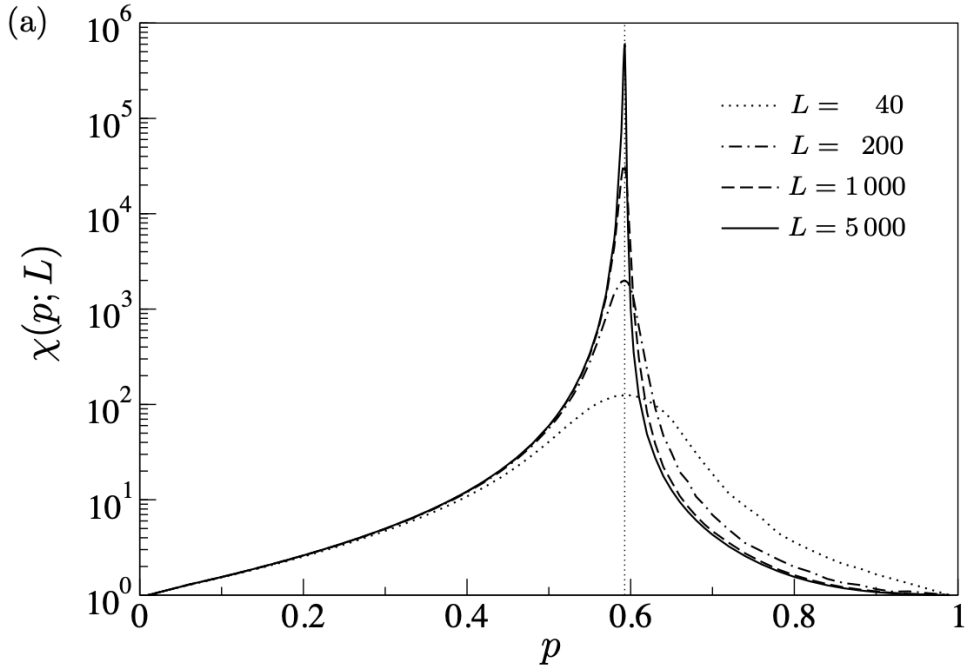

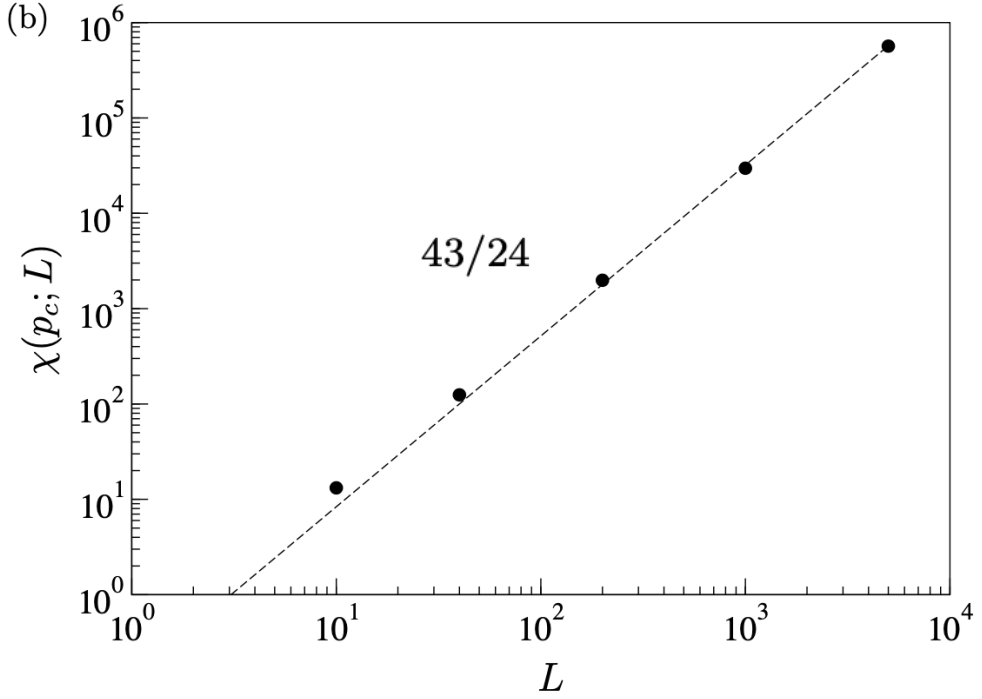

$$n(s,p;L) \propto \begin{cases} s^{-\tau}\mathcal{G}(s/\xi^D) & \text{for } p \to p_c, s \gg 1, L \gg \xi \\ s^{-\tau}\tilde{\mathcal{G}}(s/L^D) & \text{for } p \to p_c, s \gg 1, 1 \ll L \ll \xi \end{cases}$$

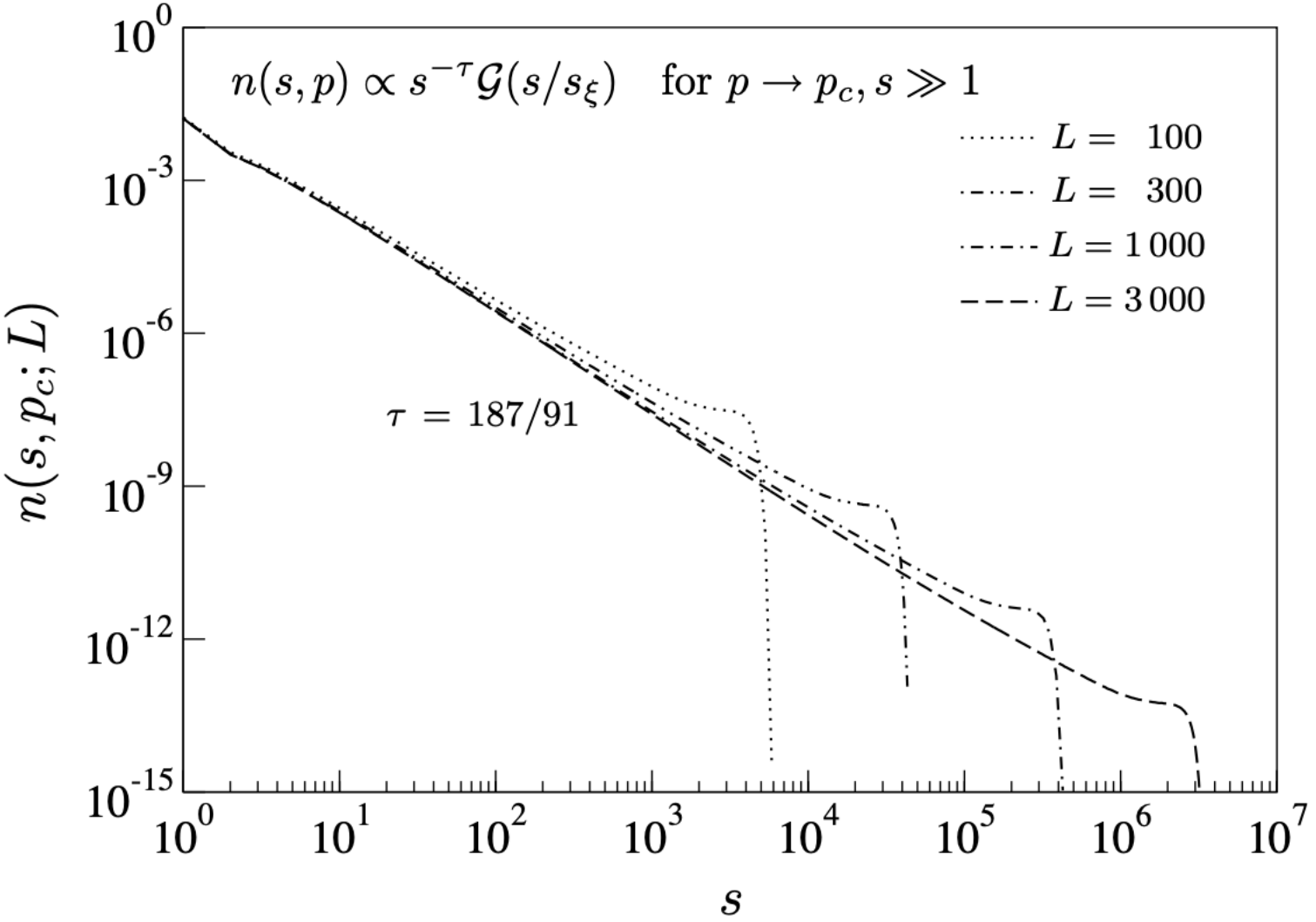

$$n(s, p_c; L) \propto s^{-\tau} \tilde{\mathcal{G}}(s/L^D)$$

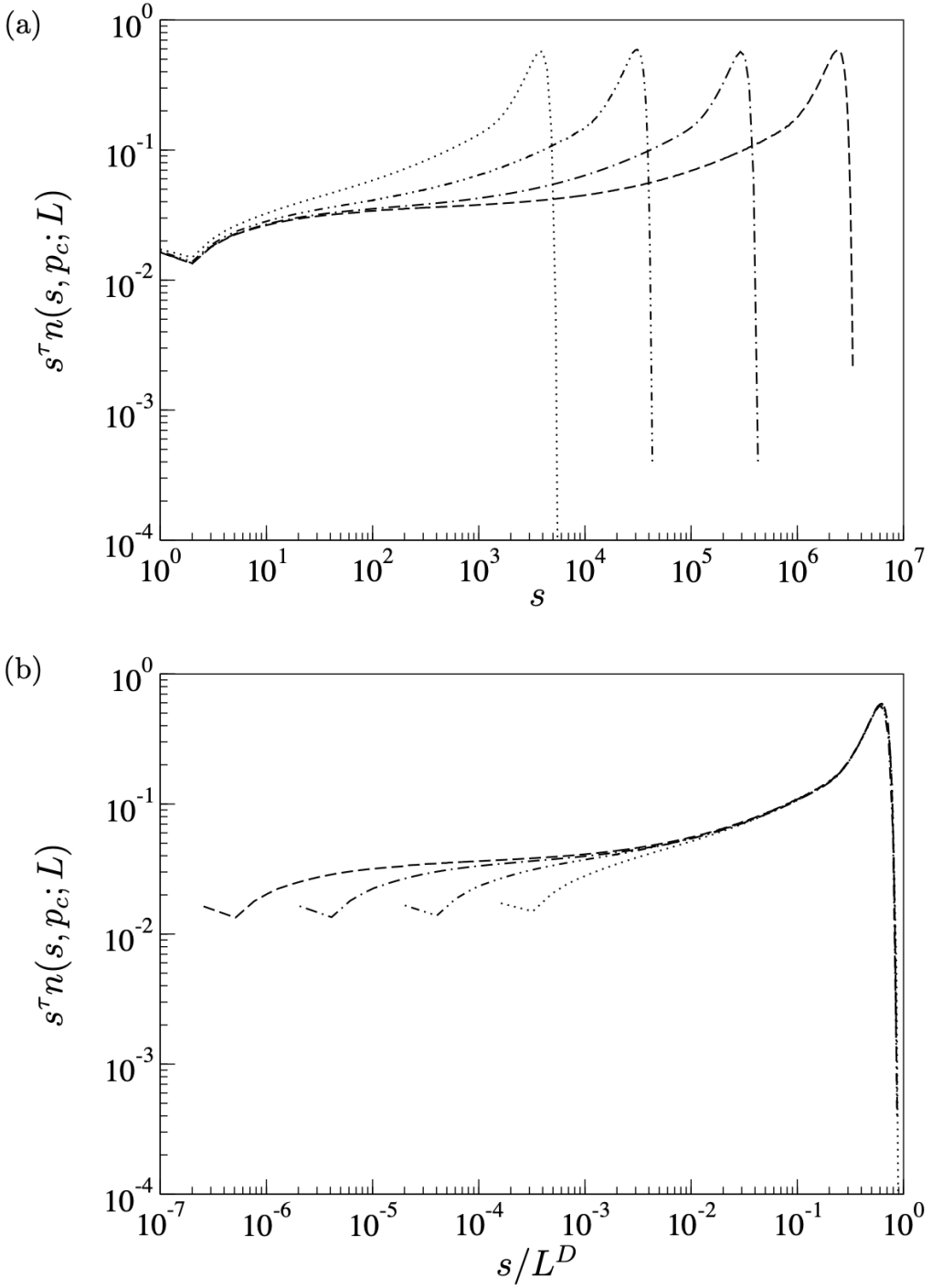

Real-space renormalisation group procedure

We now outline a three-step procedure to perform a real-space renormalisation group transformation

(1) Divide the lattice into blocks of linear size b (in terms of the lattice constant) with each block containing at least a few sites.

(2) Replace each block of sites by a single block site of size b which is occupied with probability $R_b(p)$ according to the renormalisation group transformation.

(3) Rescale all lengths by the factor b to restore the original lattice spacing.

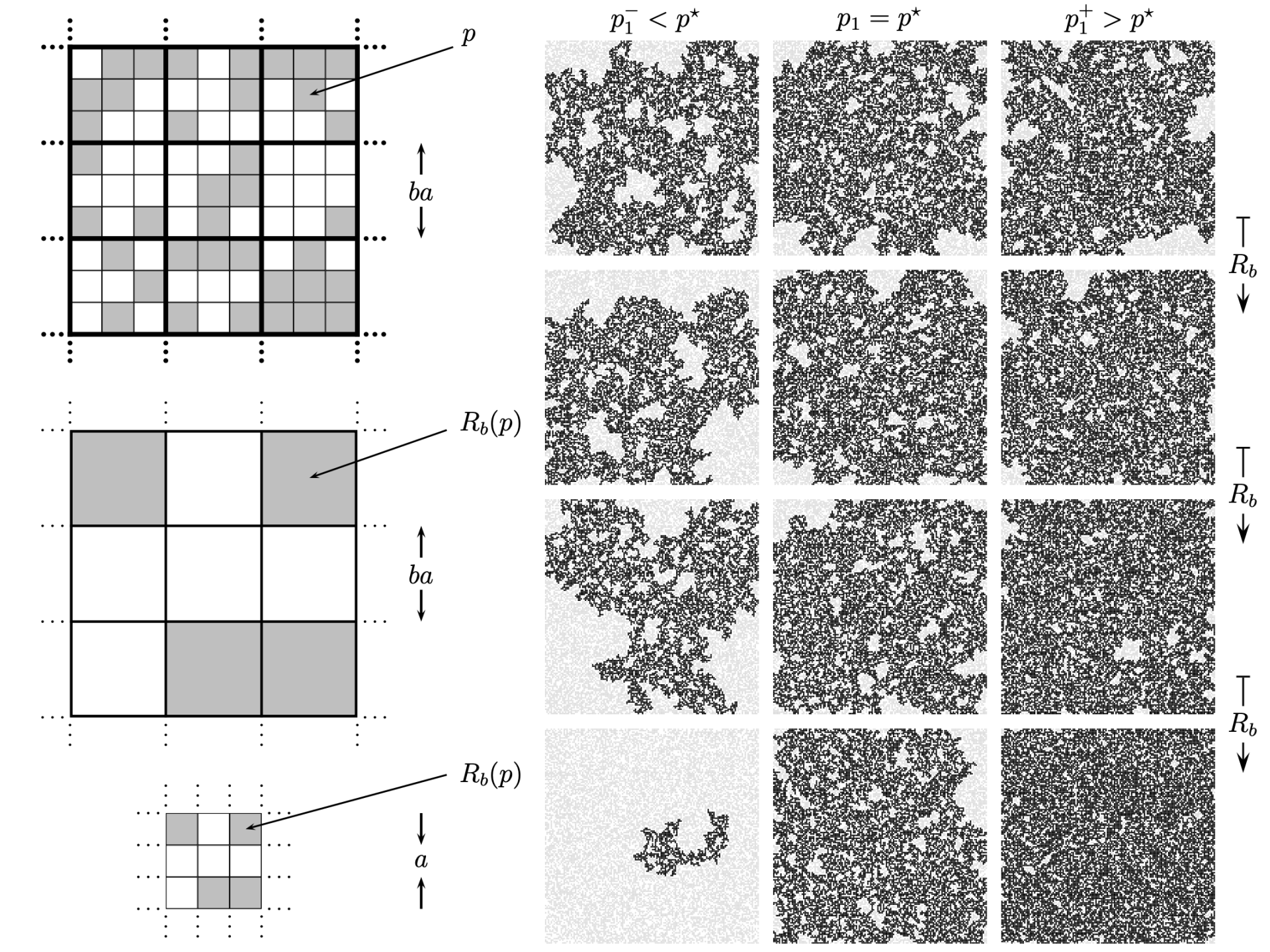
p
ba
$R_b(p)$
ba
$R_b(p)$
a
$p_1^- < p^\star$
$p_1 = p^\star$
$p_1^+ > p^\star$
R_b
R_b
R_b

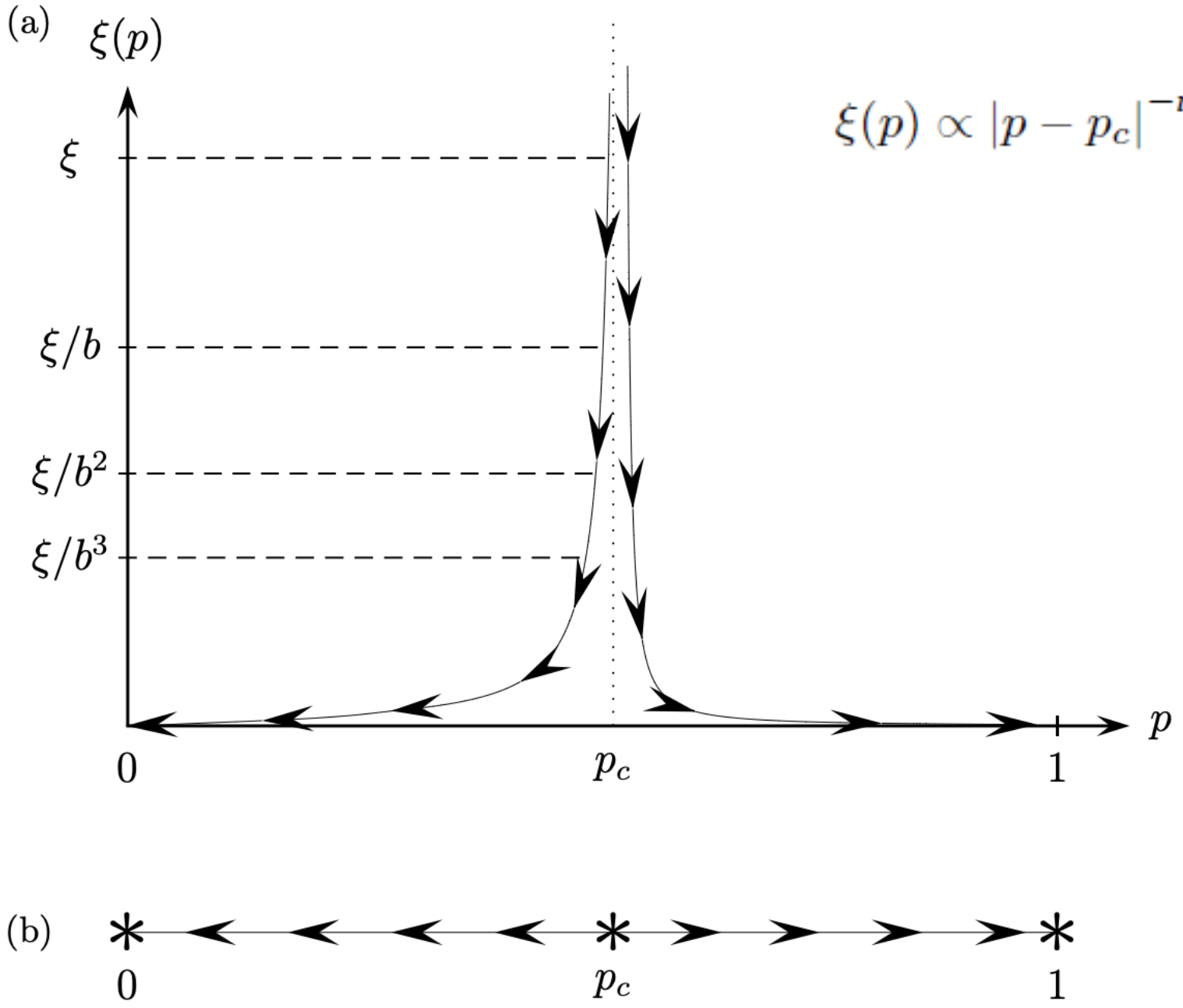
(a)
$\xi(p)$
$\xi(p) \propto |p - p_c|^{-\nu}$
ξ
ξ/b
ξ/b^2
ξ/b^3
p
0
p_c
1
(b)
0
p_c
1

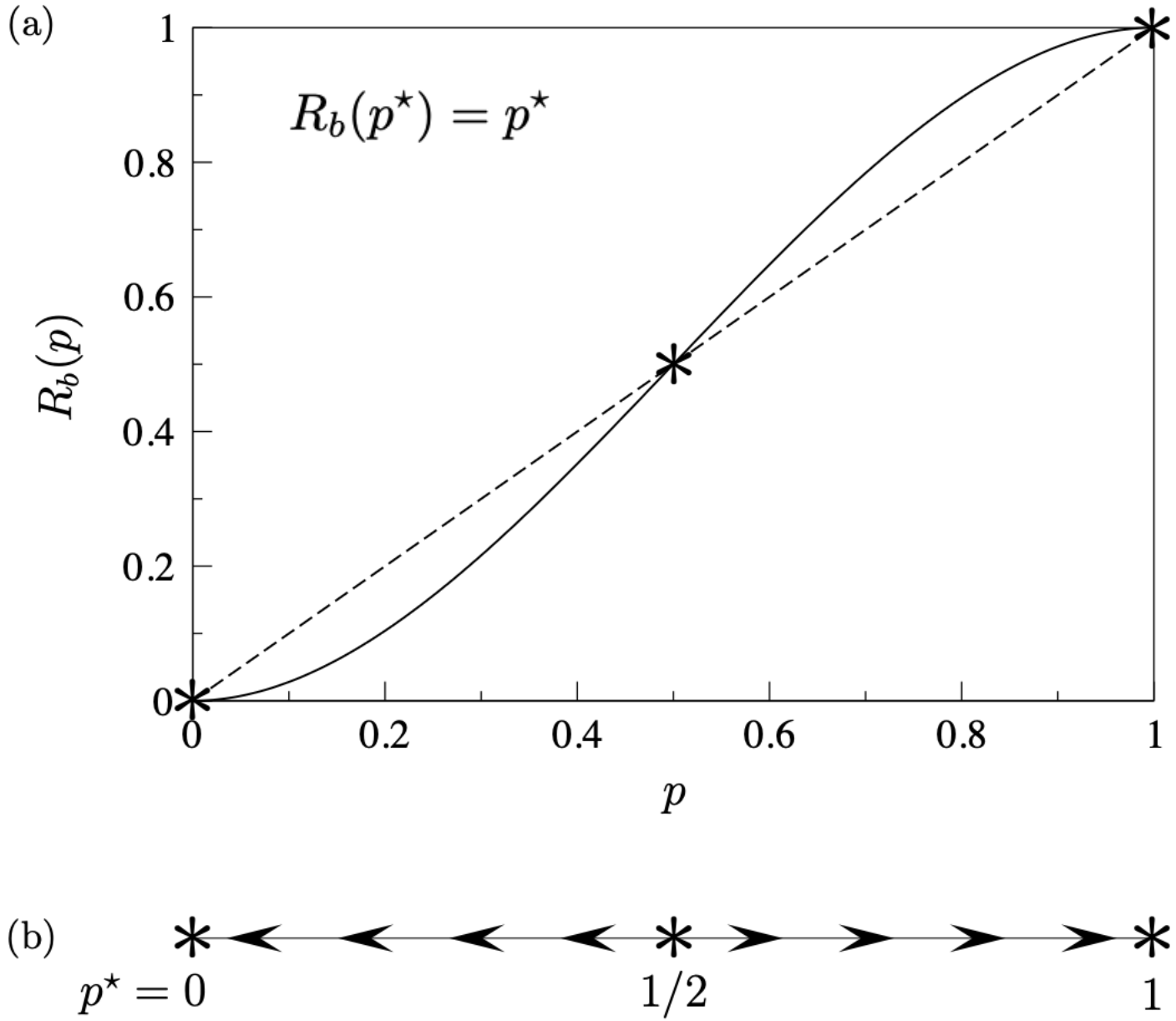
(a)
$R_b(p^\star) = p^\star$
$R_b(p)$
p
0
0.2
0.4
0.6
0.8
1
(b)
$p^\star = 0$
$1/2$
1

$$\frac{\xi}{b} \propto \frac{|p - p_c|^{-\nu}}{b} = |R_b(p) - p_c|^{-\nu} \propto \xi'$$

$$R_b(p^\star) = p^\star$$

$$\begin{aligned} \nu &\approx \frac{\log b}{\log\left(\frac{|R_b(p) - R_b(p^\star)|}{|p - p^\star|}\right)} && \text{for } p \to p^\star \\ &= \frac{\log b}{\log\left(\left.\frac{dR_b}{dp}\right|_{p^\star}\right)} && \text{for } p \to p^\star \end{aligned}$$

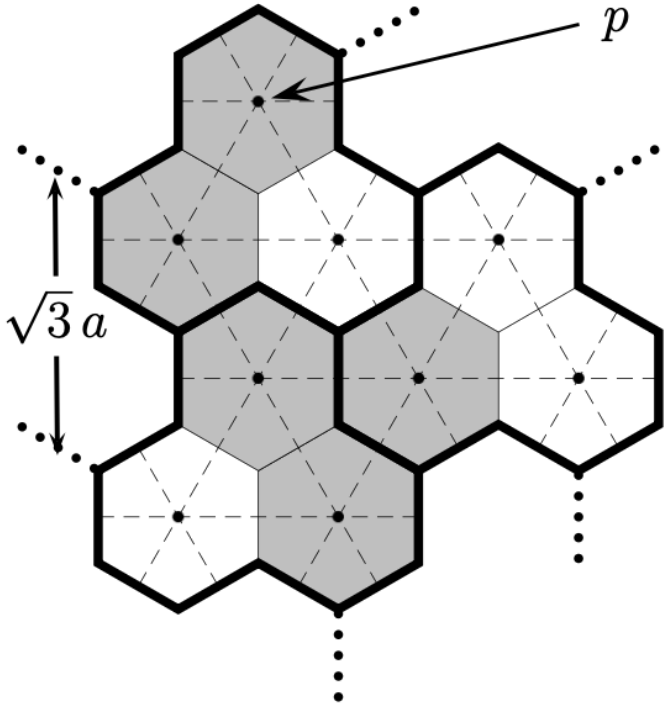

$$b = \sqrt{3}$$

$$R_b(p) = p^3 + 3p^2(1-p) = 3p^2 - 2p^3$$

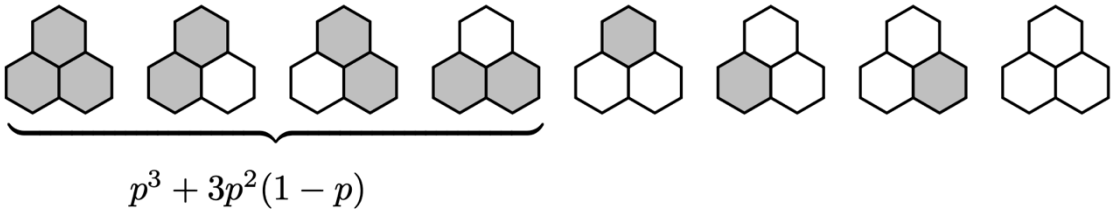

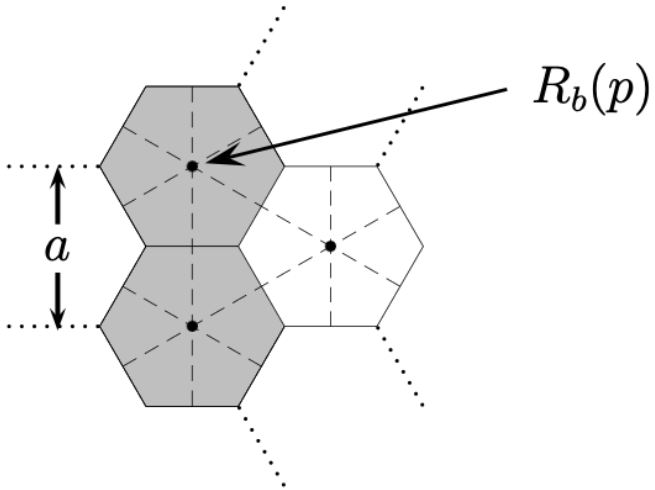

$$R_b(p^\star) = 3p^{\star 2} - 2p^{\star 3} = p^\star$$

$$p^\star(p^\star - 1)(2p^\star - 1) = 0 \quad \Leftrightarrow \quad p^\star = \begin{cases} 0 \\ 1/2 \\ 1. \end{cases}$$

$$R_b(p) = p^3 + 3p^2(1-p) = 3p^2 - 2p^3$$

$$\left.\frac{dR_b}{dp}\right|_{p^\star=\frac{1}{2}} = \left.(6p^\star - 6p^{\star 2})\right|_{p^\star=\frac{1}{2}} = \frac{3}{2}$$

$$\nu = \frac{\log b}{\log\left(\left.\frac{dR_b}{dp}\right|_{p^\star=\frac{1}{2}}\right)} = \frac{\log\sqrt{3}}{\log(3/2)} \approx 1.355$$

(exact value) $\nu = \frac{4}{3}$

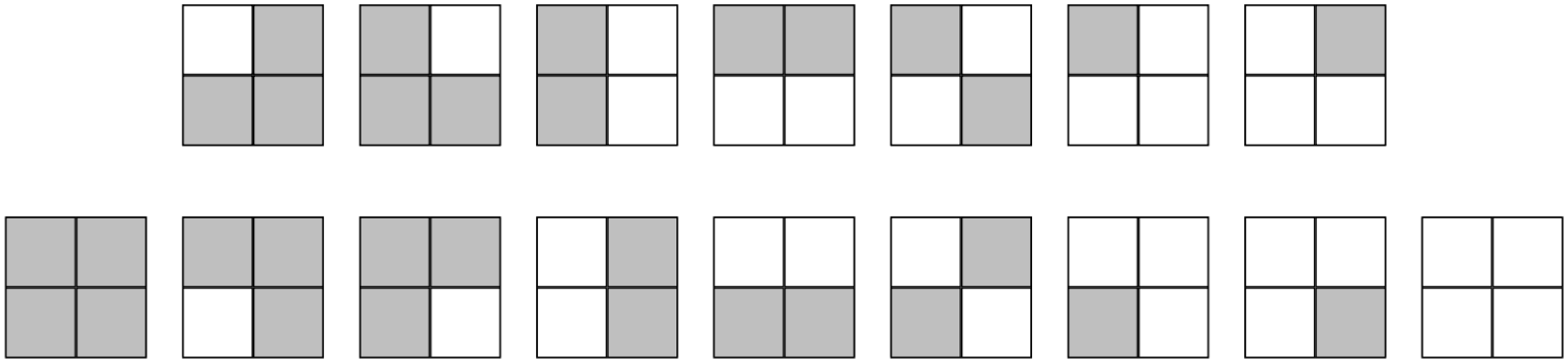

$p^4 + 4p^3(1-p) + 2p^2(1-p)^2$

$$R_b(p) = p^4 + 4p^3(1-p) + 2p^2(1-p)^2 = 2p^2 - p^4$$

$$R_b(p^\star) = 2p^{\star 2} - p^{\star 4} = p^\star$$

$$p^\star(p^\star - 1)(p^{\star 2} + p^\star - 1) = 0 \quad \Leftrightarrow \quad p^\star = \begin{cases} 0 \\ (-1 \pm \sqrt{5})/2 \\ 1. \end{cases}$$

(exact value) $p_c = 0.59274621$

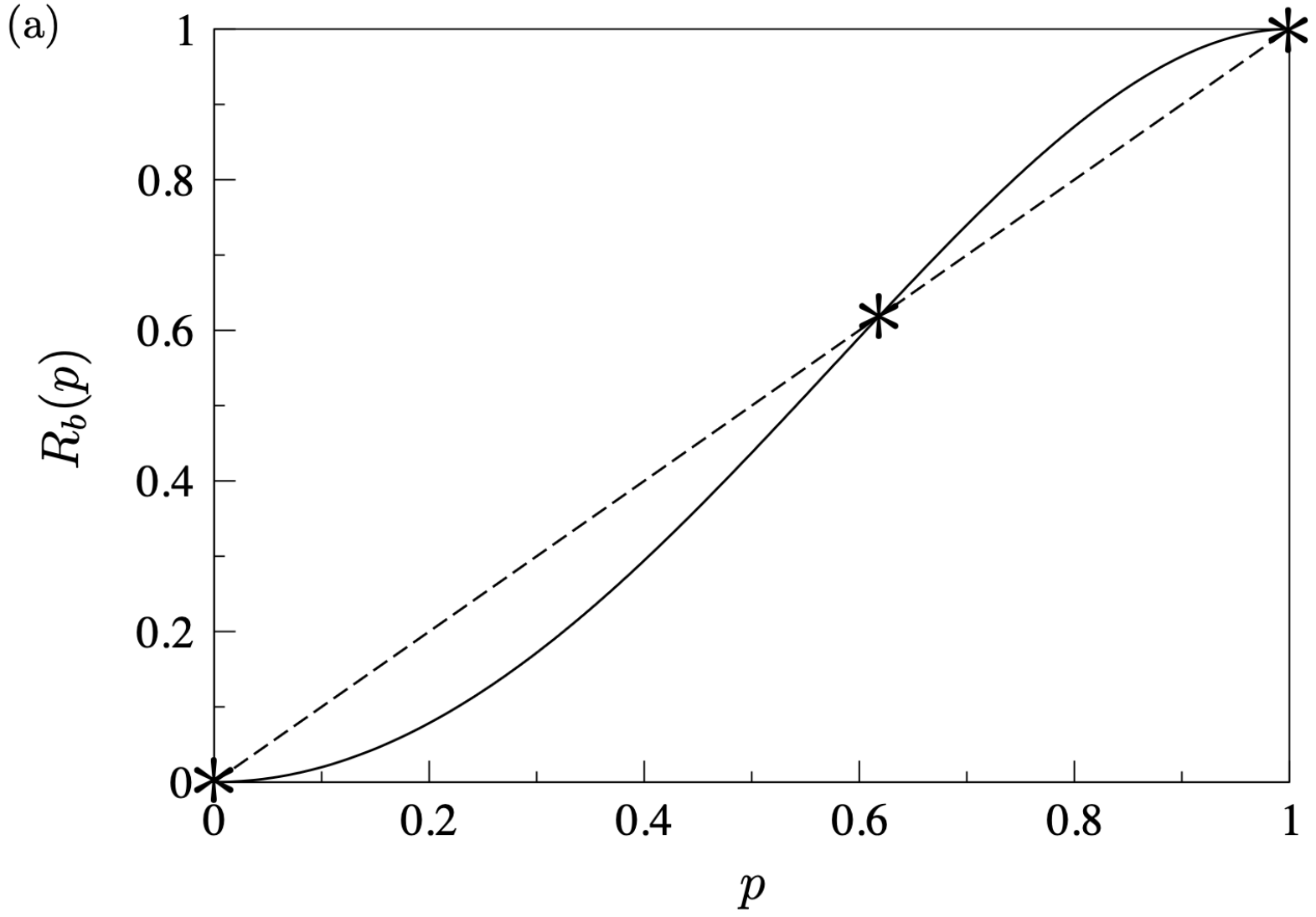
(a)
1
0.8
0.6
0.4
0.2
0
$R_b(p)$
0
0.2
0.4
0.6
0.8
1
p

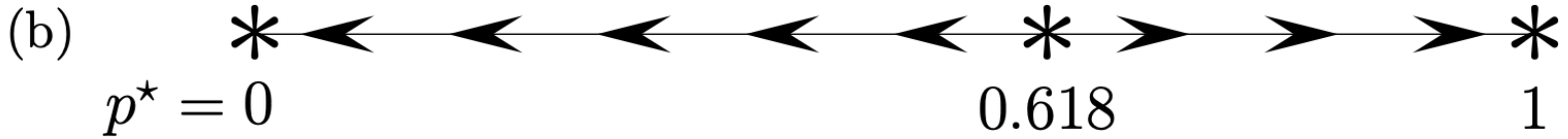
(b)
$p^\star = 0$
0.618
1

$$R_b(p) = p^4 + 4p^3(1-p) + 2p^2(1-p)^2 = 2p^2 - p^4$$

$$\left.\frac{dR_b}{dp}\right|_{p^\star} = \left.(4p^\star - 4p^{\star 3})\right|_{p^\star} = (\sqrt{5}-1)^2$$

$$\nu = \frac{\log b}{\log\left(\left.\frac{dR_b}{dp}\right|_{p^\star}\right)} = \frac{\log 2}{2\log(\sqrt{5}-1)} \approx 1.635$$

(exact value) $\nu = \frac{4}{3}$

Small cell renormalization

√3×√3 triangular lattice

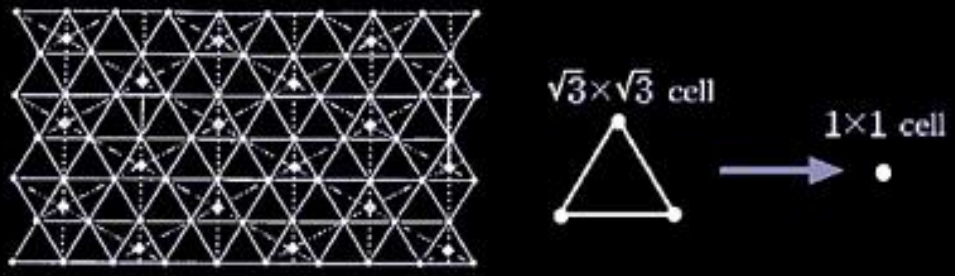

$$\lambda_p = \left.\frac{\partial p'}{\partial p}\right|_{p=p^*} = \frac{3}{2}, \qquad \nu_p = \frac{\ln\sqrt{3}}{\ln(3/2)} = 1.3547\ldots$$

2×2 square lattice bond percolation (?)

$$p' = p^5 + 5p^4(1-p) + 8p^3(1-p)^2 + 2p^2(1-p)^3$$
$$= 2p^5 - 5p^4 + 2p^3 + 2p^2$$

$$p^* = \frac{1}{2}, \quad b = 2 \quad \text{and} \quad \lambda = \left.\frac{dp'}{dp}\right|_{p=p^*} = \frac{13}{8}$$

$$\nu = 1.428$$

Recursion relation

$$p' = R_b(p) = p^3 + 3p^2(1-p)$$

Fixed point $p^* = 0, \ \frac{1}{2}, \ 1$

$$p_c = \frac{1}{2} \ \text{(exact)}, \quad \nu = \frac{4}{3} \ \text{(exact)}$$

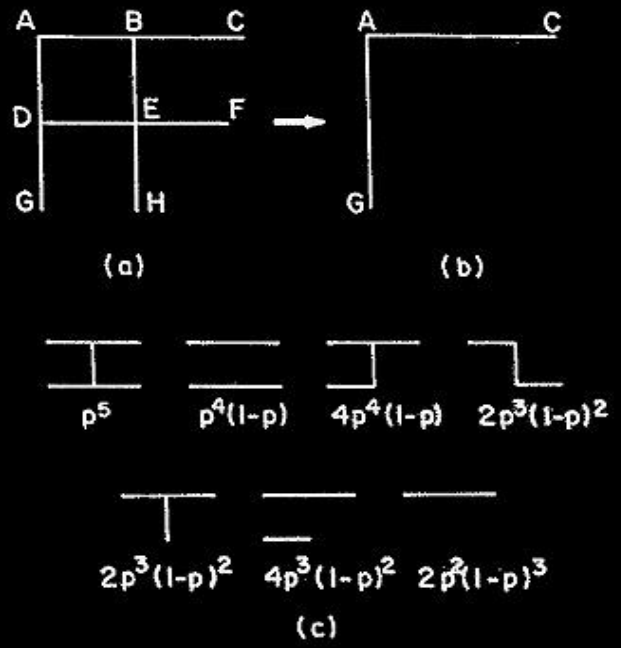

The **Ising model** becomes scale invariant at (Tc,0), where the correlation length is infinite.

Kadanoff's block spin transformation

(1) Divide the lattice into blocks, I, of linear size b (in terms of the lattice constant) with each block containing b^d spins.

(2) Replace each block I of spins with a single block spin, s_I, according to some coarse graining rule which is some function of the spins within block I.

(3) Rescale all lengths by the dimensionless scale factor b to restore the original lattice spacing.

$$t = \frac{T - T_c}{T_c},$$

$$h = \frac{H}{k_B T} = \beta H$$

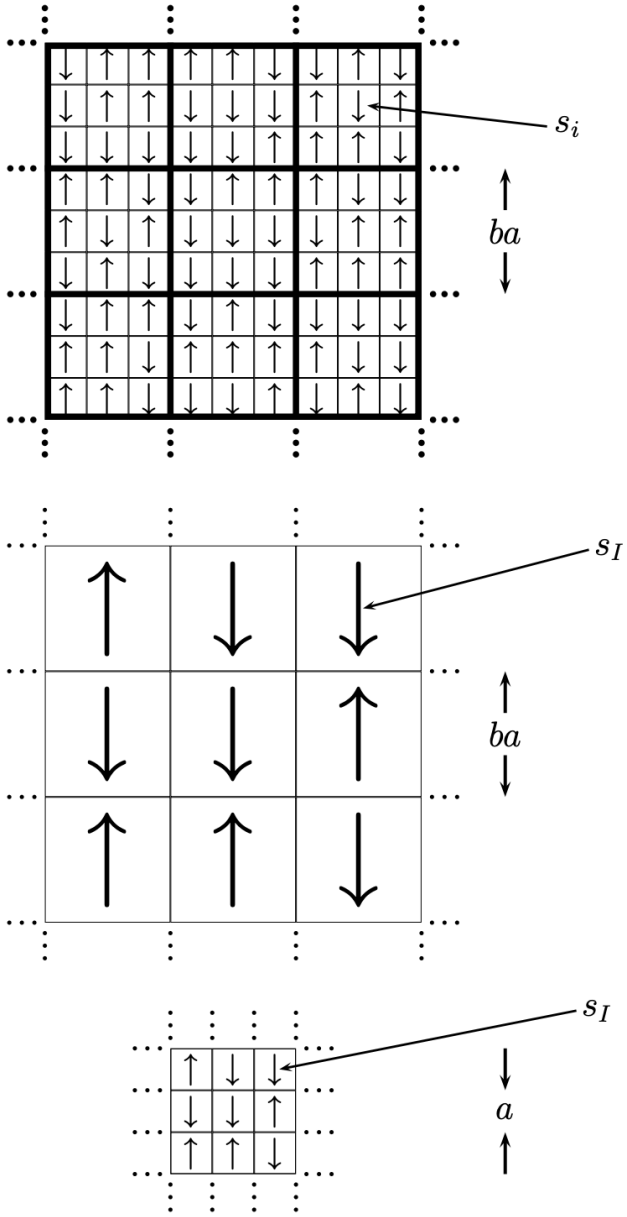

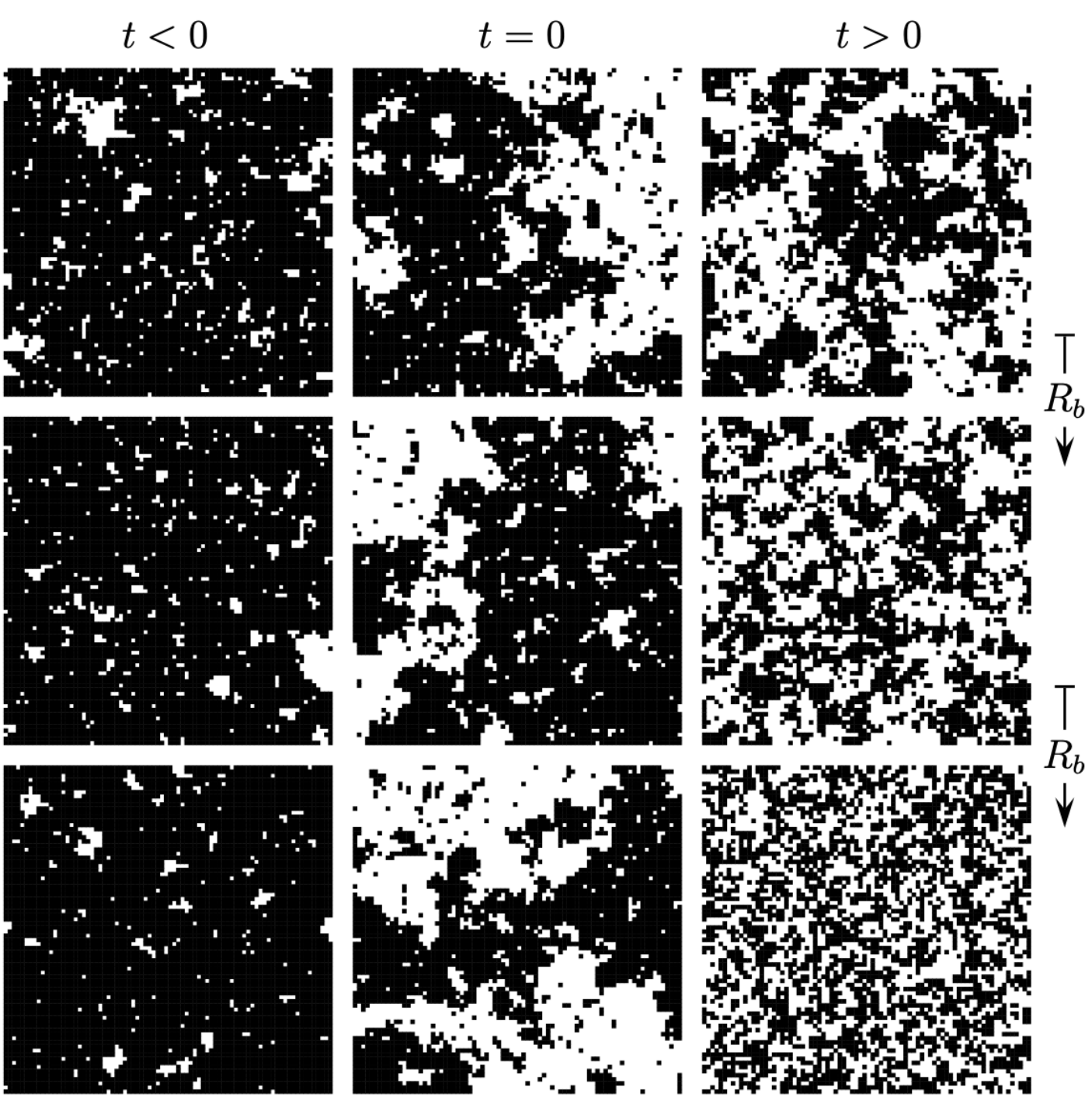
$t < 0$
$t = 0$
$t > 0$
R_b
R_b

In the vicinity of the critical point, $t' = \lambda_t(b)t, \quad b > 1, \lambda_{t(b)} > 1$

$$t'' = \lambda_t(b_2)t' = \lambda_t(b_2)\lambda_t(b_1)t = \lambda_t(b_1 b_2)t$$

$$\lambda_t(b_2)\lambda_t(b_1) = \lambda_t(b_1 b_2) \qquad \lambda_t(1) = 1$$

Power law

$$t' = b^{y_t} t \quad \text{for } t \to 0^{\pm}, \text{ with } y_t > 0,$$
$$h' = b^{y_h} h \quad \text{for } h \to 0^{\pm}, \text{ with } y_h > 0.$$

$$\xi' = \frac{\xi}{b} \qquad \xi' \sim |t'|^{-\nu} = |b^{y_t} t|^{-\nu} = b^{-\nu y_t} |t|^{-\nu} \sim \frac{1}{b}|t|^{-\nu} \qquad y_t = \frac{1}{\nu}$$

$$\begin{aligned} f(t,h) &= -\frac{1}{N} k_B T \ln Z(t,h,N) \\ &= -b^{-d} \frac{1}{N'} k_B T \ln Z(t',h',N') \\ &= b^{-d} f(t',h'). \end{aligned}$$

$$f(t,h) = b^{-d} f(b^{y_t} t, b^{y_h} h) \quad \text{for } t \to 0^{\pm}, h \to 0.$$

Generalised homogeneous function

$$f\left(\lambda^a x, \lambda^b y\right) = \lambda f(x, y)$$

$$\begin{aligned} f(x, y) &= \frac{1}{\lambda} f\left(\pm 1, \lambda^b y\right) \\ &= |x|^{1/a} f\left(\pm 1, y/|x|^{b/a}\right) \\ &= |x|^{1/a} \mathcal{G}_{\pm}\left(y/|x|^{b/a}\right) \end{aligned}$$

scaling form

$$f_s(t,h) = b^{-d} f_s(b^{y_t} t, b^{y_h} h) \quad \text{for } t \to 0^{\pm}, h \to 0.$$

$$b = |t|^{-1/y_t} \propto \xi$$

$$\begin{aligned} f_s(t,h) &= \left[|t|^{-1/y_t}\right]^{-d} f_s\left(\left[|t|^{-1/y_t}\right]^{y_t} t, \left[|t|^{-1/y_t}\right]^{y_h} h\right) \\ &= |t|^{\nu d} f_s\left(t/|t|, h/|t|^{y_h/y_t}\right) \\ &= |t|^{\nu d} f_s\left(\pm 1, h/|t|^{y_h/y_t}\right) \quad \text{for } t \to 0^{\pm}, h \to 0. \end{aligned}$$

$$2 - \alpha = \nu d,$$

$$\Delta = y_h / y_t,$$

$$f_s(t,h) = |t|^{2-\alpha} \mathcal{F}_{\pm}\left(h/|t|^{\Delta}\right) \quad \text{for } t \to 0^{\pm}, h \to 0$$

Widom Scaling Ansatz

$$m(t,h) = -m(t,-h).$$

$$\lim_{h \to 0^{\pm}} m(t,h) \propto \begin{cases} 0 & \text{for } t \geq 0 \\ \pm |t|^{\beta} & \text{for } t \to 0^{-} \end{cases}$$

$$m(0,h) \propto \operatorname{sign}(h)|h|^{1/\delta} \quad \text{for } h \to 0^{\pm}$$

$$m(t,h) = |t|^{\beta} \mathcal{M}_{\pm}\left(h/|t|^{\Delta}\right) \quad \text{for } t \to 0^{\pm}, h \to 0$$

$$\mathcal{M}_{\pm}(x) = -\mathcal{M}_{\pm}(-x) \qquad \mathcal{M}_{\pm}(x) \propto \operatorname{sign}(x)|x|^{1/\delta} \quad \text{for } x \to \pm\infty$$

$$m(t,h) \propto |t|^{\beta}\text{sign}(h)\left(|h|/|t|^{\Delta}\right)^{1/\delta} \quad \text{for } h \to 0^{\pm}, h/|t|^{\Delta} \to \pm\infty$$
$$\propto \text{sign}(h)|h|^{1/\delta} \quad \text{for } h \to 0^{\pm}, h/|t|^{\Delta} \to \pm\infty$$

$$\Delta = \beta\delta$$

$$f_s(t,h) = |t|^{2-\alpha}\mathcal{F}_{\pm}\left(h/|t|^{\Delta}\right) \quad \text{for } t \to 0^{\pm}, h \to 0$$

$$m(t,h) = -\frac{1}{k_B T}\left(\frac{\partial f_s}{\partial h}\right)_t \qquad 2-\alpha-\Delta = \beta$$
$$= -\frac{1}{k_B T}|t|^{2-\alpha-\Delta}\mathcal{F}'_{\pm}\left(h/|t|^{\Delta}\right)$$
$$= |t|^{2-\alpha-\Delta}\mathcal{M}_{\pm}\left(h/|t|^{\Delta}\right) \quad \text{for } t \to 0^{\pm}, h \to 0$$

$$\chi(t,h) = \frac{1}{k_B T}\left(\frac{\partial m}{\partial h}\right)_t$$
$$= -\frac{1}{k_B^2 T^2}|t|^{2-\alpha-2\Delta}\mathcal{F}''_{\pm}\left(h/|t|^{\Delta}\right)$$
$$= |t|^{2-\alpha-2\Delta}\mathcal{X}_{\pm}\left(h/|t|^{\Delta}\right) \quad \text{for } t \to 0^{\pm}, h \to 0$$

$$2 - \alpha - 2\Delta = -\gamma$$

Free energy density

$$f_s(t,0) \propto |t|^{2-\alpha} \quad \text{for } t \to 0$$

$$2 - \alpha = \nu d$$

$$f_s(t,0) \propto \xi^{-d} \propto |t|^{\nu d} \quad \text{for } t \to 0$$

$$k_B T \chi(t,h) = \int_V g(\mathbf{r}_i, \mathbf{r}_j) d\mathbf{r}_j$$

$$k_B T_c \chi(t,0) \propto |t|^{-\gamma} \quad \text{for } t \to 0 \qquad\qquad \gamma = \nu(2-\eta)$$

$$\begin{aligned}
\int_V g(\mathbf{r}_i, \mathbf{r}_j) d\mathbf{r}_j &\propto \int_0^\infty r^{-(d-2+\eta)} \mathcal{G}_\pm(r/\xi, 0) r^{d-1}\, dr \\
&= \int_0^\infty r^{1-\eta} \mathcal{G}_\pm(r/\xi, 0)\, dr && \text{for } t \to 0^\pm \\
&= \int_0^\infty (u\xi)^{1-\eta} \mathcal{G}_\pm(\tilde{r}, 0)\, \xi\, du && \text{with } r = u\xi \\
&= \xi^{2-\eta} \int_0^\infty u^{1-\eta} \mathcal{G}_\pm(u, 0)\, du \\
&= |t|^{-\nu(2-\eta)} \int_0^\infty u^{1-\eta} \mathcal{G}_\pm(u, 0)\, du && \text{for } t \to 0.
\end{aligned}$$

Exponent: Quantity	$d=1$[a]	$d=2$	$d=3$	$d\geq 4$	Mean-field
$\alpha:\ c(t,0)\propto \lvert t\rvert^{-\alpha}$	$2-2/k$	0 (log)	0.111(2)	0	0 (dis)
$\beta:\ m(t,0)\propto (-t)^{\beta}$	0	1/8	0.3262(13)[b]	1/2	1/2
$\gamma:\ \chi(t,0)\propto \lvert t\rvert^{-\gamma}$	$2/k$	7/4	1.237(3)	1	1
$\delta:\ m(0,h)\propto \mathrm{sign}(h)\lvert h\rvert^{1/\delta}$	∞	15	4.792(18)	3	3
$\nu:\ \xi(t,0)\propto \lvert t\rvert^{-\nu}$	$2/k$	1	0.6297(8)[b]	1/2	1/2
$\eta:\ g(r,t,0)\propto r^{-(d-2+\eta)}\mathcal{G}_{\pm}(r/\xi,0)$	1	1/4	0.036(5)	0	0

[a] Using the reduced 'temperature' $t=\exp(-kJ/k_BT)$, where $k>0$ is a constant.
[b] [Binder and Luijten, 2001].

$$\beta\delta = \beta + \gamma,$$
$$\alpha + 2\beta + \gamma = 2,$$
$$\gamma = \nu(2-\eta),$$
$$2-\alpha = \nu d \qquad \text{for } d \leq 4$$

Surface roughness

Ballistic deposition (BD)

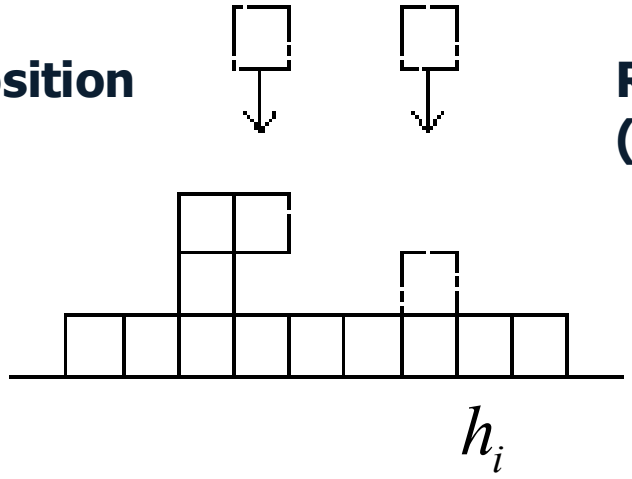

Random deposition (RD)

$$\bar{h} = \frac{1}{L}\sum_i h_i$$

$$W(t) \equiv \sqrt{\frac{1}{L}\sum_{i=1}^{L}\left[h(i,t) - \bar{h}(t)\right]^2}$$

$$w(L,t) \sim t^{\beta} \qquad t \ll t_{\times}$$

$$t_{\times} \sim L^{z}$$

$$w_{sat}(L) \sim L^{\alpha} \qquad t \gg t_{\times}$$

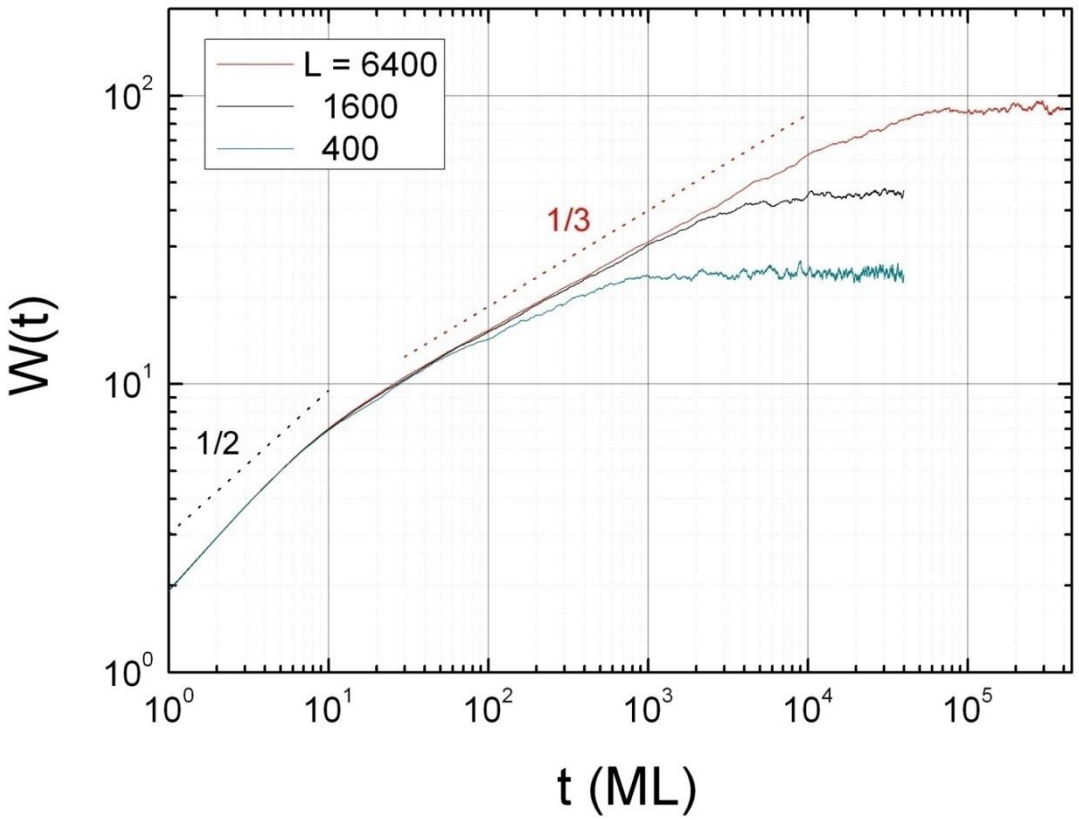

Dynamic Scaling in Surface Growth

- Surface roughness *W(t)*
- Growth exponent *β*
- Roughness exponent *α*
- Dynamic exponent *z*

$$W(t) \equiv \sqrt{\frac{1}{L}\sum_{i=1}^{L}\left[h(i,t)-\bar{h}(t)\right]^2}$$

$$z = \frac{\alpha}{\beta}$$

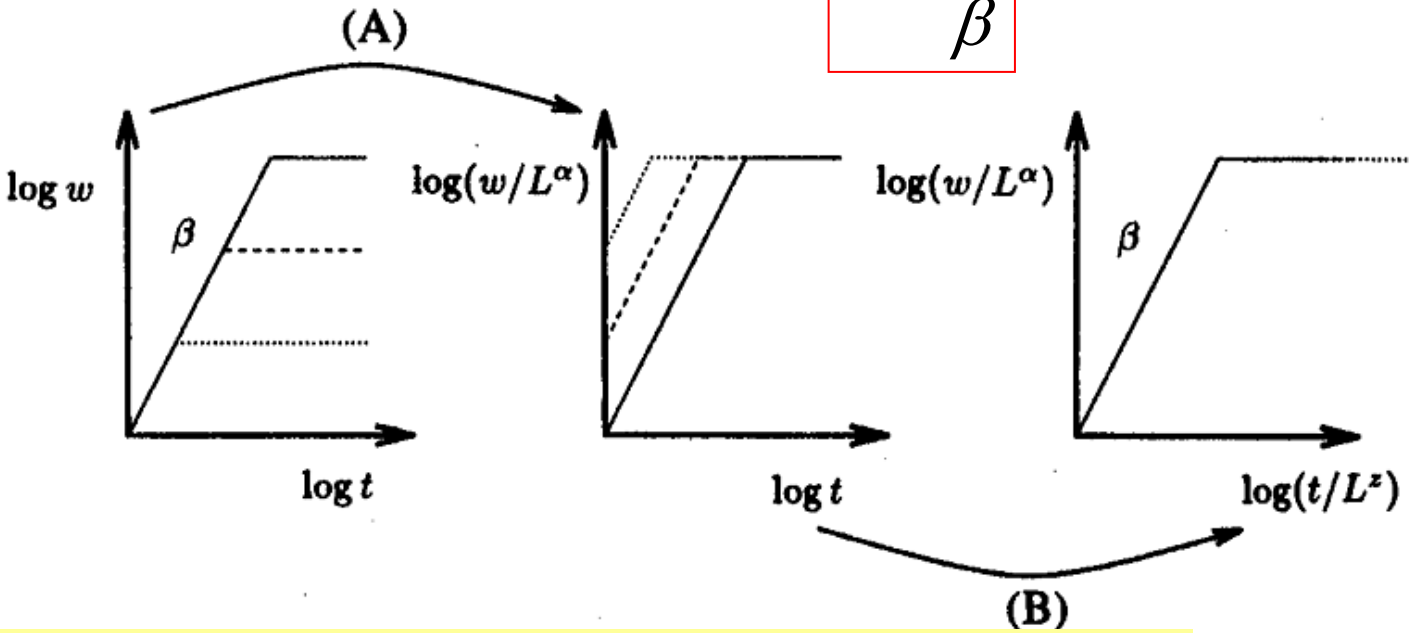

Ref.: A.-L.Barabasi and H.E. Stanley, Fractal Concepts in Surface Growth, Cambridge Univ. Press.

Finite-Time and Finite-Size Scaling of the Kuramoto Oscillators

Mi Jin Lee, Su Do Yi, and Beom Jun Kim*
Department of Physics, Sungkyunkwan University, Suwon 440-746, Korea
(Received 6 August 2013; published 21 February 2014)

Phase transition in its strict sense can only be observed in an infinite system, for which equilibration takes an infinitely long time at criticality. In numerical simulations, we are often limited both by the finiteness of the system size and by the finiteness of the observation time scale. We propose that one can overcome this barrier by measuring the nonequilibrium temporal relaxation for finite systems and by applying the finite-time–finite-size scaling (FTFSS) which systematically uses two scaling variables, one temporal and the other spatial. The FTFSS method yields a smooth scaling surface, and the conventional finite-size scaling curves can be viewed as proper cross sections of the surface. The validity of our FTFSS method is tested for the synchronization transition of Kuramoto models in the globally coupled structure and in the small-world network structure. Our FTFSS method is also applied to the Monte Carlo dynamics of the globally coupled q-state clock model.

DOI: 10.1103/PhysRevLett.112.074102 PACS numbers: 05.45.Xt, 05.70.Fh, 64.60.Ht

Introduction.—In the frame of statistical physics, it is important to find critical exponents in a system aiming to understand its critical behavior. For a limited number of model systems, it might be possible to analytically obtain the exponents via the mean-field analysis, the transfer-matrix calculation, the renormalization group approach, and other analytic tools [1]. In most realistic model systems, however, a rigorous analytic calculation of critical exponents is often a formidable task, making numerical approaches unavoidable and essential.

A phase transition manifests itself as a singularity of the free energy, which exists only in thermodynamic limit of the infinite system size. On the other hand, one can only

is chosen in such a way that its anomalous dimension is null [4], the scaling form of Q is written as $Q(t, L, K) = f(tL^{-z}, (K - K_c)L^{1/\nu})$. In words, the first scaling variable tL^{-z} describes the competition of the two time scales, the finite observation time t and the relaxation time τ, while the second scaling variable $(K - K_c)L^{1/\nu}$ is for the competition of the two length scales, the finite system size L and the correlation length ξ. It is straightforward to extend the scaling form for the globally coupled system, which reads

$$Q(t, N, K) = f(tN^{-\bar{z}}, (K - K_c)N^{1/\bar{\nu}}), \qquad (1)$$

$$Q(t) \equiv \left\langle \operatorname{sgn}\left[\sum_{i=1}^{N} \cos\theta_i(t)\right]\right\rangle$$

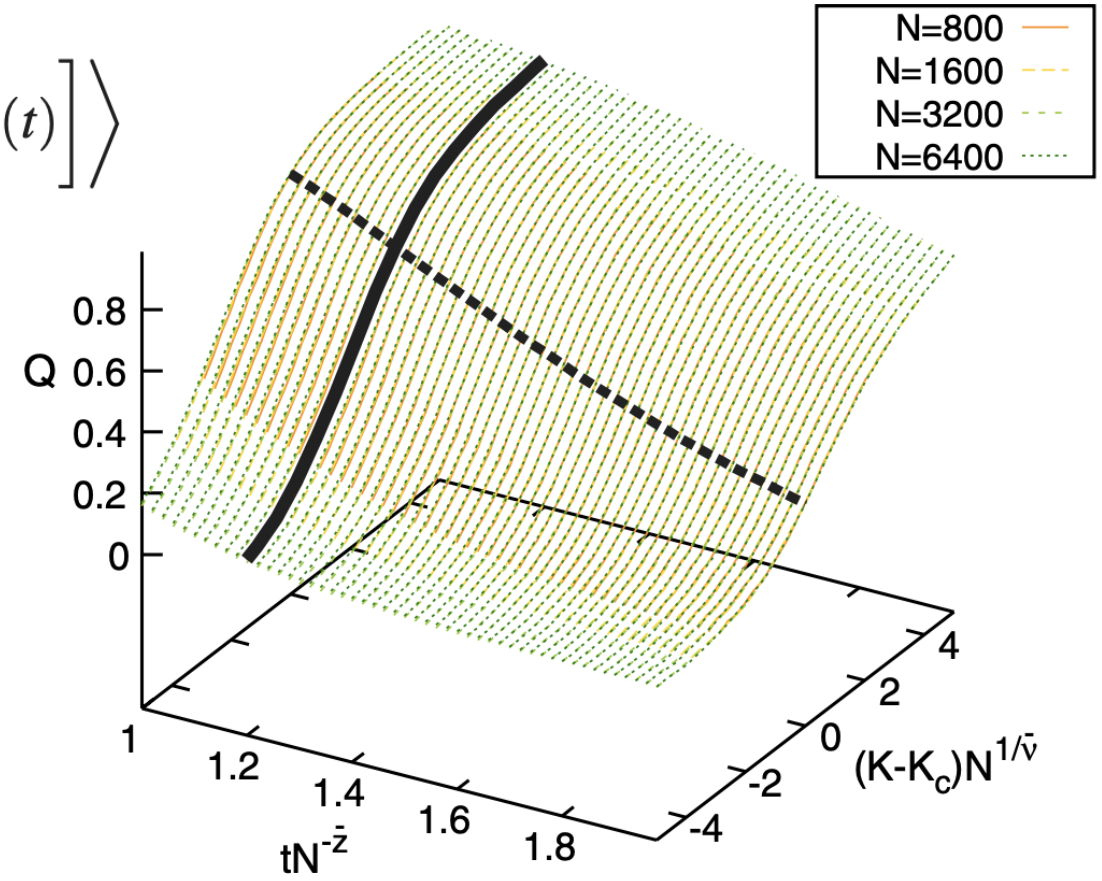

FIG. 1 (color online). Finite-time–finite-size scaling (FTFSS): $Q(t,N,K) = f(tN^{\bar{z}}, (K-K_c)N^{1/\bar{\nu}})$ for the globally coupled Kuramoto oscillators with quenched disorder yields a smooth scaling surface with $\bar{\nu} = 5/2$, $\bar{z} = 2/5$, and $K_c = 1.595\,769$. The scaling collapse is good enough to make the difference of surfaces obtained from different sizes $N = 800$, 1600, 3200, and 6400 almost invisible. The thick dashed and solid lines are two cross sections of the surface at $K = K_c$ and at $tN^{-\bar{z}} = 1.2$ displayed in Figs. 2(b) and (d), respectively.

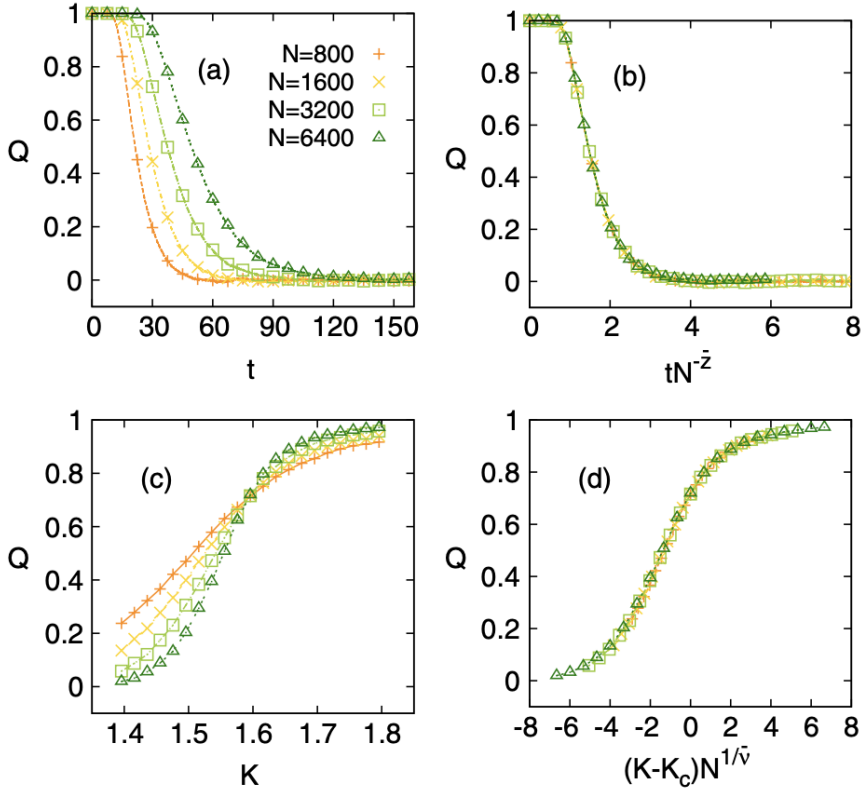

FIG. 2 (color online). The two-variable FTFSS form (1) in Fig. 1 at zero temperature is cross sectioned to one variable scaling form (b) $Q = f(tN^{-\bar{z}}, 0)$ at $K = K_c$ and (d) $Q = f(tN^{-\bar{z}} = 1.2, (K - K_c)N^{1/\bar{\nu}})$. The raw data [(a) and (c)] obtained for various system sizes are scaled into smooth scaling curves [(b) and (d)] with the critical exponents (b) $\bar{z} = 2/5$ and (d) $\bar{\nu} = 5/2$ with the critical coupling strength $K_c = 1.595\,769$.

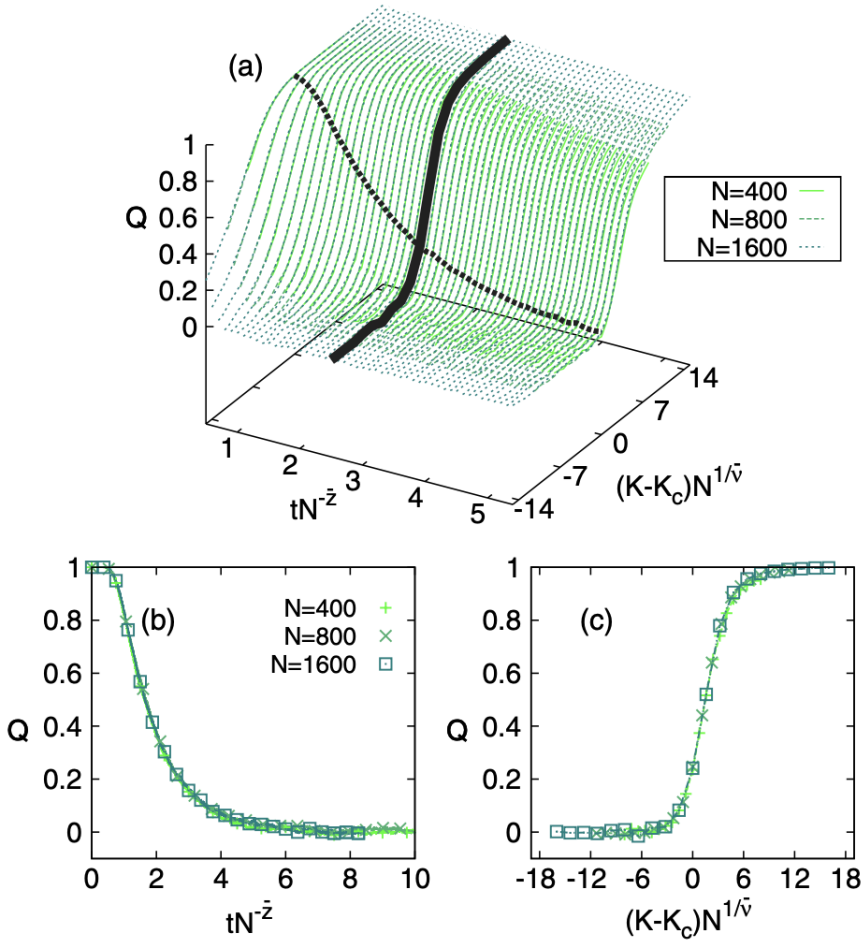

FIG. 3 (color online). The FTFSS for the globally coupled Kuramoto oscillators with thermal disorder only: $\bar{\nu} = 2$ and $\bar{z} = 1/2$ are obtained at $K_c = 2$ (in units of the temperature T). The thick dashed and solid lines are two cross sections of the surface at $K = K_c$ and at $tN^{-\bar{z}} = 2.5$ displayed in (b) and (c), respectively.